ELECTROCHEMICAL STUDIES OF REDOX SYSTEMS FOR ENERGY STORAGE

Report No. II

by

Cherng-Dean Wu

Daniel Scherson

Ernest Yeager

Annual Report : December 1981 to November 1982

NASA Project

Contract : NAG 3-219

NASA-Lewis

Cleveland, Ohio 44106

Case Center for Electrochemical Sciences

and The Chemistry Department

Case Western Reserve University

Cleveland, Ohio 44106

1 December 1982

TABLE OF CONTENTS

I. ABSTRACT OF REPORT

Both chromium(II)/(III) and iron(II)/(III) couples have been studied on various electrode surfaces in acidic perchlorate solution by using rotating ring-disk techniques. It was found that chloride which forms inner sphere coordination complexes with the redox species enhances the electrode kinetics dramatically. Those are consistent with the results of Weaver for chromium(II)/(III) couple and those of Weber for iron(II)/(III) couple.

The effects of lead underpotential deposition and surface alloy formation on the kinetics of the chromium(II)/(III) couple on gold have been studied using both linear sweep voltammetry and potential step techniques. The lead UPD was found to slow down the kinetics of the reduction of the Cr(III) species on gold surface although increase the hydrogen overvoltage. The effect on the chromium(II)/(III) kinetics can be explained in terms of principally a double layer effect. The UPD lead species with its positive charge results in a decrease in the concentration of the Cr(III) species at the electrode surface. Similar phenomena were also observed with bismuth underpotential deposition on gold for the iron(II)/(III) couple.

II. INTRODUCTION AND OBJECTIVES OF RESEARCH

NASA-Lewis has developed a promising redox electrochemical system for energy storage. This system is based on an electrochemical cell with two compartments separated by an ion selective membrane. The electrode reaction at the negative electrode involves the chromium(II)/(III) couple while that at positive electrode involves the iron(II)/(III) couple. Solutions containing these species are circulated through carbon felt electrodes where the reduction of Cr(III) and oxidation of Fe(II) occur during charging and the reverse reaction occur during discharge.

NASA-Lewis has greatly improved the performance of the carbon electrodes used for the chromium(II)/(III) reactions by incorporating gold in the carbon felt matrix and by adding lead chloride to the solution. The resulting gold-lead catalyst greatly reduces the overvoltage normally associated with this redox couple while maintaining the hydrogen overvoltage sufficiently high to depress the competing H_2 generation reaction.

While the gold-lead catalyzed carbon felt electrodes afford high performance, a full understanding of the electrochemical and other processes involved at these electrodes has not yet been achieved. The proposed research is directed to the study of the factors controlling the kinetics of oxidation-reduction couples on various electrode surfaces.

During the past 12 months, NASA-Lewis has sponsored research at Case Center for Electrochemical Sciences on the behavior of the chromium(II)/(III) couple on electrode surfaces including gold, lead and graphite. This investigation is aimed at understanding the role of the electrode and electrolyte components in controlling the electrode reaction kinetics. Such fundamental understanding should provide the insight necessary for the optimization of the present system and for the identification of alternative and perhaps more effective electrode-electrolyte systems for energy storage applications.

III. SUMMARY OF RESEARCH

The research during the first 12 months of this project is summarized.

The experimental studies have included the following measurements :

1. Linear sweep voltammetry studies

   The underpotential electrodeposition of lead has been examined on gold surface using linear sweep voltammetry. At more cathodic potential, bulk deposition and alloy formation occur. The underpotential deposition of bismuth on gold surface also has been studied.

2. Rotating ring-disk electrode studies of the chromium(II)/(III) couple

   Rotating ring-disk electrode techniques have been used to examine the effect of the underpotential deposition of lead on the kinetics of the chromium(II)/(III) couple on gold. This technique permits the separation of the current components for the redox couple and for the underpotential deposition of lead. In some instances it should also be possible to examine the reduction kinetics for the chromium (II)/(III) couple in the presence of a substantial H_2 generation current using a ring with high hydrogen overvoltage to monitor either the consumption of Cr(III) or the production of Cr(II). The rotating disk electrode provides quantitative control of the transport of reactant and products to and from the rotating disk electrode surface.

3. Potential step studies of the effects of UPD layers on the kinetics of chromium(III) reduction

   These experiments involve polarizing a rotating gold disk electrode at a potential where UPD does not occur and then stepping the potential to a value where UPD occurs. Under these conditions with a low bulk concentration of the UPD species, the deposition of the UPD layer occurs very slowly under pure diffusion control. The coverage of the UPD layer can then be calculated as a function of time from the diffusion flux. With chromium(III) also present, the dependence of the rate of the chromium(III) reduction on the UPD coverage can be determined from the time dependence of the chromium(III) reduction current.

4. Raman studies of adsorbed chromium complexes on electrode surfaces

   Surface enhancement of the Raman signals (SERS) by factors of up to 10^6 are obtained with adsorbed species on metals such as silver and gold. Advantage is being taken of this enhancement to check on the possible specific adsorption of various inner sphere chromium(III) complexes on these electrode surfaces. So far, preliminary measurements have been carried out with the mono- and di-thiocyanate chromium

complexes adsorbed on silver. Strong signals have been obtained, presumably from monolayers, but detailed analyses of the Raman data have not yet been made. Further work is planned.

5. Ultraviolet-visible absorption spectroscopy

The $[Cr(H_2O)_6]^{3+}$, $[Cr(H_2O)_5Cl]^{2+}$ and $[Cr(H_2O)_4Cl_2]^{+}$ species have been monitored using UV-visible absorption spectroscopy. Further measurements using UV-visible absorption are planned to establish the concentration changes for these species as a consequence of the electrode processes as well as homogeneous processes.

The voltammetry and polarization measurements have led to the following conclusions :

1. The reversible potentials differ substantially for the $[Cr(H_2O)_6]^{3+}$, $[Cr(H_2O)_5Cl]^{2+}$ and $[Cr(H_2O)_4Cl_2]^{+}$ couples.

2. The UPD lead on the gold slows down the kinetics of the reduction of the various chromium(III) species on the gold surface. This effect is probably principally associated with a double layer effect. The UPD lead species with its positive charge results in a decrease in the concentration of the chromium(III) species at the electrode surface (in the outer Helmholtz plane).

3. The principal beneficial role of the lead on the reduction of chromium (III) species on gold is to increase the hydrogen overvoltage and thus suppress the competing H_2 generation reaction.

4. Anion bridging does not play an important role in the reduction of $[Cr(H_2O)_5Cl]^{2+}$ on gold, probably because the negative charge on the cathode causes this complex to approach the electrode surface in the outer Helmholtz plane with the chloride ligand directed away from the electrode surface.

5. Anion-bridging does appear to be important in the oxidation of chromium (II) to chromium(III). The model proposed to explain the kinetics is that the chloride ion is specifically adsorbed on the electrode surface and then transfered into the inner coordination sphere of the chromium (III) ion to yield $[Cr(H_2O)_5Cl]^{2+}$. UPD can increase the surface concentration of adsorbed Cl^- and thus promote the formation of the chloride complex. In addition to the UPD of lead, the UPD of bismuth has also been examined on gold. Some kinetic measurements have also been carried out for the iron(II)/(III) couple on the UPD Bi/Au surfaces.

IV. DATA AND PRELIMINARY DISCUSSION

1. $Cr(H_2O)_6^{3+}/Cr(H_2O)_6^{2+}$ Couple on Nickel-Mercury Disk Electrode

A. Nickel-Mercury Electrode

The chromium(II)/(III) couple in an acidic aquo solution is a simple one-electron transfer reaction having very irreversible kinetics in the absence of bridging ligands. It is necessary to have a high hydrogen overvoltage electrode to study the reduction kinetics of this couple. Mercury affords such a high hydrogen overvoltage and has been used for previous studies of this couple at Case Center for Electrochemical Sciences.[1] To check out this couple under steady state and well defined transport conditions, a rotating mercury coated nickel disk electrode has been used in the early phases of the present study. For practical purposes the electrochemical surface properities are close to those of a mercury electrode. The solubilities of nickel in mercury and vice verse are very low. The surface layer is almost pure mercury.

The mercury coated electrode is easily made and is easy to use. The following procedure will give a nickel-mercury electrode with high hydrogen overvoltage. A polished nickel disk is subjected to a few minutes of ultrasonic cleaning immediately before the mercury-deposition procedure to remove any organic film and trapped particles on the electrode. The electrode is then introduced into a solution of ca. 0.5 mM $Hg(NO_3)_2$ and 0.1 M $HClO_4$. A potential of -1.10 V vs SCE is then applied to the nickel disk electrode and maintained until hydrogen evolution is apparent from bubble formation. A nickel grid is used as

---

(1). S. Donovan and E. Yeager, " The Electrode Kinetics of the Chromous-Chromic Couple " ONR. Technical Report No. 24, Case Western Reserve University, Cleveland, Ohio, Oct. 1969.

counter electrode. Deposition is repeated for several times.

The mercury coated surface of the electrode has a reasonable high hydrogen overvoltage, although not as high as very pure mercury. Actually the hydrogen overvoltage on a stationary film of mercury was intermediate between that on smooth solid electrode and on dropping mercury.

B. The $NaClO_4$ Supporting Electrolyte

The specific adsorption of the ions of the supporting electrolyte has long been known to influence profoundly the rate of electron-transfer reactions at metal-solution interfaces. A difficulty faced with redox couples of the type M^{2+}/M^{3+} with high charged ions is that the double-layer effects in the kinetics are quite significant even in concentrated electrolytes. The double-layer corrections are smallest and can be applied with greatest confidence using supporting electrolytes at high ionic strengths in the absence of specific ionic adsorption with the concentration of the redox species small in comparison with that of the supporting electrolyte. Perchlorate was chosen because this anion combines weak specific adsorption with only a very small tendency toward complex formation in the bulk of the solution. Perchlorate ions are adsorbed to a very low degree on conventional electrodes such as Pt, Au and Hg. Their adsorbability is far lower than for sulfate ions and, except at higher positive potential, their adsorption can be neglected. Inner coordination complexes between chromium ions and the ClO_4^- form only to a very small extent except in

very high concentration of perchlorate.[2] The concentration of chromium (III) employed was always kept sufficiently below those of the supporting electrolytes so that these ions made a negligible contribution to the diffuse-layer structure.

Among the solid electrodes, it seems that a mercury coated electrode is the only one which can be seen both cathodic and anodic waves of chromium(II)/(III) couple in perchlorate electrolyte. In perchlorate supporting electrolyte, the chromium(II)/(III) couple gives well defined cathodic and anodic waves, as is shown later. The reduction of Cr^{3+} proceeds at negative potential where the perchlorate is not significantly specifically adsorbed. The reduction and oxidation waves are well separated and have different shapes that reflect, in part, the different influence of the diffuse double layer on the reduction and oxidation reactions, respectively.

Rotating nickel-mercury disk electrode data are shown in fig.2.

(2). K. M. Jones and J. Bjerrum, Acta. Chem. Scand. 19 (1965) 974.

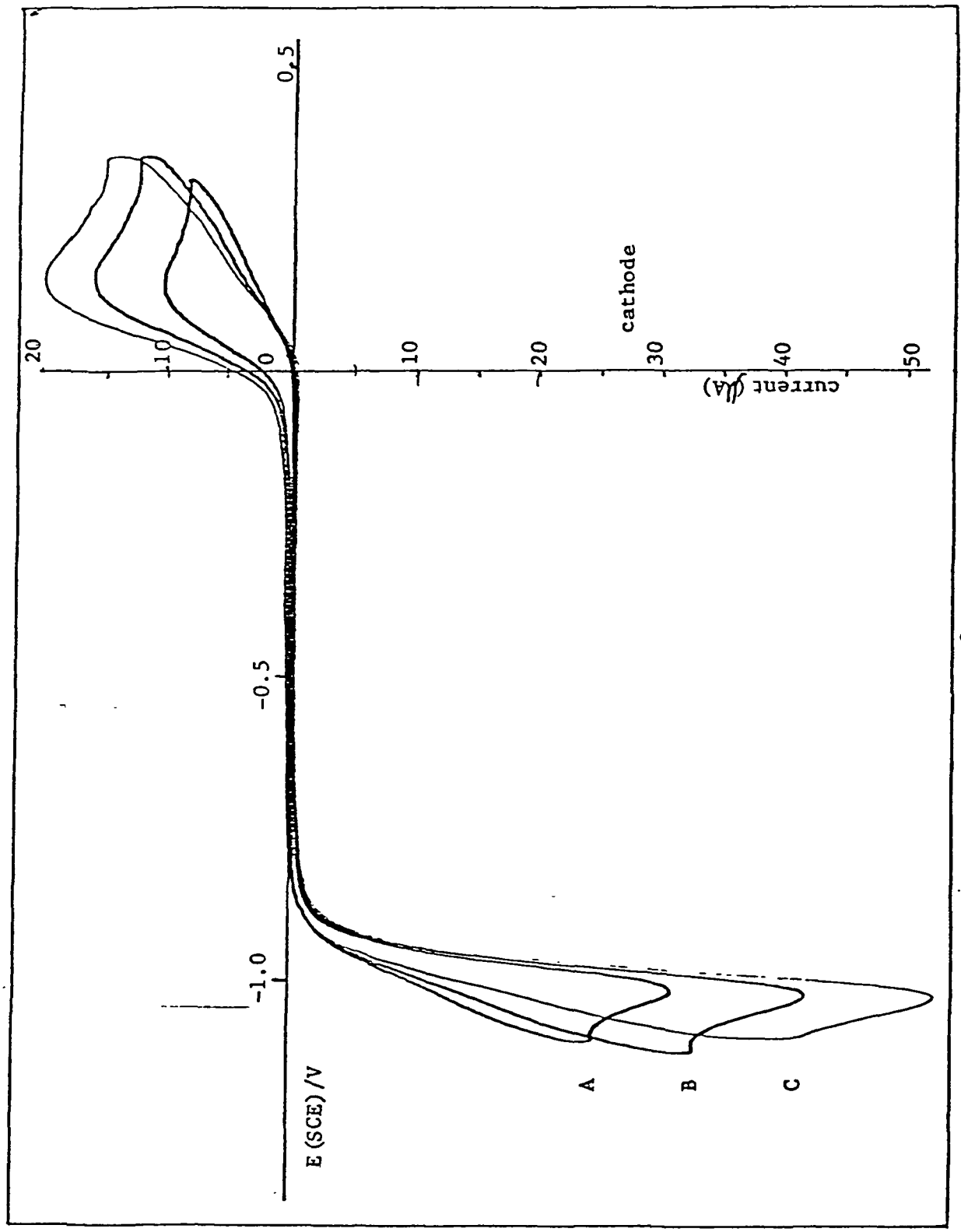

Figure 1: Voltammetry curves for 2mM $Cr(H_2O)_6^{3+}$ on stationary nickel-mercury disk electrode. Electrolyte: 0.1M $HClO_4$ (pH: 1.6). Electrode area: 0.2 cm^2. Sweep rate: A. 50mV/s, B. 100mV/s, C. 150mV/s. Temperature: 25°C.

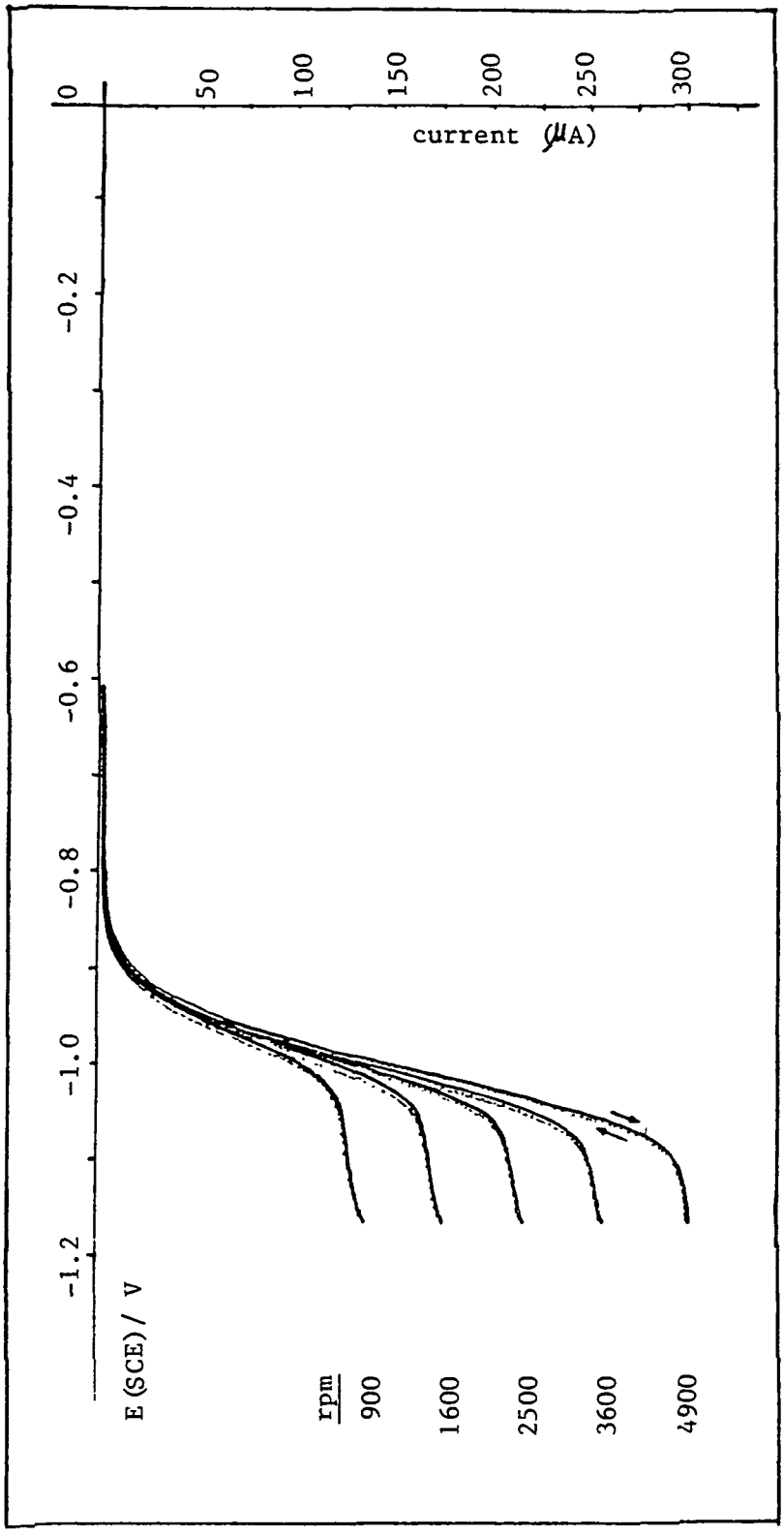

Figure 2: Polarization curves for $Cr(H_2O)_6^{3+}$ reduction on mercury coated nickel disk electrode. Solution: 0.61mM $Cr(ClO_4)_3$ in 0.01M $HClO_4$, 2mM $NaClO_4$. Electrode area: 0.2 cm^2. Sweep rate: 10 mV/s. Rotation rate: as indicated.

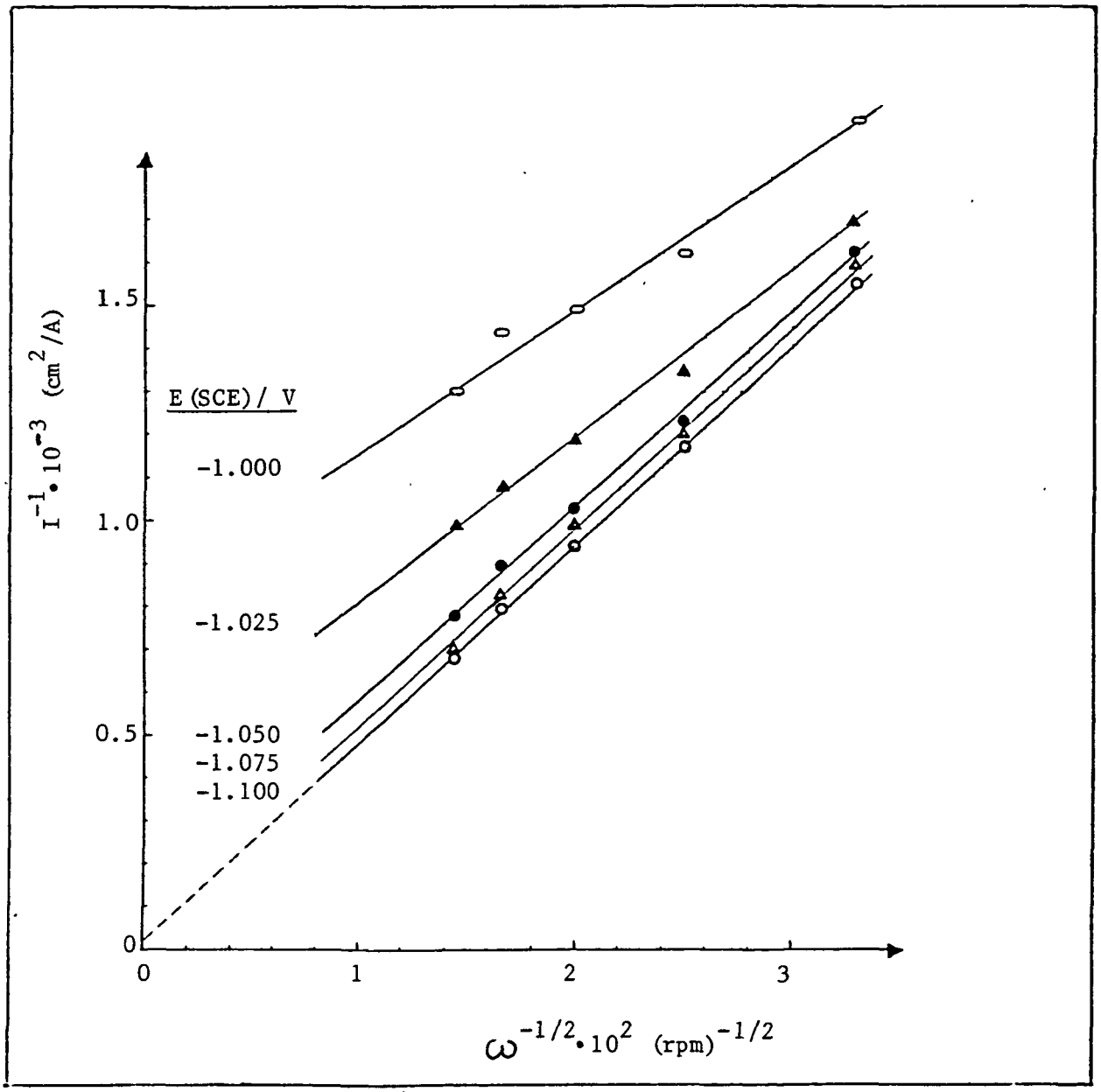

Figure 3: I^{-1} vs. $\omega^{-1/2}$ plots of data in Fig. 2 for reduction of $Cr(H_2O)_6^{3+}$ on nickel-mercury electrode.

C. Effect of Halides

In perchlorate supporting electrolyte with a pH of 2 or less (to avoid hydrolysis), the hexaaquochromium(II)/(III) couple exhibits an irreversible wave. With halides in solution, the anodic wave of couple is shifted toward more negative potential. When the supporting electrolyte contains bromide ions, the couple produces two reduction waves: one corresponding to the uncomplexed chromium(III) reduction, the other to the bromide complex chromium(III) reduction. Only a single anodic wave is apparent corresponding to the formation of the complexed chromium(III) from chromium (II). The bromide is adsorbed on the electrode surface and transfered into the inner coordination sphere of the Cr. The kinetics are very slow for the reduction without the bridging bromide ligand. A representative voltammetry curve with bromide is given in Fig. 4.

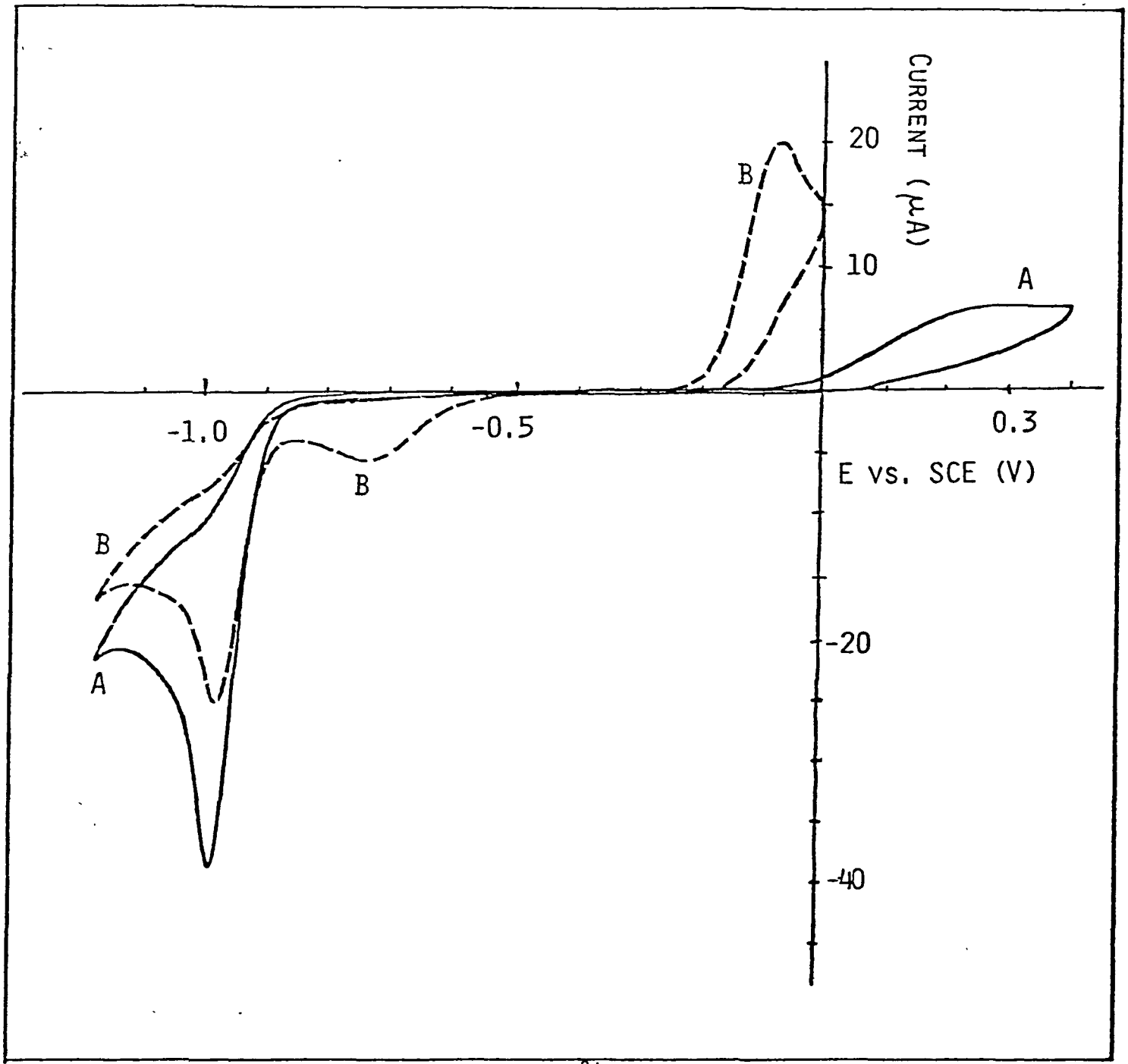

Figure 4: Voltammetry curves for 2mM $Cr(H_2O)_6^{3+}$ on stationary nickel-mercury disk electrode. Electrolyte: 0.01M $NaClO_4$ and 0.01M $HClO_4$. Electrode area: 0.2 cm^2. Sweep rate: 50 mV/s. Temperature: 22°C. A. without NaBr added. B. with 1.67 mM NaBr added. Quasi-steady-state measurement (curves recorded after many cycles).

D. NH_4X as Supporting Electrolyte

In 0.1 M ammonium chloride or ammonium bromide, chromium(II)/(III) couple gives well defined anodic and cathodic waves. The voltammetry curve of chromium (II)/(III) couple shows a much more reversible behavior in NH_4X supporting electrolyte than that in pure perchlorate solution. While the cathodic wave potentials are not changed very much and remain almost the same, the anodic potentials vary with the supporting electrolyte used.

In presence of ammonium halide the anodic wave potential is found to be more negative than that with NaX in acidic solution. It appears that both ammonium and halide ions have an influence on the behavior of the chromium (II)/(III) couple. It is likely that ammonium ions (NH_4^+) adsorb on mercury surface to modify the kinetics of electrode reaction.

When NH_4Br was used as supporting electrolyte, the cyclic voltammetry curve was changed from what it was in a NH_4Cl supporting electrolyte. (Fig.6). The original cathodic peak was slightly changed from what it was in the pure perchlorate or NH_4Cl media, the anodic peak was shifted toward negative potentials, and a new cathodic peak at potentials positive to the original cathodic peak appeared. The new cathodic peak which was not seen in NH_4Cl electrolyte corresponds to the reduction of $[Cr(H_2O)_5Br]^{2+}$. It is believed some bromide ions have already coordinated to the Cr to form $[Cr(H_2O)_5Br]^{2+}$ during the back scan, but not chloride ions.

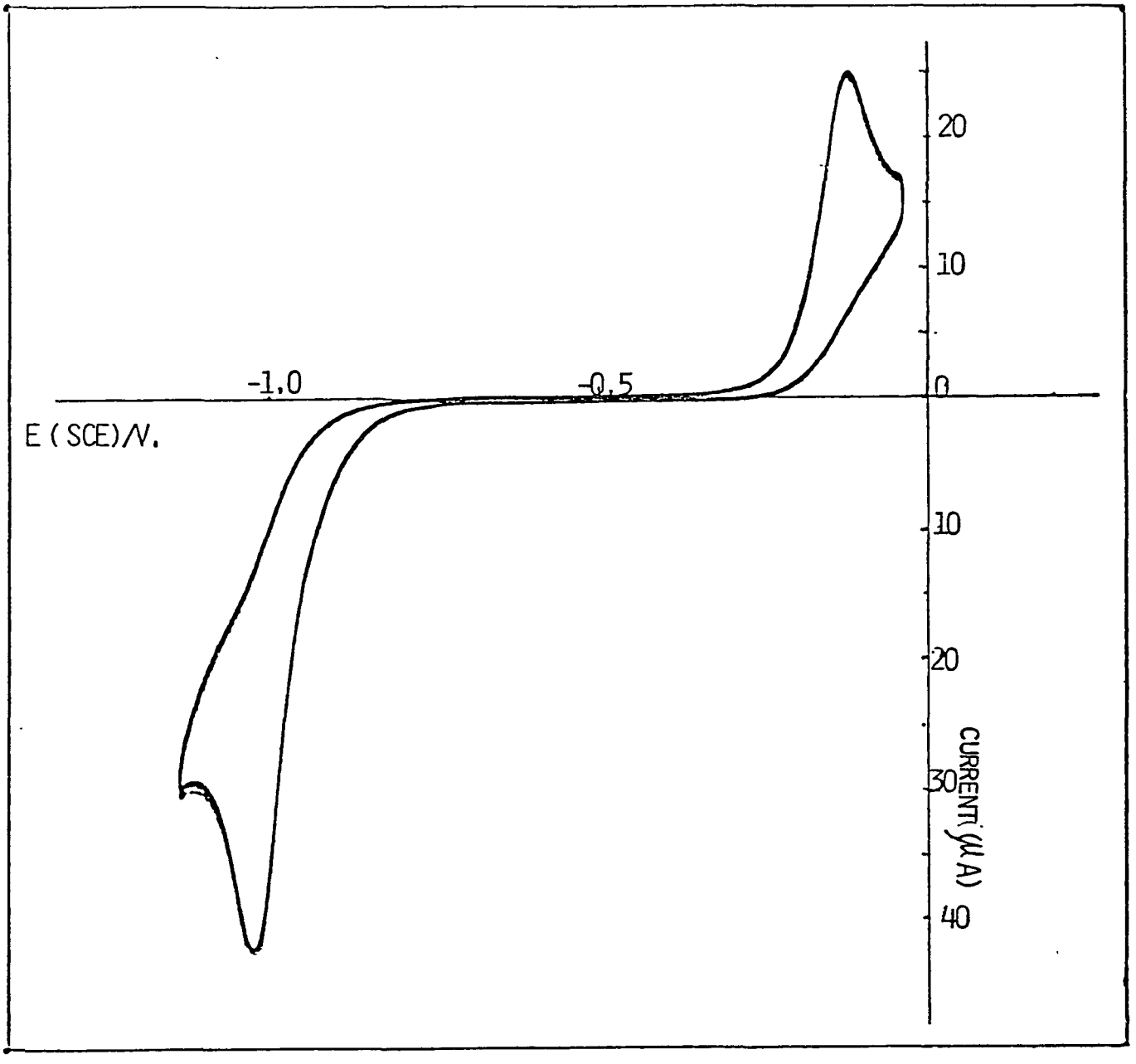

Figure 5: Voltammetry curve for 2 mM $Cr(H_2O)_6^{3+}$ on nickel-mercury disk electrode. Quasi steady-state measurement. (curve recorded after many cycles). Electrolyte: 0.01M $HClO_4$, 0.1M NH_4Cl (pH: 2.4). Electrode area: 0.2 cm^2. Sweep rate: 100 mV/s.

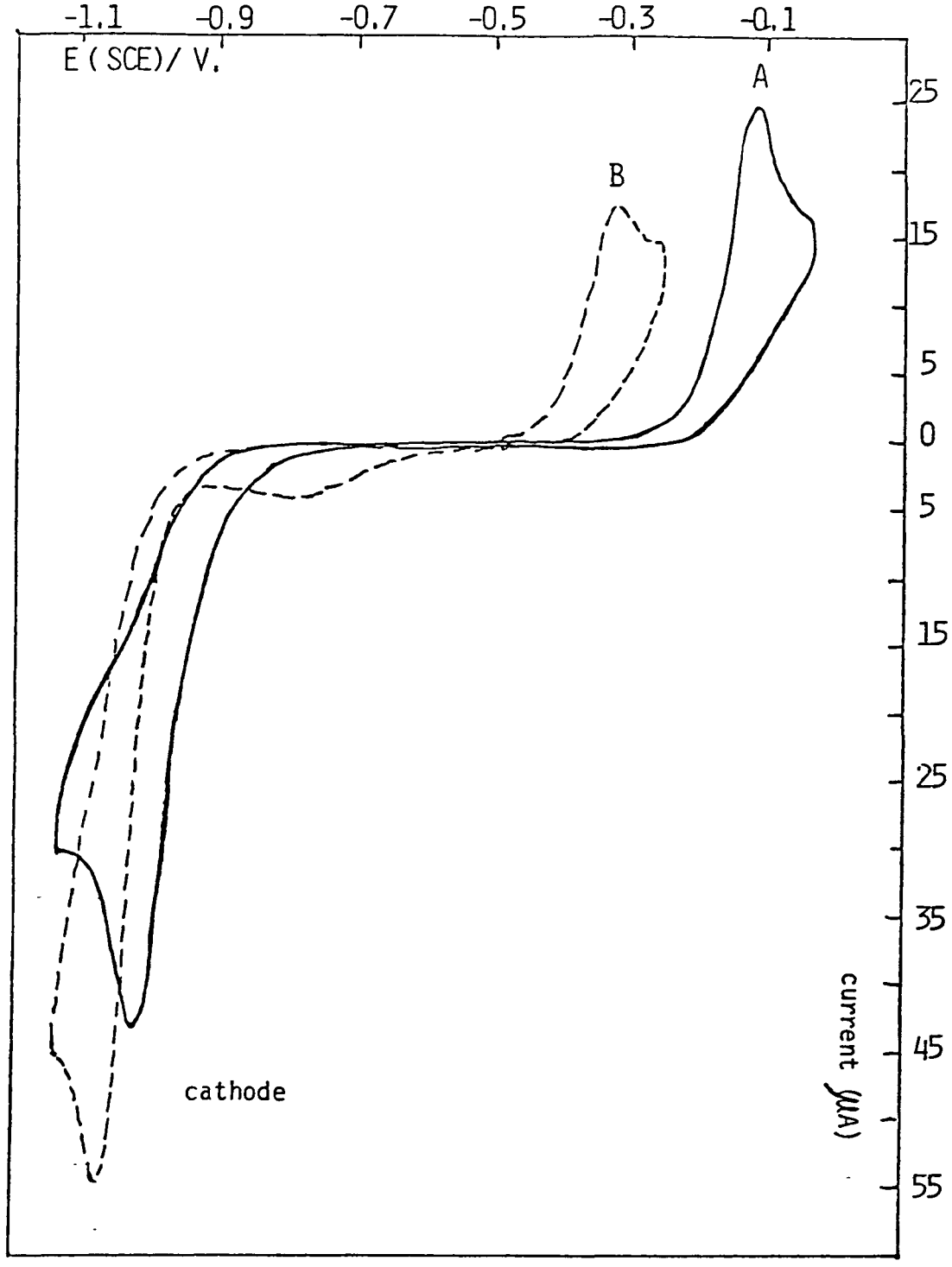

Figure 6: Voltammetry curves for 2 mM $Cr(H_2O)_6^{3+}$ on nickel-mercury disk electrode with NH_4X as supporting electrolyte. Quasi steady-state measurements. Electrode area: 0.2 cm^2.
A. in 0.01 M $HClO_4$, 0.1 M NH_4Cl (pH: 2.4)
B. in 0.01 M $HClO_4$, 0.1 M NH_4Br (pH: 2.3)

2. Chromic Chloride Reduction in Acid Media on Au, Pb/Au and Graphite Electrodes

A. Gold Electrode

As indicated in section 1, the $Cr(H_2O)_6^{3+}/Cr(H_2O)_6^{2+}$ couple has sluggish electrode kinetics on nickel-mercury electrode in acid media at pH of 2. Such low pH solution was used to prevent the hydrolysis of chromium couple. Under these conditions, the reduction wave of $Cr(H_2O)_6^{3+}$ occurs at potentials close to that for hydrogen evolution. It is difficult to study the reduction of $Cr(H_2O)_6^{3+}$ without interference of hydrogen evolution.

The high overvoltage for Cr(III) reduction is due to the high free energy of activation just as in the homogeneous case. In contrast to the nickel-mercury electrode, the reduction of $Cr(H_2O)_6^{3+}$ does not occur on crystalline gold disk electrode without hydrogen evolution. Unlike $Cr(ClO_4)_3$, the reduction in solutions prepared from $CrCl_3$ occurs on gold disk electrode before hydrogen evolution with a well defined reduction wave. Voltammetry and polarization curves are shown in Fig. 7-10. In view of the results for the $Cr(H_2O)_6^{3+}/Cr(H_2O)_6^{2+}$ couple even with the introduction chloride into solution, the inner coordination sphere complexes of chromium with chloride play the major role in the reduction on gold electrode in chromic chloride solution. From a coordination-complex standpoint the binding chloride perturbs the transition-state of the electron-transfer process as well as the initial-state of the chromic complex. From a electrochemical standpoint the bound chloride may adsorb on the electrode surface and participate as a bridging ligand,

thus facilitating the electron transfer.

It was found that the results are not reproducible; currents increase with extended cycles. Probable reason for this is the changing of solution composition with time. The commercially available chromic chloride is assigned the molecular formula $[Cr(H_2O)_4Cl_2]Cl \cdot 2H_2O$. On dissolving this complex in water, however, the metal-bound chlorides are successively replaced by water molecules, giving first blue-green $[Cr(H_2O)_5Cl]Cl_2 H_2O$ and finally violet $[Cr(H_2O)_6]Cl_3$.

With bridging chloride adsorbs on electrode surface to facilitate electron transfer, both $Cr(H_2O)_5Cl^{2+}$ and $Cr(H_2O)_4Cl_2^+$ are electrode active species. Unfortunately their electrode kinetics are not the same making the analysis work difficult. $Cr(H_2O)_5Cl^{2+}$ with its dipositive charge will have a higher concentration in the outer Helmholtz plane than $Cr(H_2O)_4Cl_2^+$ at potentials negative to the potential of zero charge. Beside that, the steric interactions between ligands are unfavorable to $Cr(H_2O)_4Cl^+$ within the double layer. The closest distance of $Cr(H_2O)_5Cl^{2+}$ to electrode surface is therefore shorter than that of $Cr(H_2O)_4Cl_2^+$. Among these components in chromic chloride solution, the $Cr(H_2O)_5Cl^{2+}$ has the fastest kinetics on gold electrode. As time passing after freshly prepared, the $Cr(H_2O)_4Cl_2^+$ loses its bridging chloride producing more $Cr(H_2O)_5Cl^{2+}$ species in solution and therefore the current increases with extended cycles. (Fig. 8).

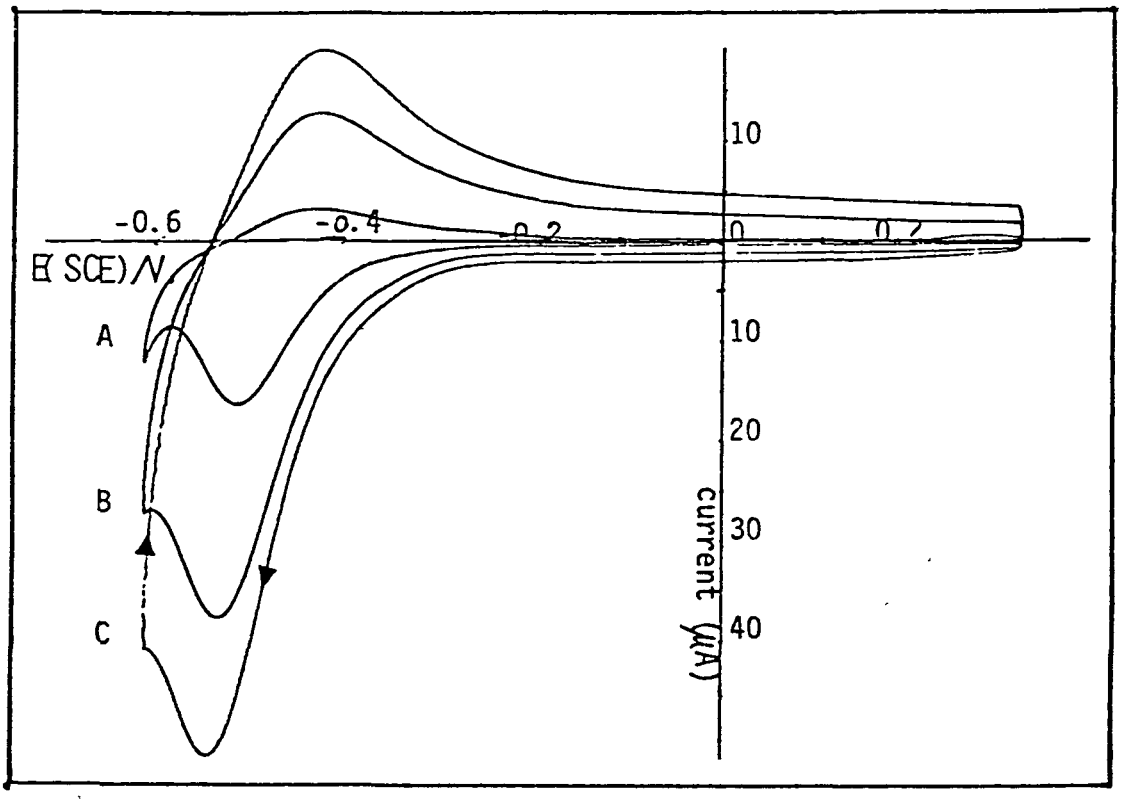

Figure 7: Voltammetry curves for 3mM $CrCl_3$ on gold disk electrode. Electrolyte: 0.1M $NaClO_4$ and 0.01M $HClO_4$. Electrode area: 0.2 cm^2. Sweep rate: A. 10mV/s B. 50mV/s C. 100mV/s.

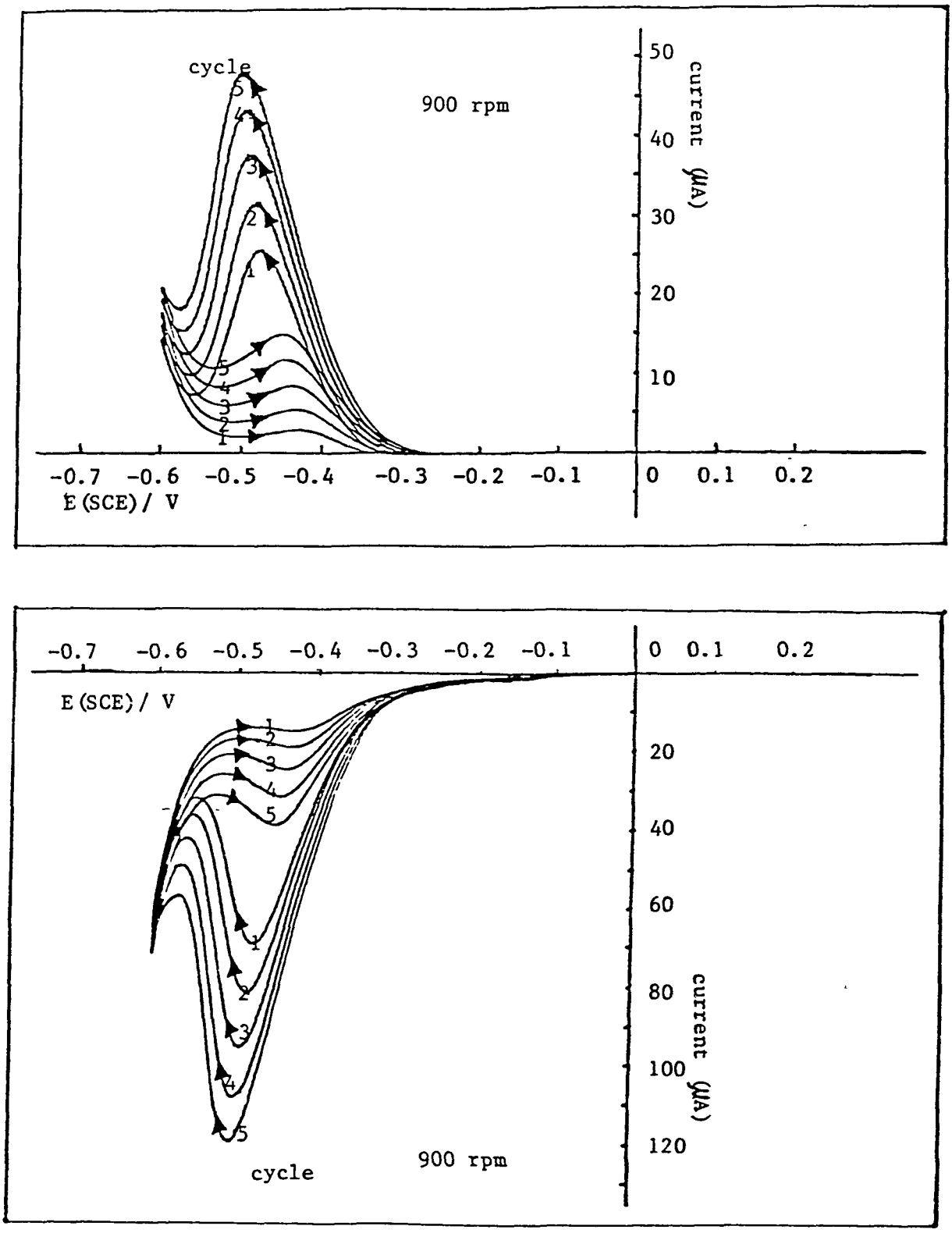

Figure 8: Polarization curves for reduction of freshly prepared $CrCl_3$ on gold ring-disk electrode. Ring potential: 0.6V. Rotation rate: 900 rpm. Sweep rate: 10mV/s. Solution: 3mM $CrCl_3$ in 0.1M $NaClO_4$ and 0.1M $HClO_4$.

Large hyteresis of $CrCl_3$ reduction on gold surface under convection was observed. (Fig. 8-10). The I-E curves do not level off at cathodic potentials, -0.57V vs. SCE, where the reduction processes are under pure diffusion control. Before the potential of hydrogen evolution, the currents decrease quickly even during the back scan of potential. A re-enhanced current occurs during back scan at the same potential where current changes dramatically during forward scan. The turnover of current occurs at -0.57V vs. SCE., which is independent of the rotation rate. (Fig. 10). This phenomenon is probably associated with the inner-sphere mechanism in which the bridging chloride adsorbs on the gold surface. At potentials negative to -0.57V vs. SCE. the bridging chloride de-adsorbs from the electrode surface. Therefore the orientation of the oxidized species on gold surface changes with the water ligand directing toward the electrode. Because of the slowness of the electron transfer with the water ligand compared with the chloride ligand, the electrode kinetics slow down at these potentials. The re-enhancement of currents during back scan is due to the re-adsorption of bridging chloride, as is shown below:

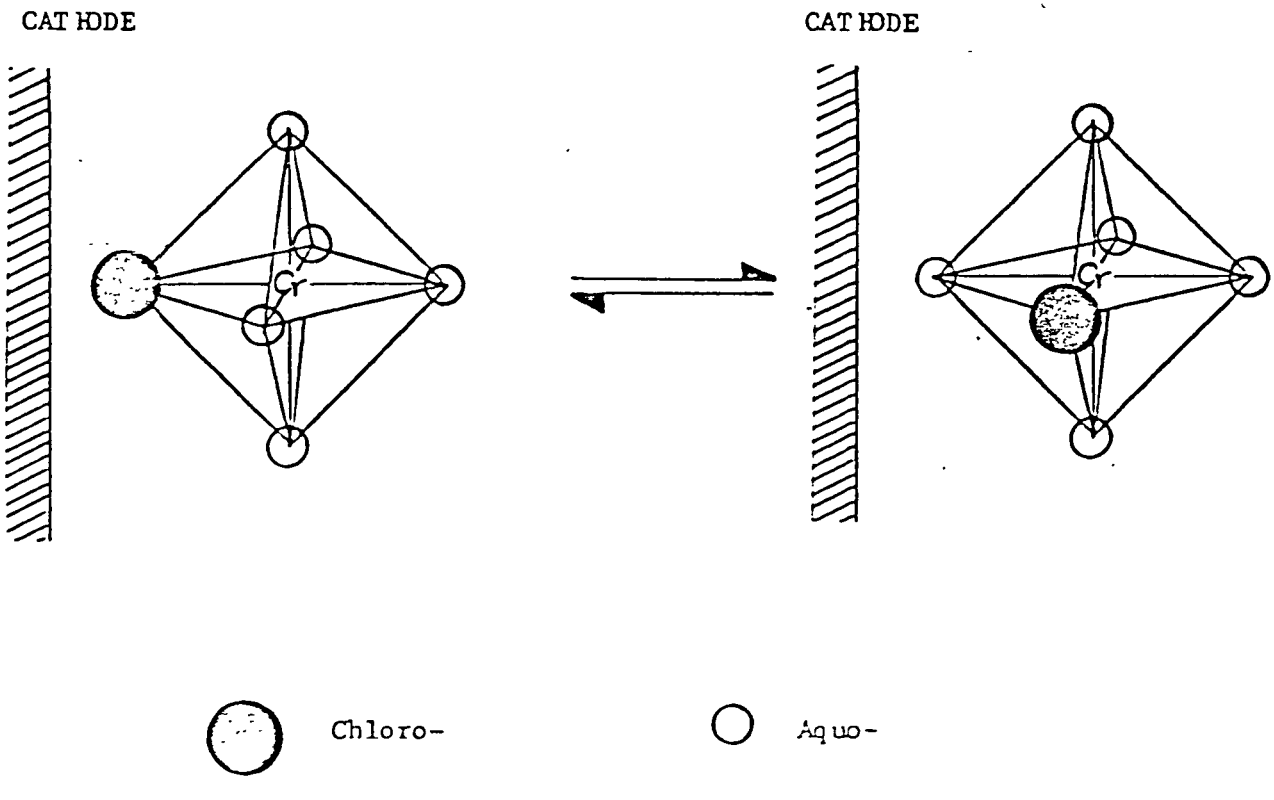

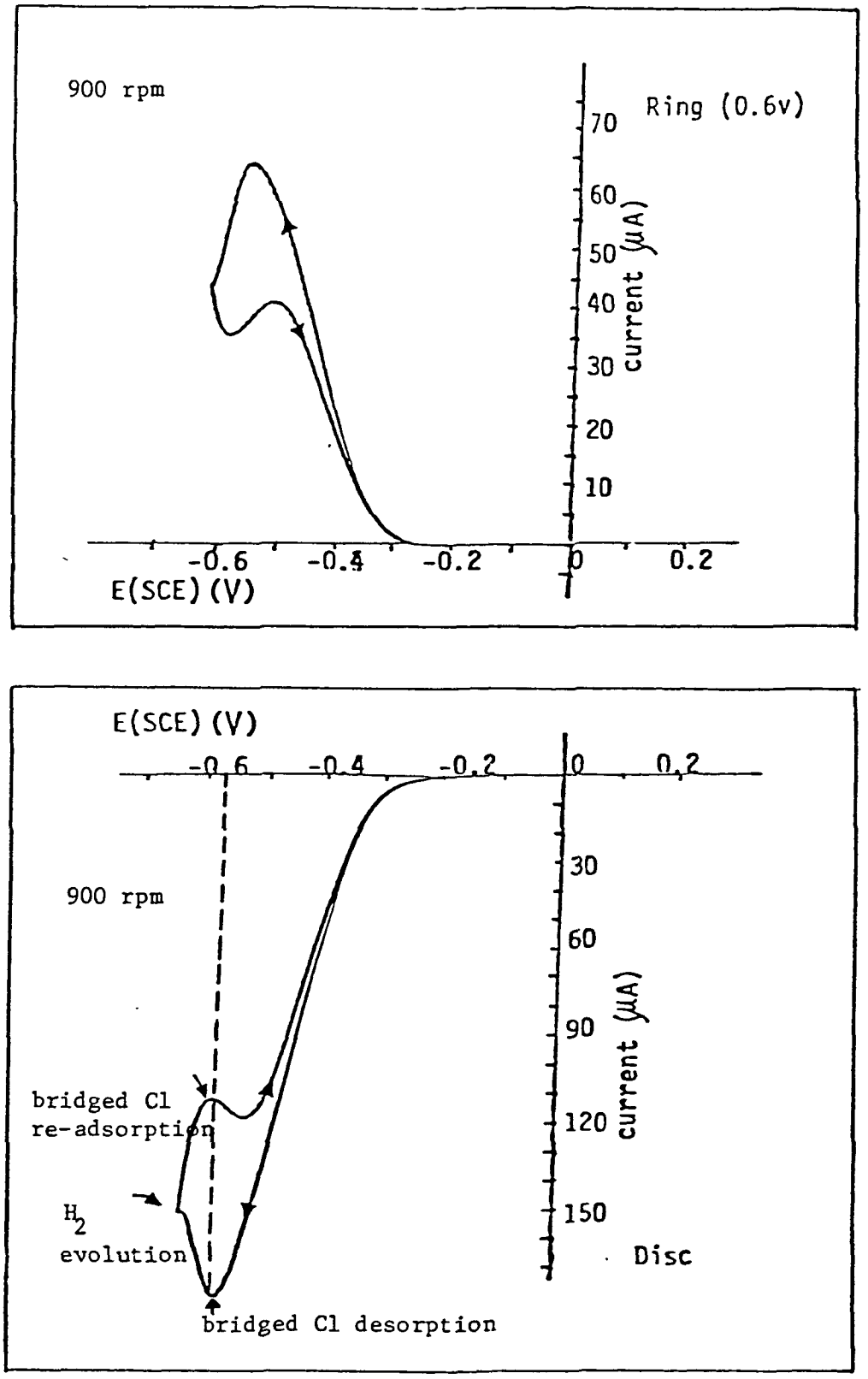

Figure 9: Polarization curve for reduction of $CrCl_3$ on gold ring-disk electrode. Ring potential: 0.6V. Rotation rate: 900 rpm. Sweep rate: 10mV/s. Solution: 3mM $CrCl_3$ in 0.1M $NaClO_4$ and 0.01M $HClO_4$.

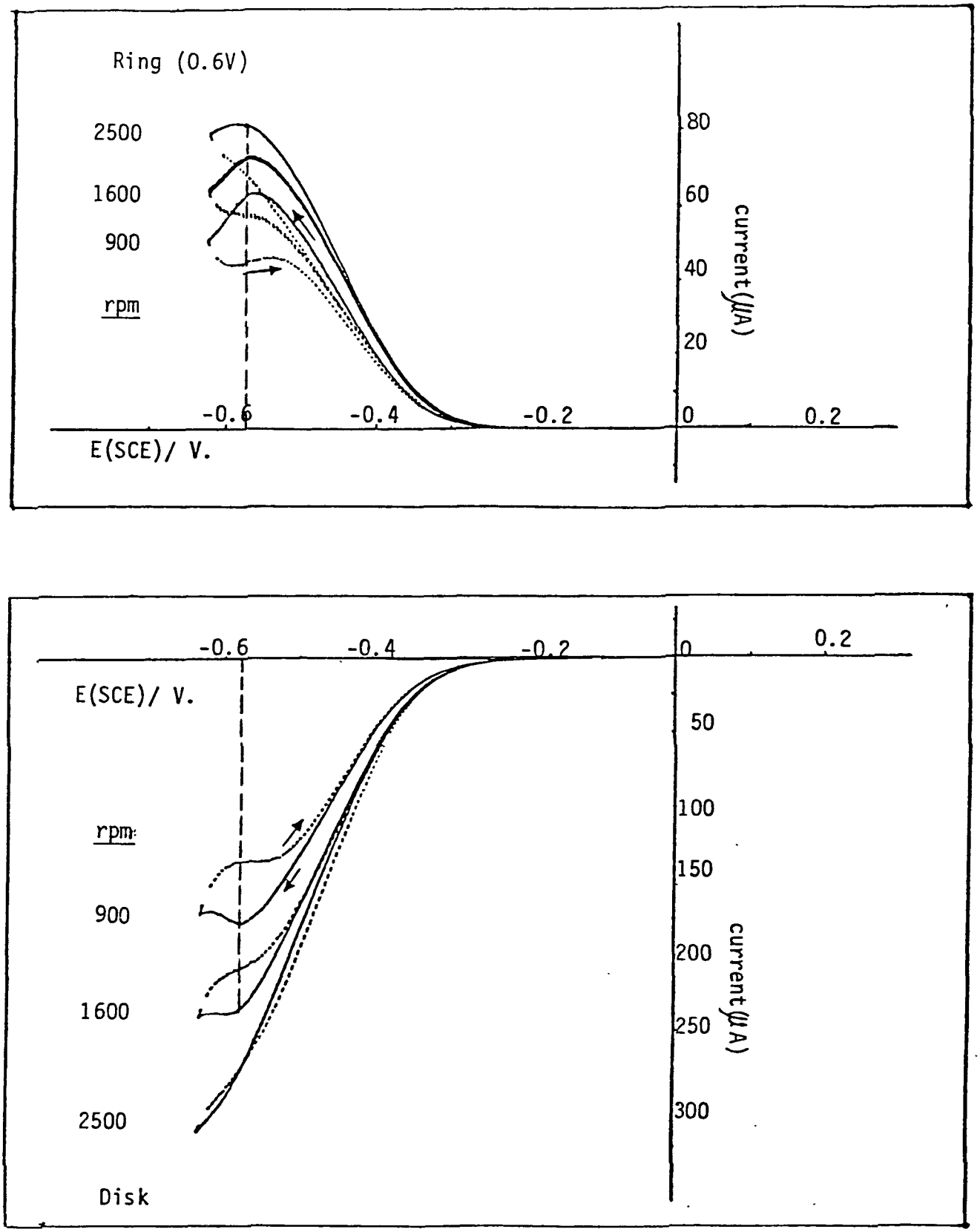

Figure 10: Polarization curves for chromic chloride reduction on rotating gold ring-disk electrode in acid media. Solution: 3mM $CrCl_3$ in 0.1 M $NaClO_4$, 0.01 M $HClO_4$. Sweep rate: 10 mv/s. Electrode area: 0.20 cm^2, Rotation rates as specified.

B. Lead/Gold System

i). Deposition and Stripping of Lead on Gold Electrode

The role of lead on gold surface is important in the understanding of the kinetics of chromium(II)/(III) couple. Underpotential deposition as well as the bulk deposition and stripping of lead on crystalline gold electrode have been studied in perchloric acid.

The effect of lead on the kinetics of the chromic reduction can be studied by rotating ring-disk electrode technique. Cr(II) which is reduced at the disk can be reoxidized to Cr(III) at the ring. The ring potential is fixed at such a positive value (0.6V vs. SCE) that the reoxidation of Cr(II) occurs under pure diffusion control. Because no lead deposition occurs at the ring, the ring currents are totally due to the oxidation of Cr(II) to Cr(III).

It was found that the underpotential deposition of lead on gold disk results in a net decrease of the reaction kinetics as compared with that on the bare metal. This effect is probably principally associated with a double layer effect. The UPD lead species with its positive charge results in a decrease in the concentration of the Cr(III) species at the electrode surface (in the outer Helmholtz plane).

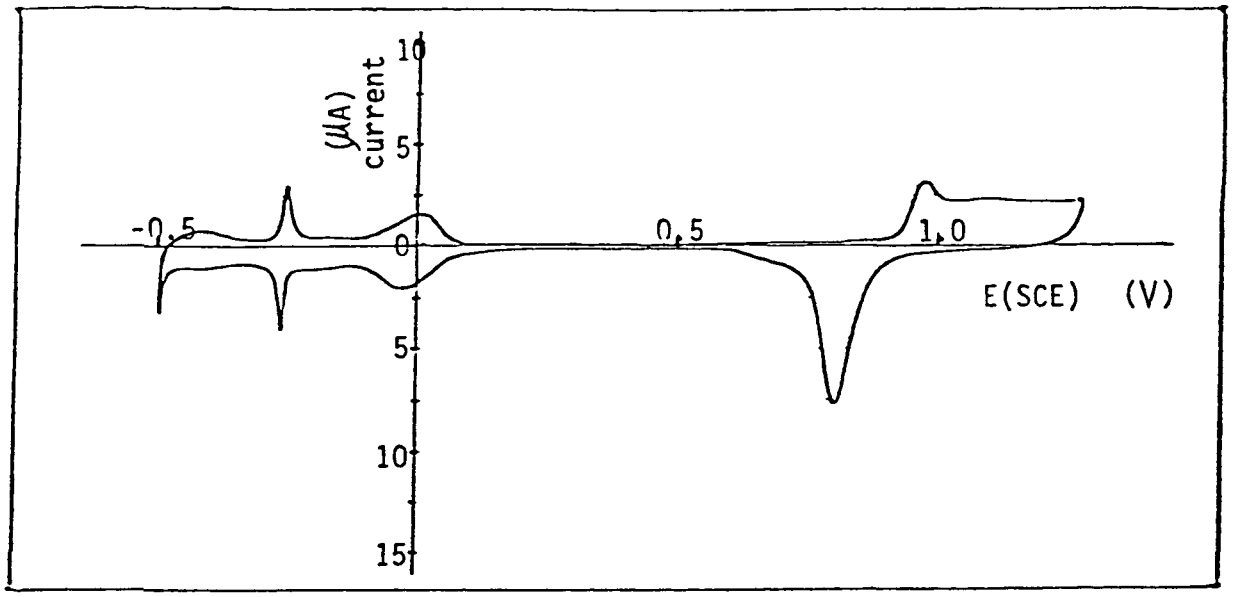

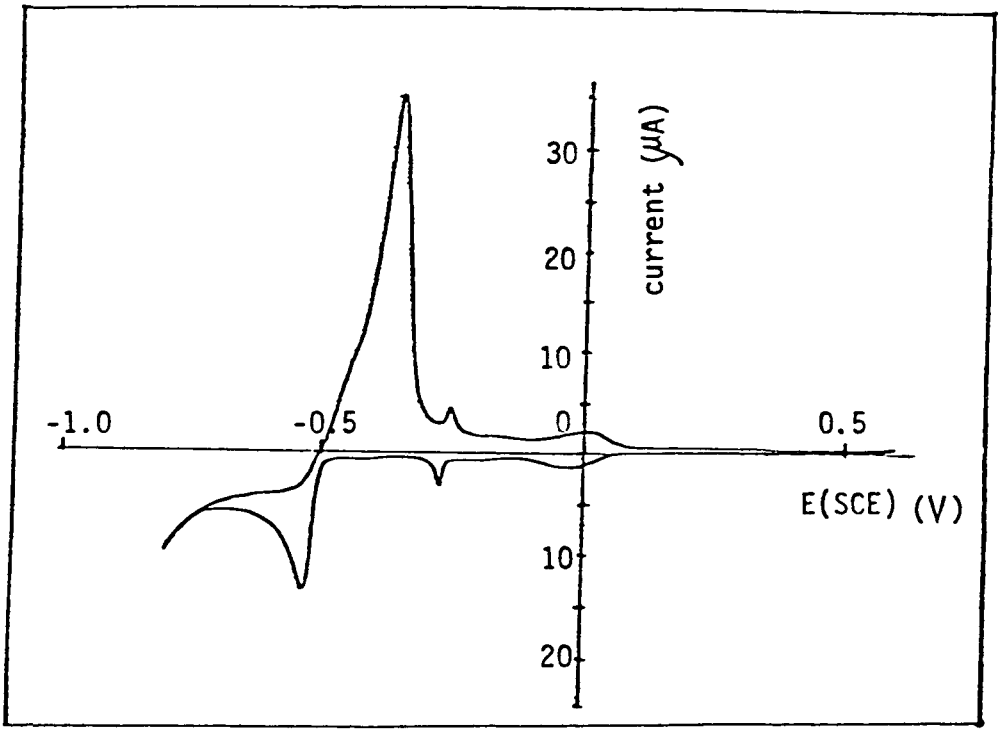

FIGURE 11: UNDERPOTENTIAL DEPOSITION OF LEAD ON GOLD ELECTRODE. SOLUTION: 0.3 mM $Pb(NO_3)_2$ IN 0.01 M $HClO_4$, 0.1 M $NaClO_4$. SCAN RATE: 10 mV/s. ELECTRODE AREA: $\sim$ 0.2 cm^2. STAGNANT SOLUTION.

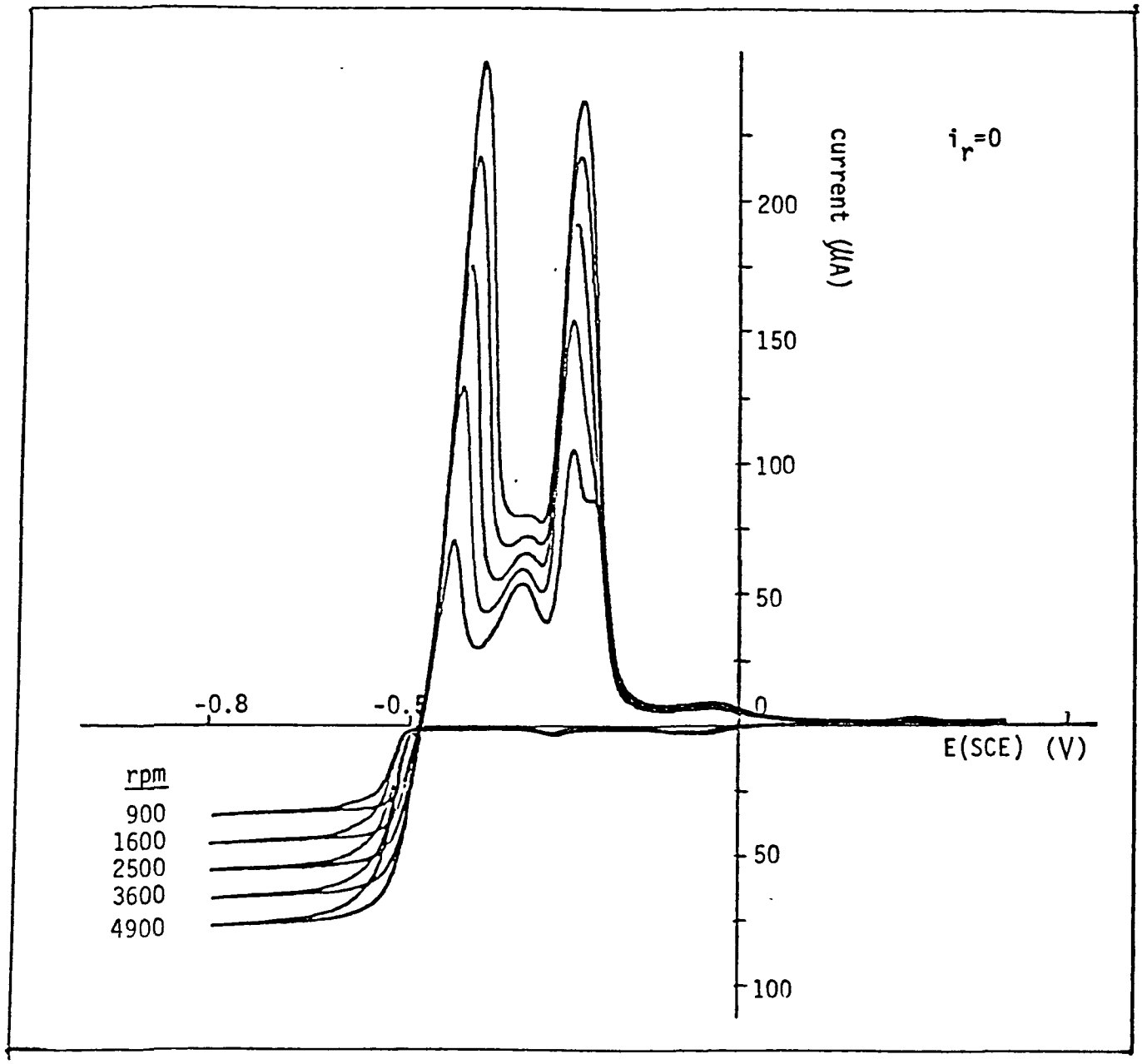

FIGURE 12: SAME AS FIG. 11 WITH ELECTRODE UNDER ROTATION. ROTATION RATES AS SPECIFIED.

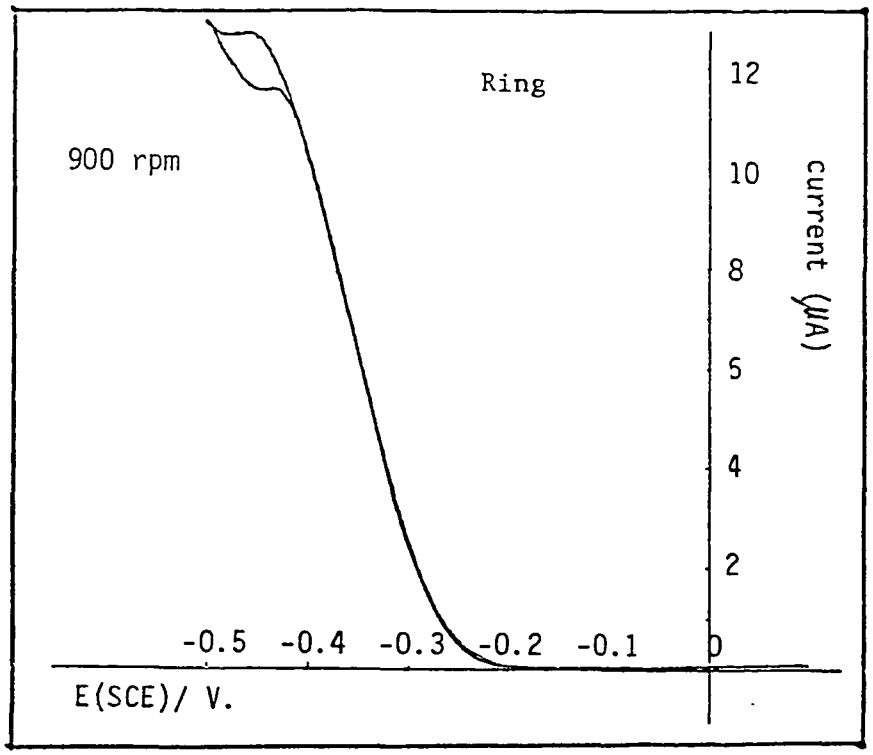

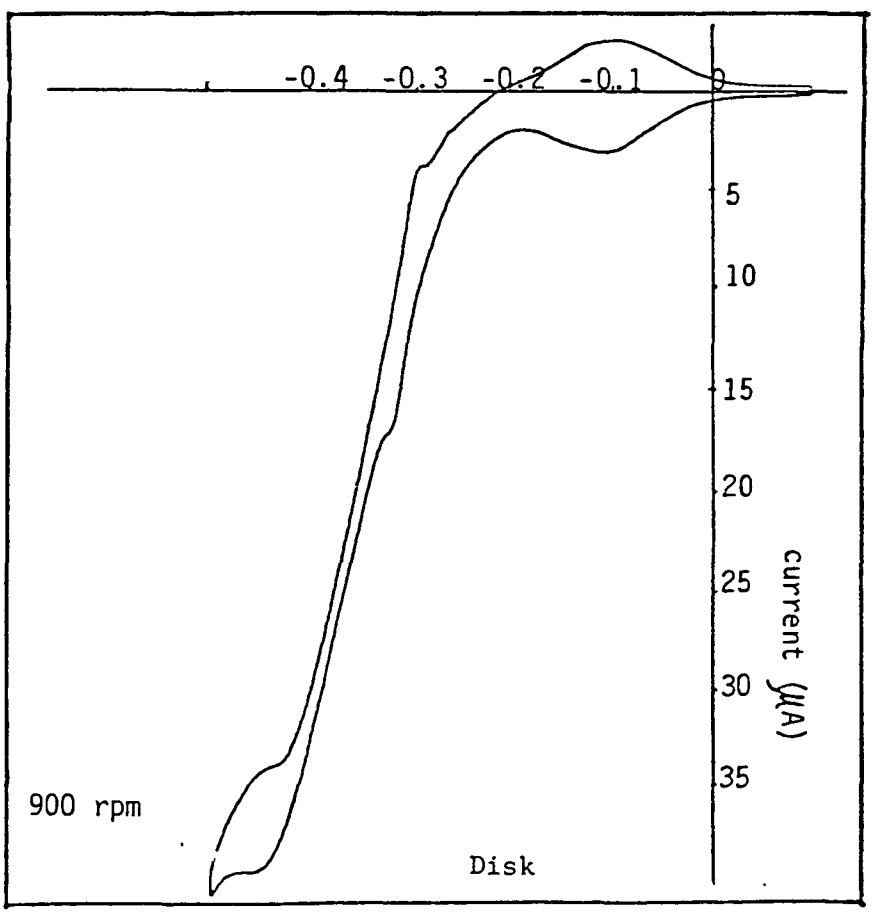

Figure 13: Polarization curves for chromic chloride reduction on rotating gold ring-disk electrode. Solution: 3 mM $CrCl_3$ in o.1 M $HClO_4$ $6 \cdot 10^{-6}$ M PbO. Sweep rate: 10 mV/s. Electrode area: 0.2 cm^2. Ring potential: 0.6V vs. SCE.

ii). Potential Step Experiments

In order to study the transient behavior of UPD and the transient effect of UPD on redox couple, controlled potential step experiments have been arranged. The working electrode potential is initially set to a known constant value where no Faradaic processes occur, and then stepped to a potential at which the kinetics are of interest. The current which is the response of the system to the step perturbation is measured as a function of time. The waveform applied in a series of potential step experiments are depicted in Fig. 14.

These experiments of UPD phenomenon studies involve polarizing a rotating gold disk electrode at a potential where UPD does not occur and then stepping the potential to a value where UPD occurs. Under these conditions with a low bulk concentration of the UPD species, the deposition of the UPD layer occurs very slowly under pure diffusion control. (Fig. 15). The coverage of the UPD layer can then be calculated as a function of time from the diffusion flux. (Fig. 17-18). With the redox couple also present, the dependence of the rate of the couple reduction on the UPD coverage can be determined from the time dependence of the couple reduction current. (Fig. 19-21). Figure 19 shows the current vs. time curves for simultaneous underpotential deposition of lead and chromic chloride reduction on gold rotating ring-disk electrode upon potential step from 0.6V vs. SCE. into specificed potential. The curve of time-depended ring current which totally results from the oxidation of Cr(II) has the same shapes as those of disk current at constant potential. Steady state currents are observed after 40 seconds with electrodes under 900 rpm rotation.

The time dependence of the chromic chloride reduction current with both Pb^{2+} and Cl^- presence in solution is shown in Figure 24.

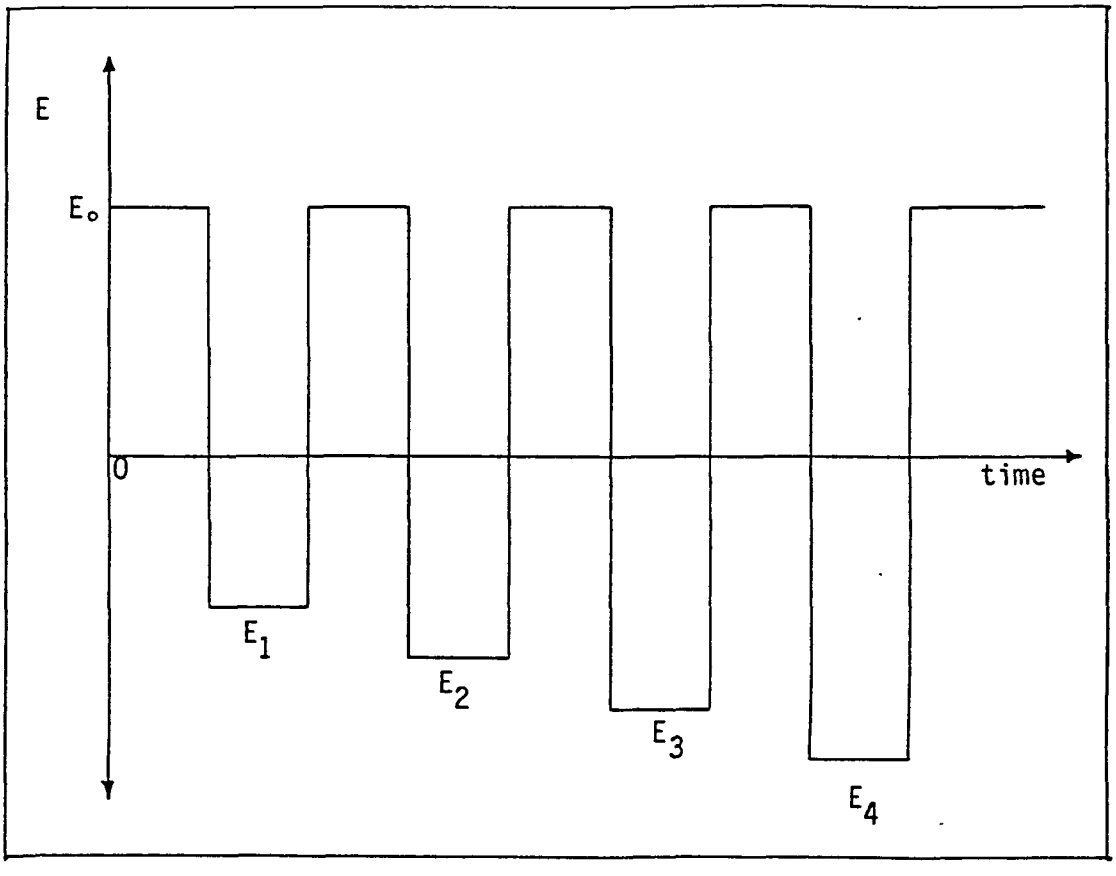

Figure 14: Step waveforms applied in a series of experiments.

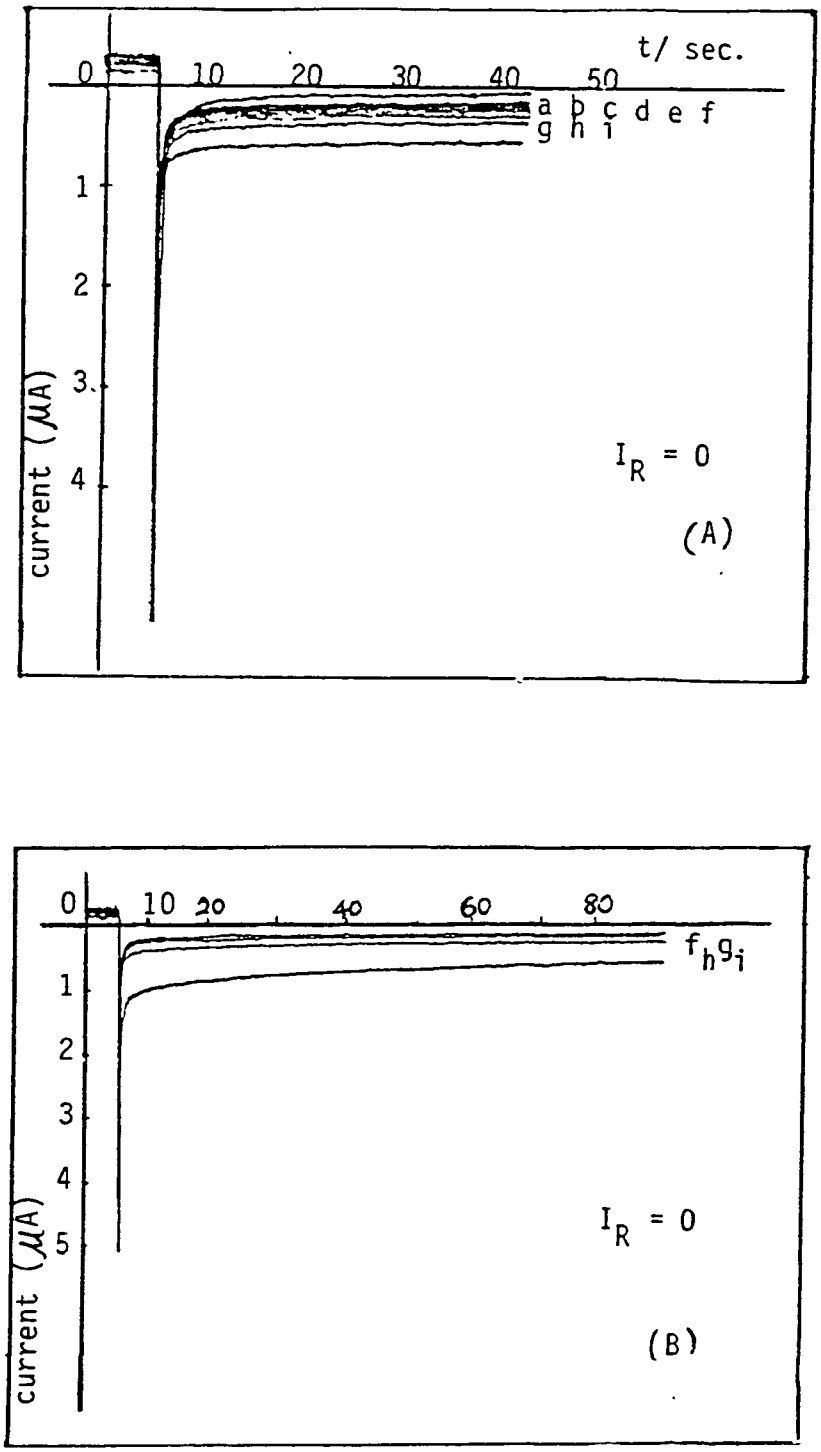

Figure 15: Disk current vs. Time curves for gold rotating ring-disk electrode in 0.1 M $HClO_4$ in absence of Cr(III) and Pb(II). Potential step from 0.6V into indicated potential. Rotation rate: 900 rpm. A. No NaCl B. with addition of 3mM NaCl. a, b, c, d, e, f, g, h, i are same as in figure 16.

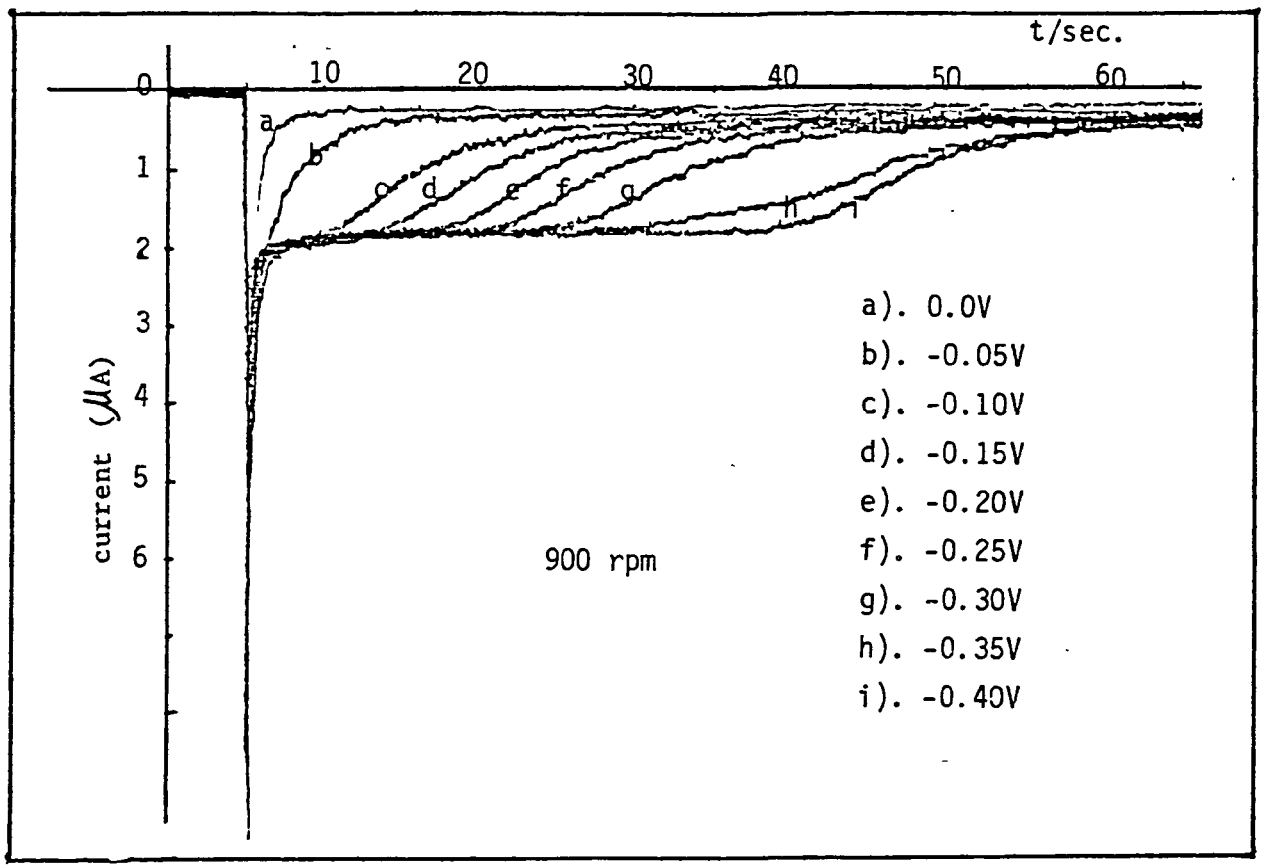

Figure 16: Current vs. Time curves for rotating gold ring-disk electrode in a solution containing 0.1 M $NaClO_4$, 0.01 M $HClO_4$ and $6 \cdot 10^{-6}$ M PbO upon potential step from 0.6V into indicated potential. Rotation rate: 900 rpm, $I_R = 0$.

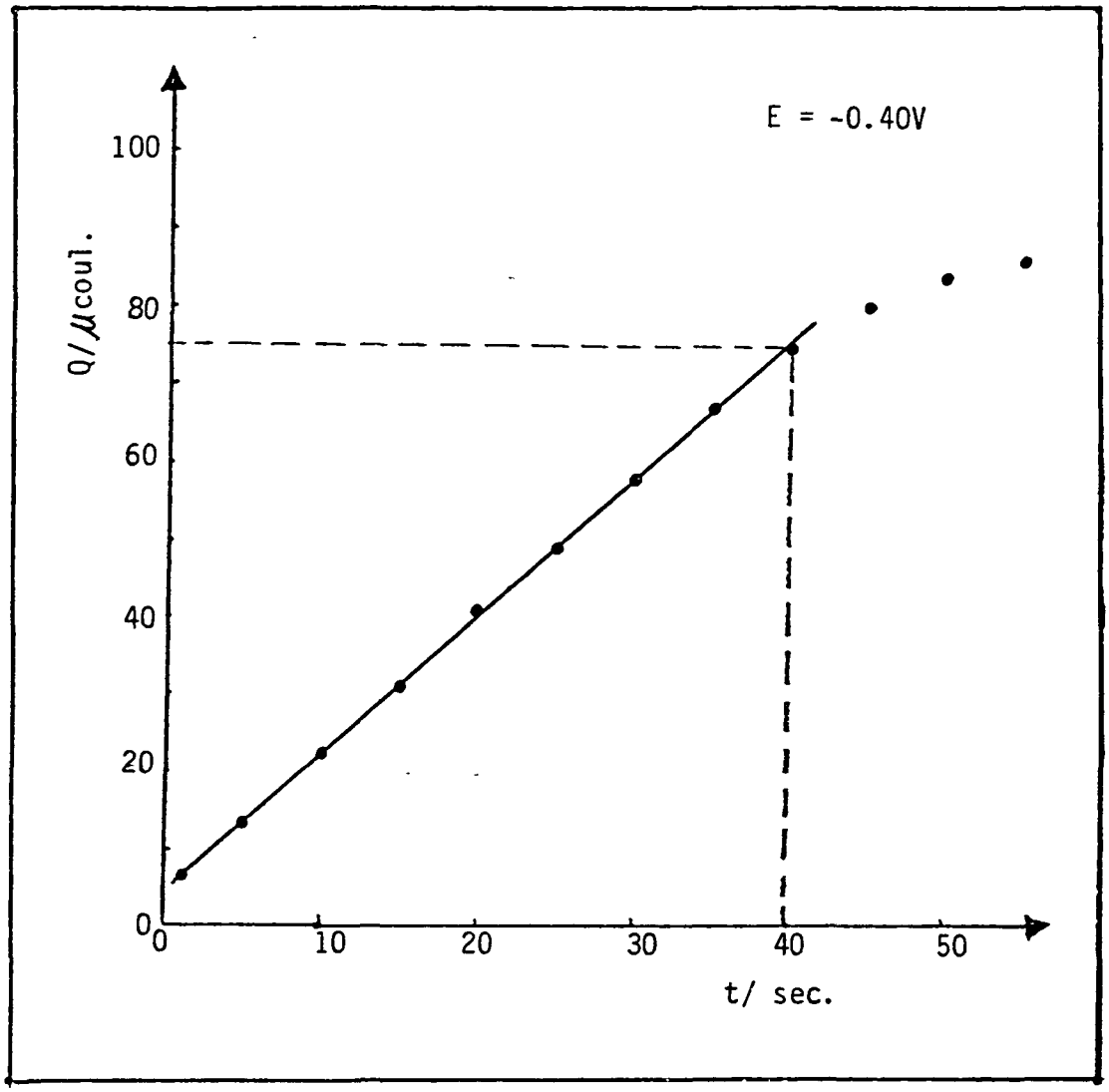

Figure 17: Charge vs. Time curve for underpotential deposition of Lead on gold at fixed applied potential. Data taken from Fig. 16.

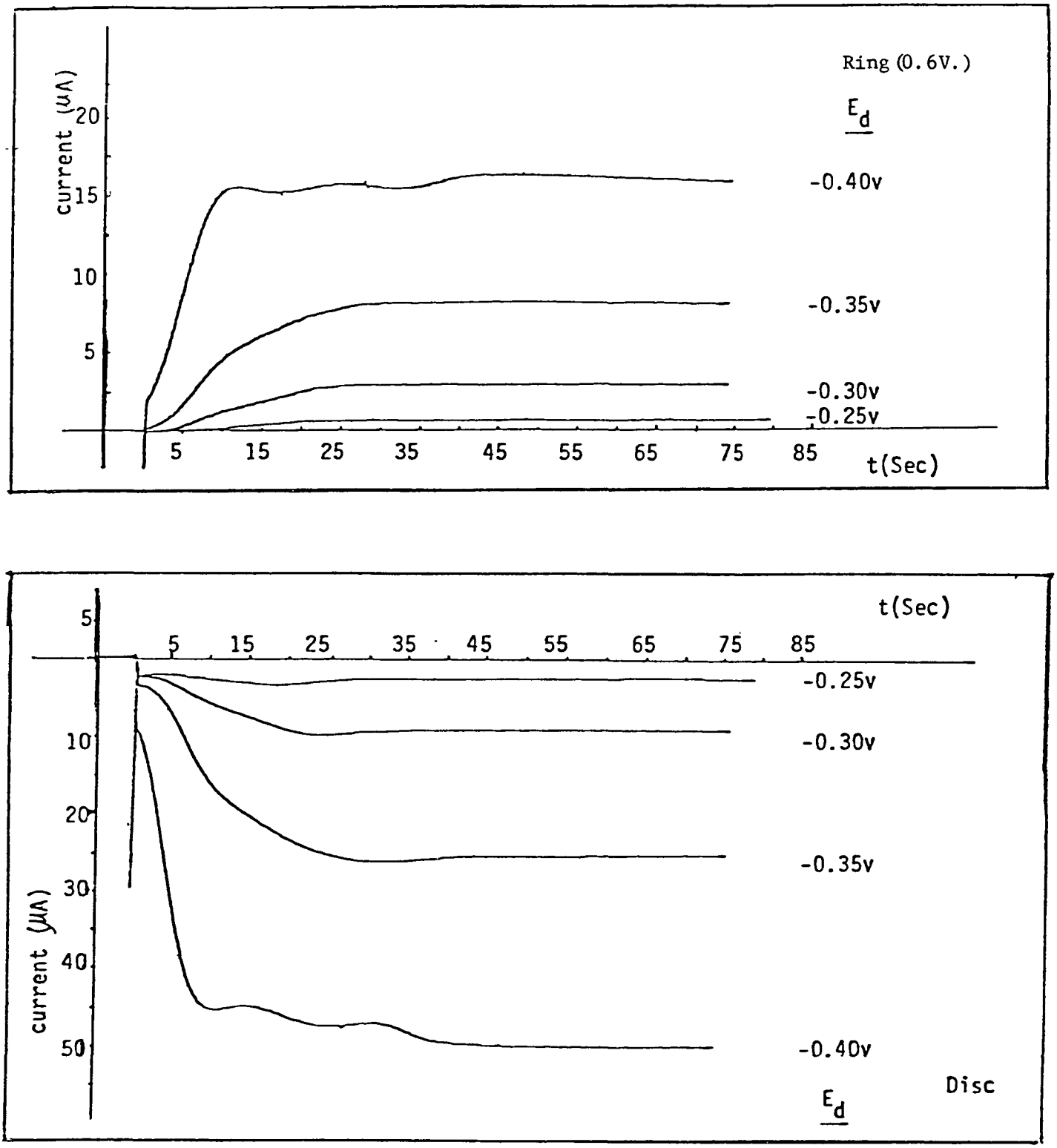

Figure 18: Current vs. Time curves for simultaneous underpotential deposition of lead and chromic chloride reduction on gold rotating ring-disk electrode upon potential step from 0.6V into indicated potential. Solution: 3 mM $CrCl_3$, 6.10^{-6} M PbO in 0.1 M $NaClO_4$ and 0.01 M $HClO_4$. Rotation rate: 900 rpm. Ring potential: 0.6V vs. SCE. Electrode area: 0.2 cm^2.

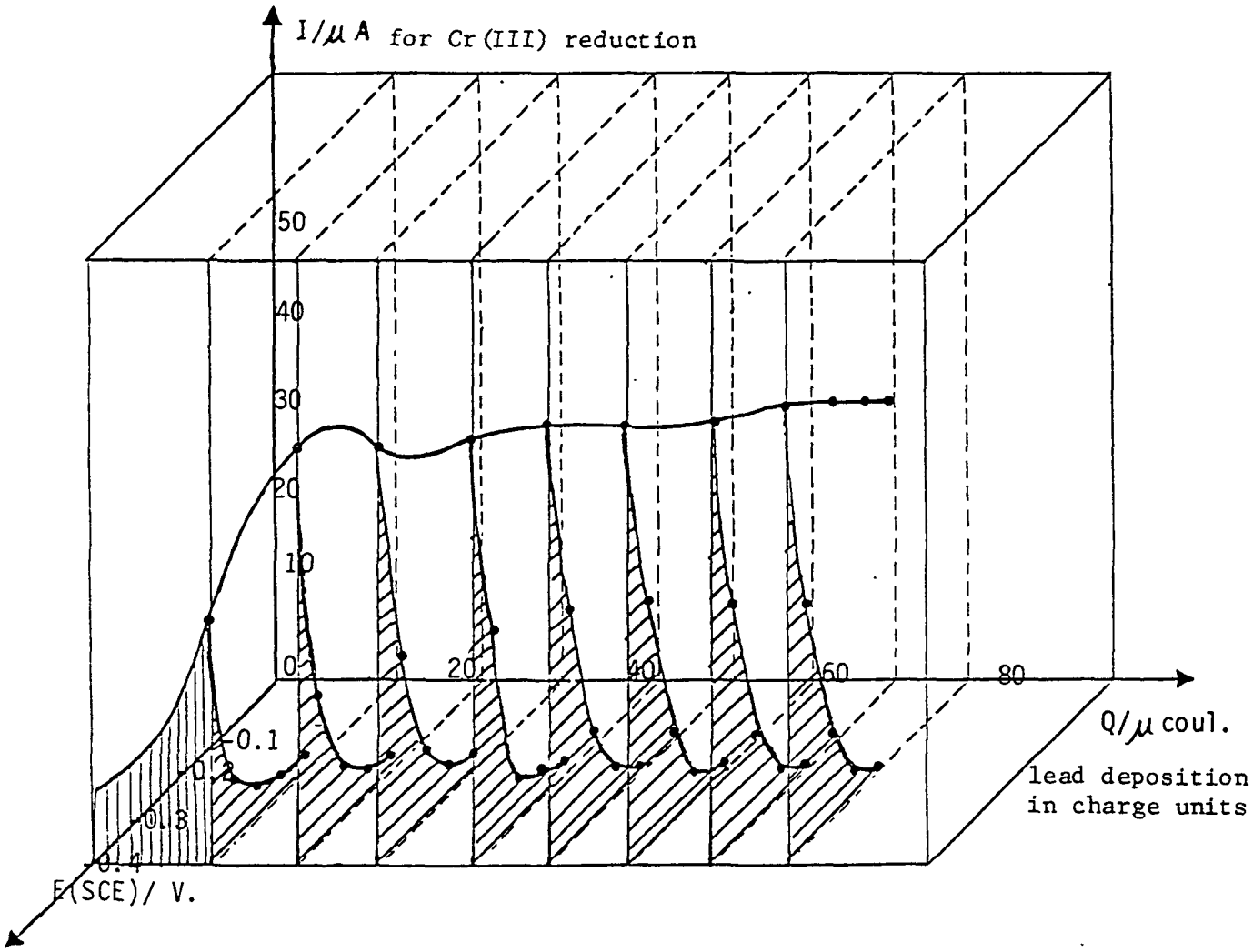

Figure 19: Three dimensional representation of current vs. potential and charge of UPD. Data from figure 16, 18.

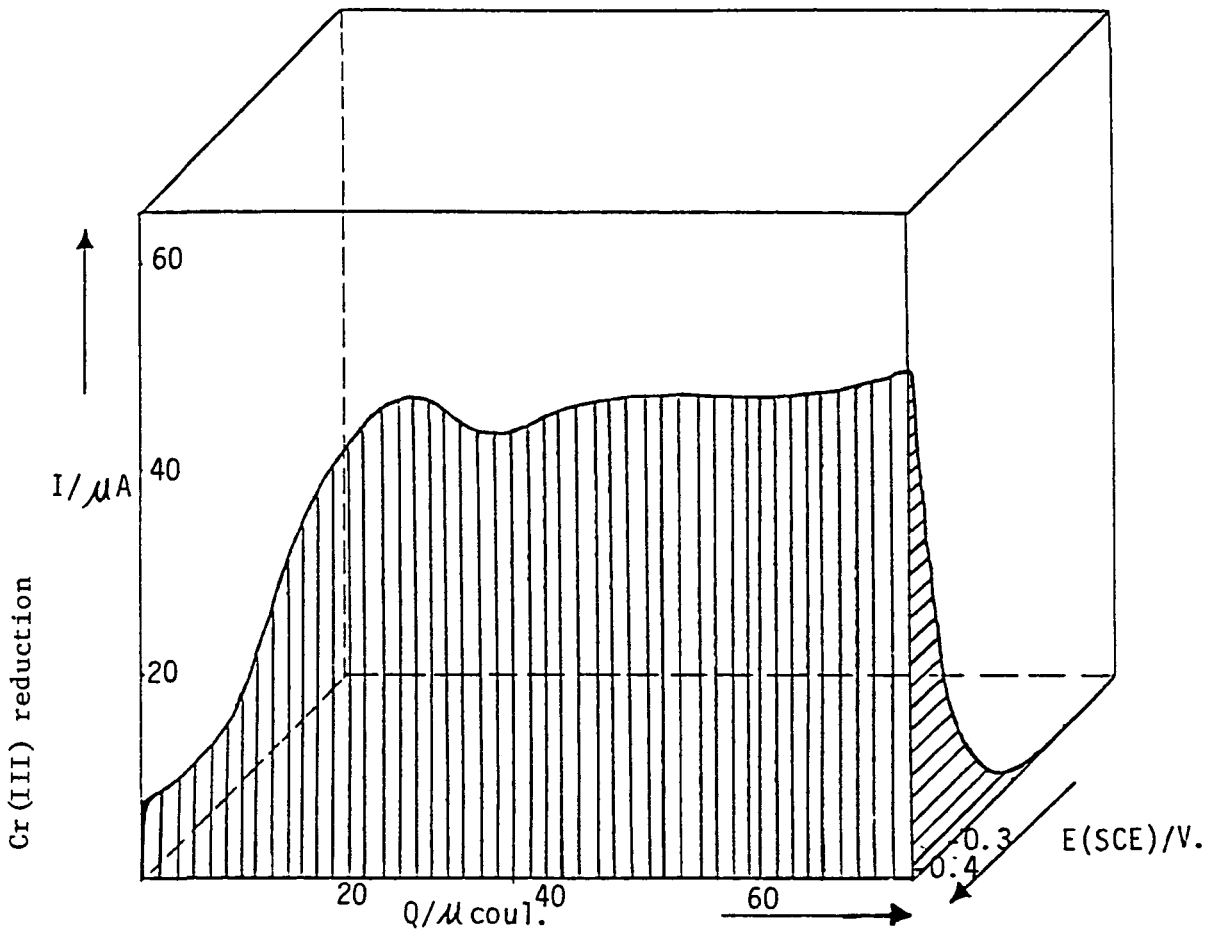

Figure 20: Same as figure 19, at Q = 74.3 μcoul., E = -0.40V

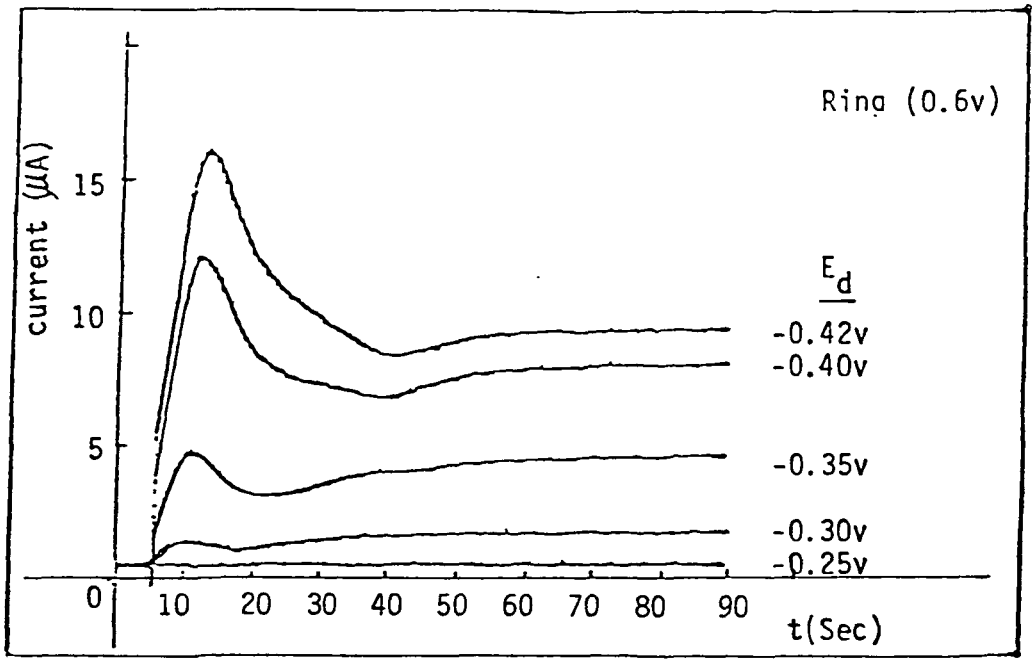

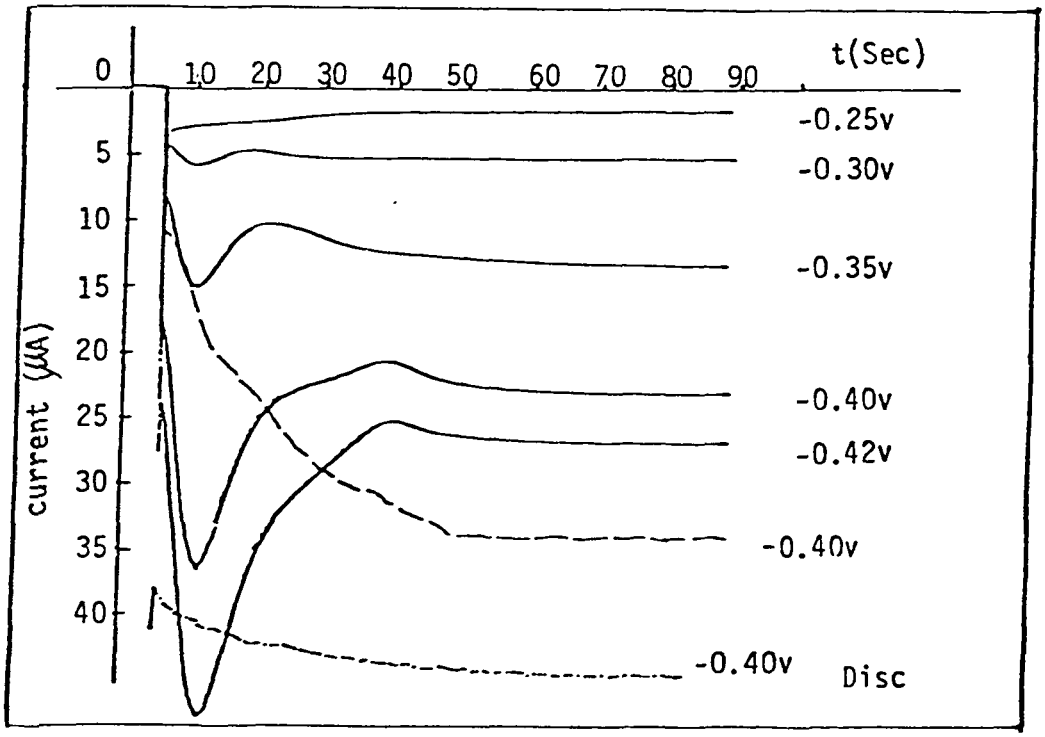

Figure 21: Current vs. Time curves for the simultaneous underpotential deposition of lead and chromic chloride reduction on a rotating ring-disk Au electrode upon potential step from 0.6V into indicated potential. Solution: 3mM $CrCl_3$ in 0.1 M $HClO_4$ and, ——— 6.10^{-6} M PbO + 3mM NaCl, - - - - - - 6.10^{-6} M PbO, ····· 3mM NaCl.
Rotation rate: 900 rpm.

The rotation dependences of the transient behavior for simultaneous underpotential deposition of lead and chromic chloride reduction on the gold disk electrode at constant potential are shown in figure 22-23. The time required to reach steady state decreases with rotation rate.

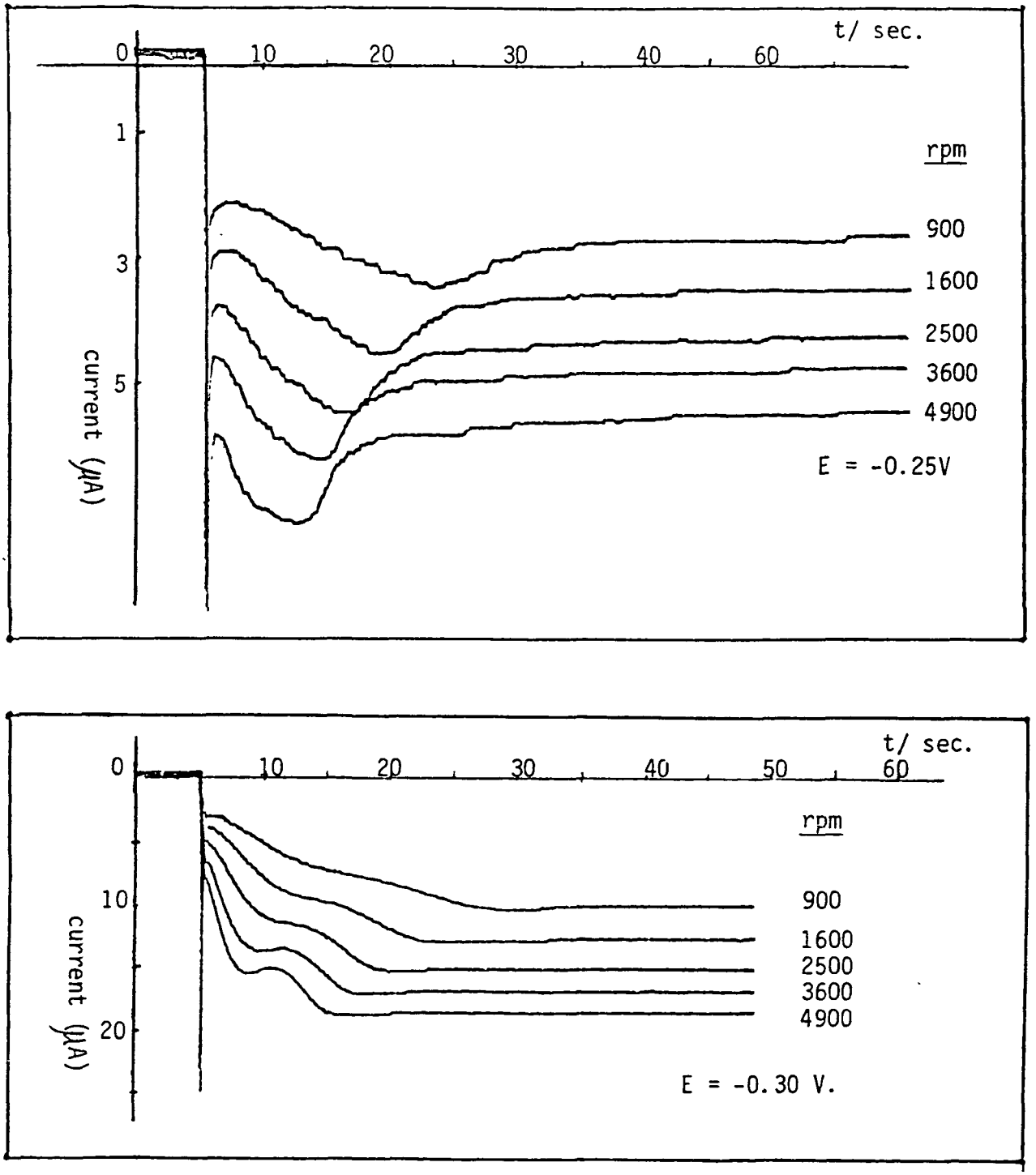

Figure 22: Disk current vs. Time curves for simultaneous underpotential deposition of lead and chromic chloride reduction on gold electrode with rotation rates change as indicated. Potential step from 0.6V into indicated potential. Solution: 3mM $CrCl_3$, $6 \cdot 10^{-6}$M PbO in 0.1 M $NaClO_4$ and 0.01M $HClO_4$.

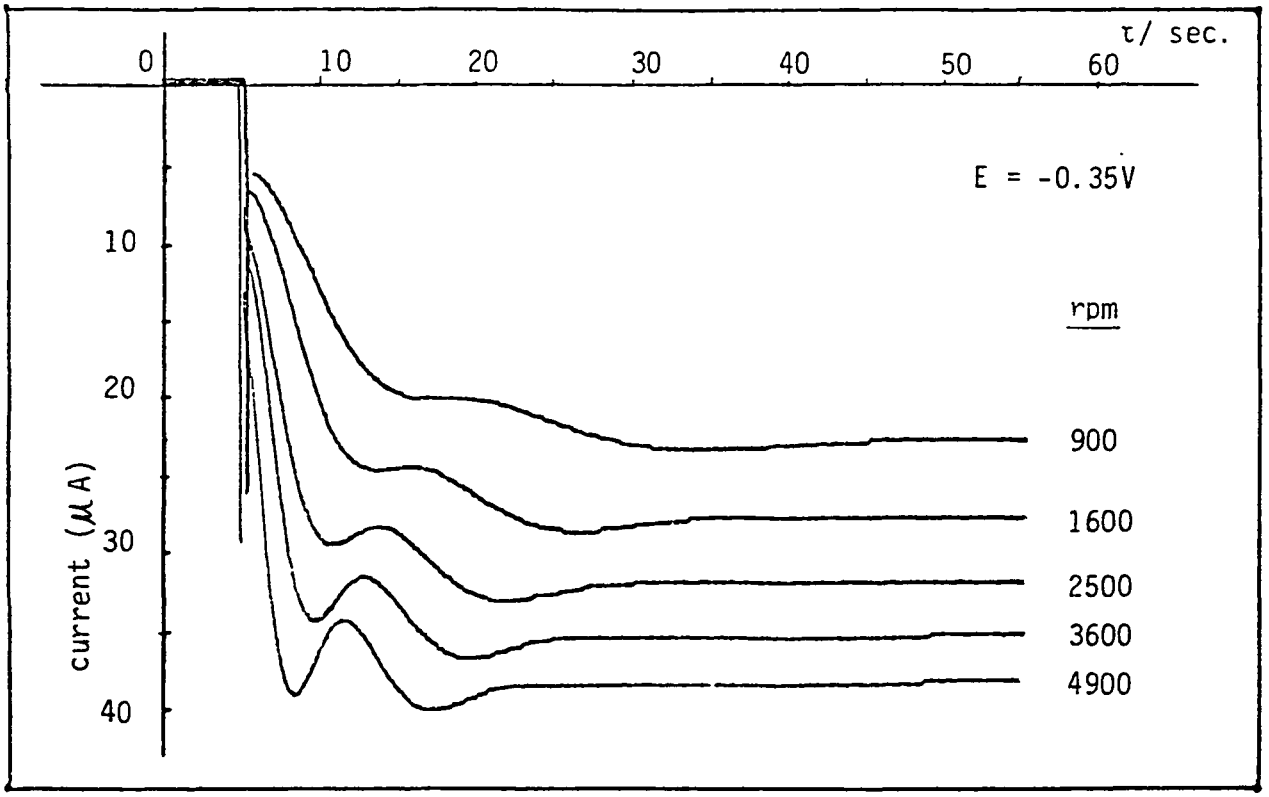

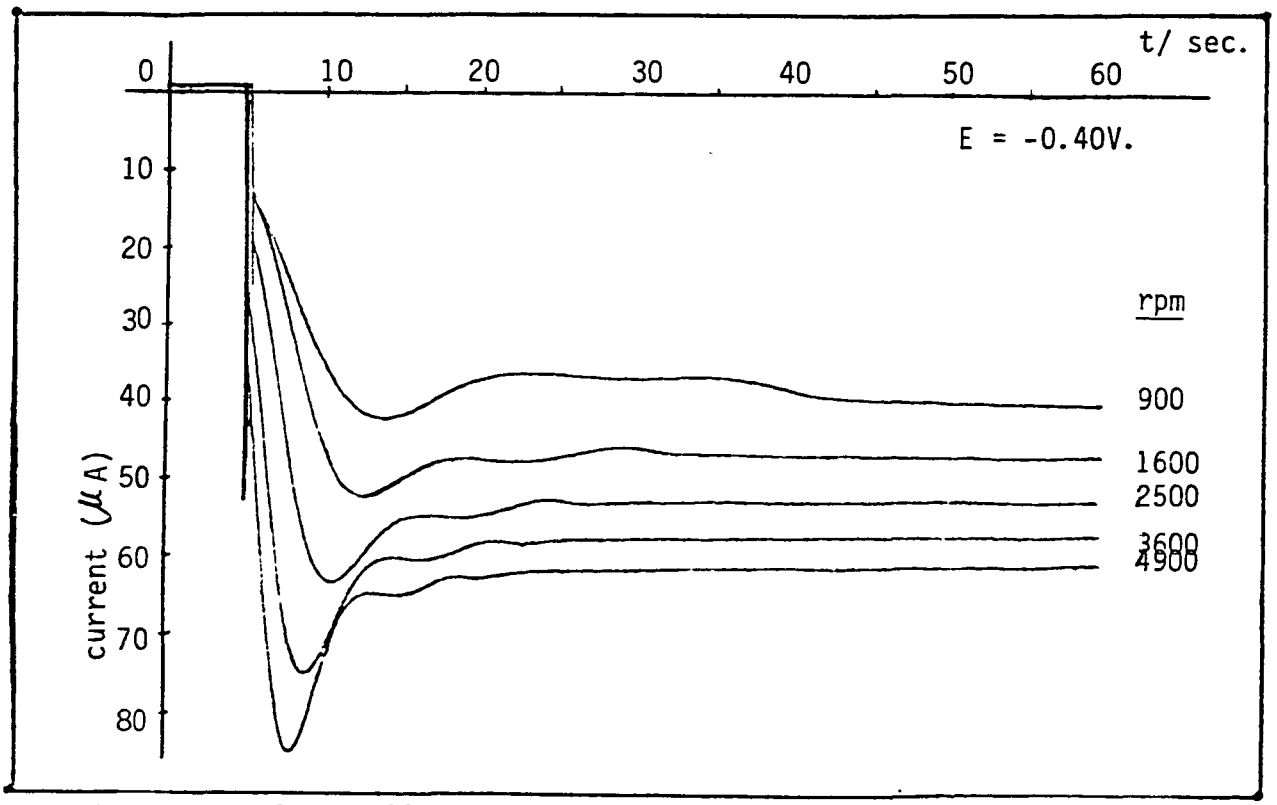

Figure 23: Same as figure 22.

C. Ordinary Pyrolytic Graphite

With lead deposited on graphite surface to prevent hydrogen evolution, both reduction and oxidation of chromic chloride couple occur on graphite electrode. Cyclic voltammogram shows two new waves for the reduction and oxidation of chromium couple. (Fig. 24)

The plating of lead on ordinary pyrolytic graphite rotating disk electrode was also investigated in the past period. Further studies are still going on.

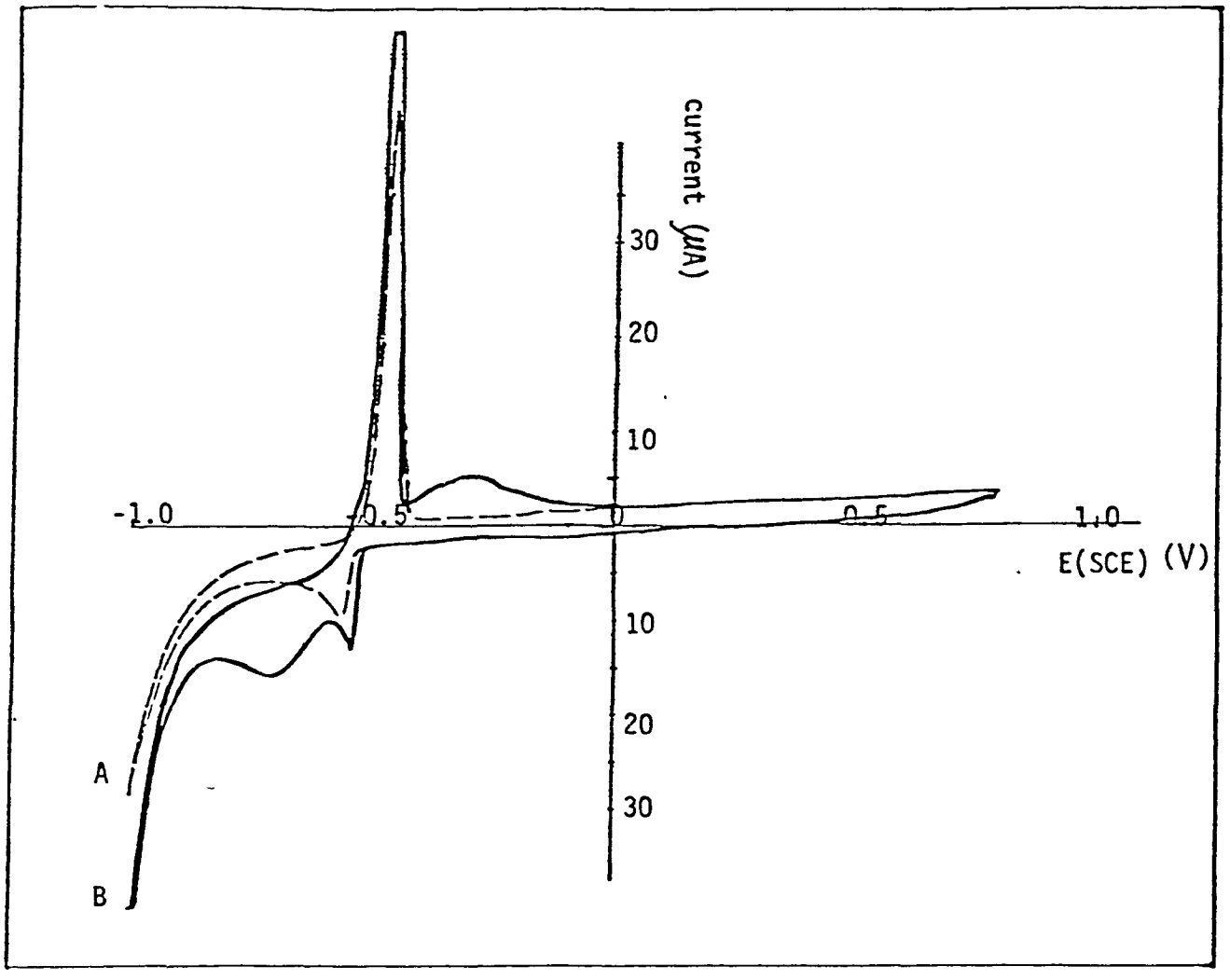

Figure 24: Cyclic voltammogram of ordinary pyrolytic graphite disk electrode in a solution containing 0.1 M $NaClO_4$, 0.01 M $HClO_4$ and 3 mM $Pb(NO_3)_2$. Sweep rate: 10 mV/s. A). No $CrCl_3$ B). with 6mM $CrCl_3$.

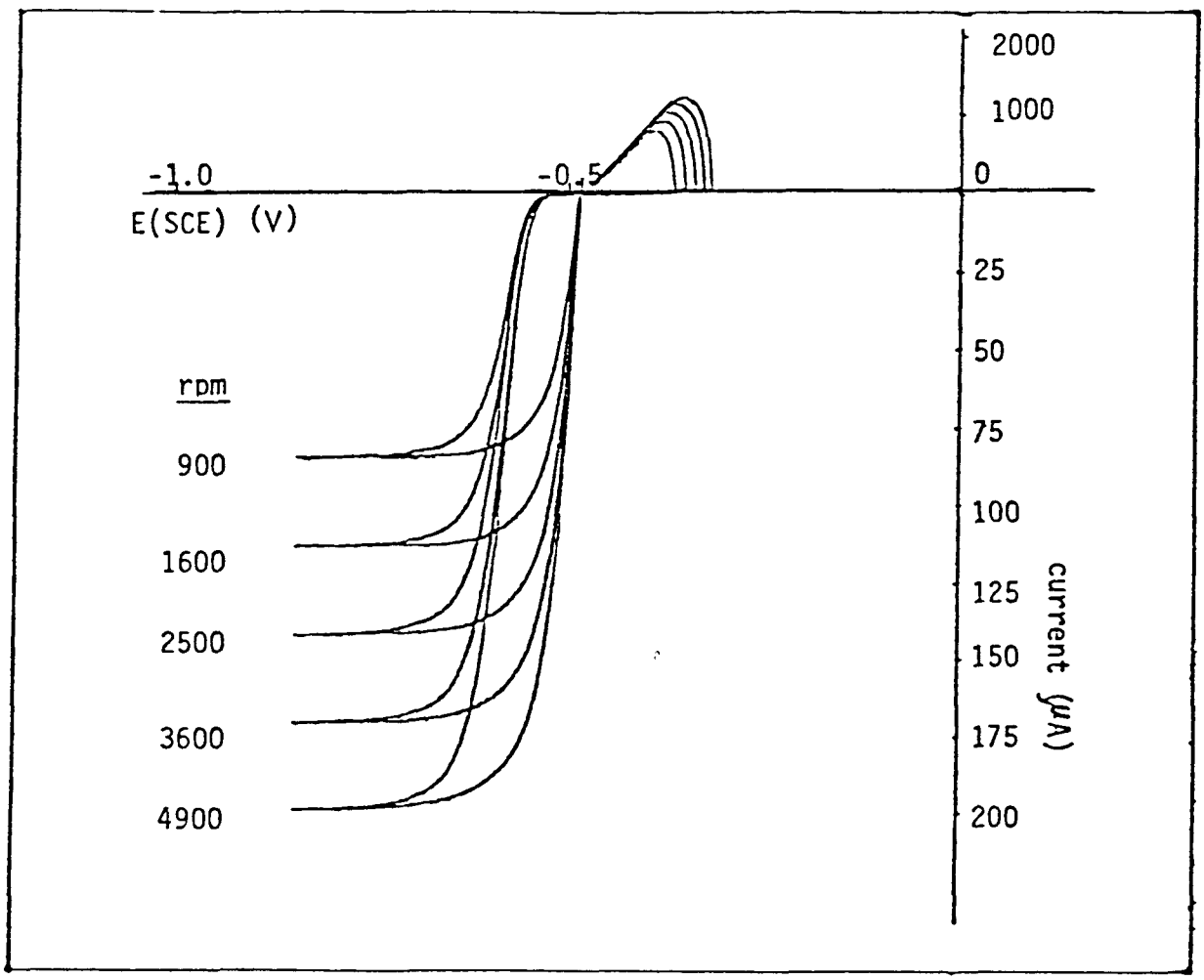

Figure 25: Polarization curve for lead deposition and stripping on ordinary pyrolytic graphite rotating disk electrode. Electrode area: 0.2cm^2. Solution: 0.1 M $NaClO_4$, 0.01 M $HClO_4$ and 3 mM PbO. Sweep rate: 10mV/s. Note: change in ordinate for anodic vs. cathodic curves.

3. $Fe(H_2O)_6^{3+}/Fe(H_2O)_6^{2+}$ Couple, Gold Ring-Disk Studies in Acid Media

The kinetics of the $Fe(H_2O)_6^{3+}/Fe(H_2O)_6^{2+}$ couple were studied on a gold rotating disk electrode in 0.5 M $HClO_4$ solution. Without anions other than the ClO_4^- of the supporting electrolyte, moderate electrode kinetics have been observed. It was found that the process is very sensitive to the surface condition; trace concentrations of impurities made the results unreproducible. The cyclic voltammogram and polarization curve of $Fe(H_2O)_6^{3+}/Fe(H_2O)_6^{2+}$ couple are shown in Figures 26 - 27.

The resulting Levich plots in which the curves are parallel confirm that the electron transfer reaction is first order in kinetics. For first order reaction: $(i)^{-1} = (i_k)^{-1} + (B\omega^{1/2})^{-1}$

i_k: current for pure kinetic control

$B\omega^{1/2} = i_d$: diffusion limiting current

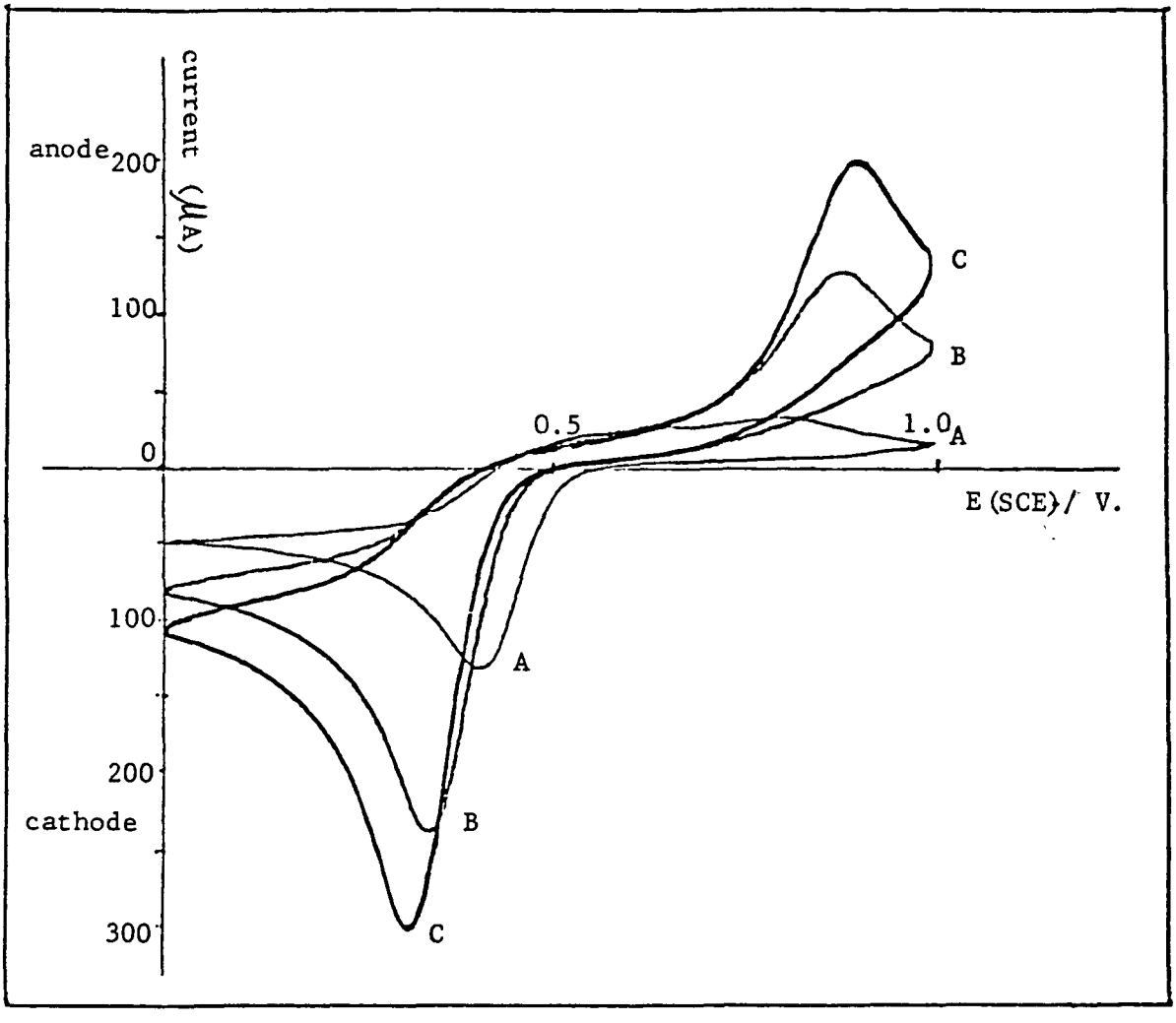

Figure 26 : Voltammetry curves for 6mM $Fe(H_2O)_6^{3+}$ on gold disk electrode in 0.5 M $HClO_4$. Electrode area: 0.458 cm^2. Sweep rate:

A: 10mV/s, B: 50mV/s, C: 100mV/s.

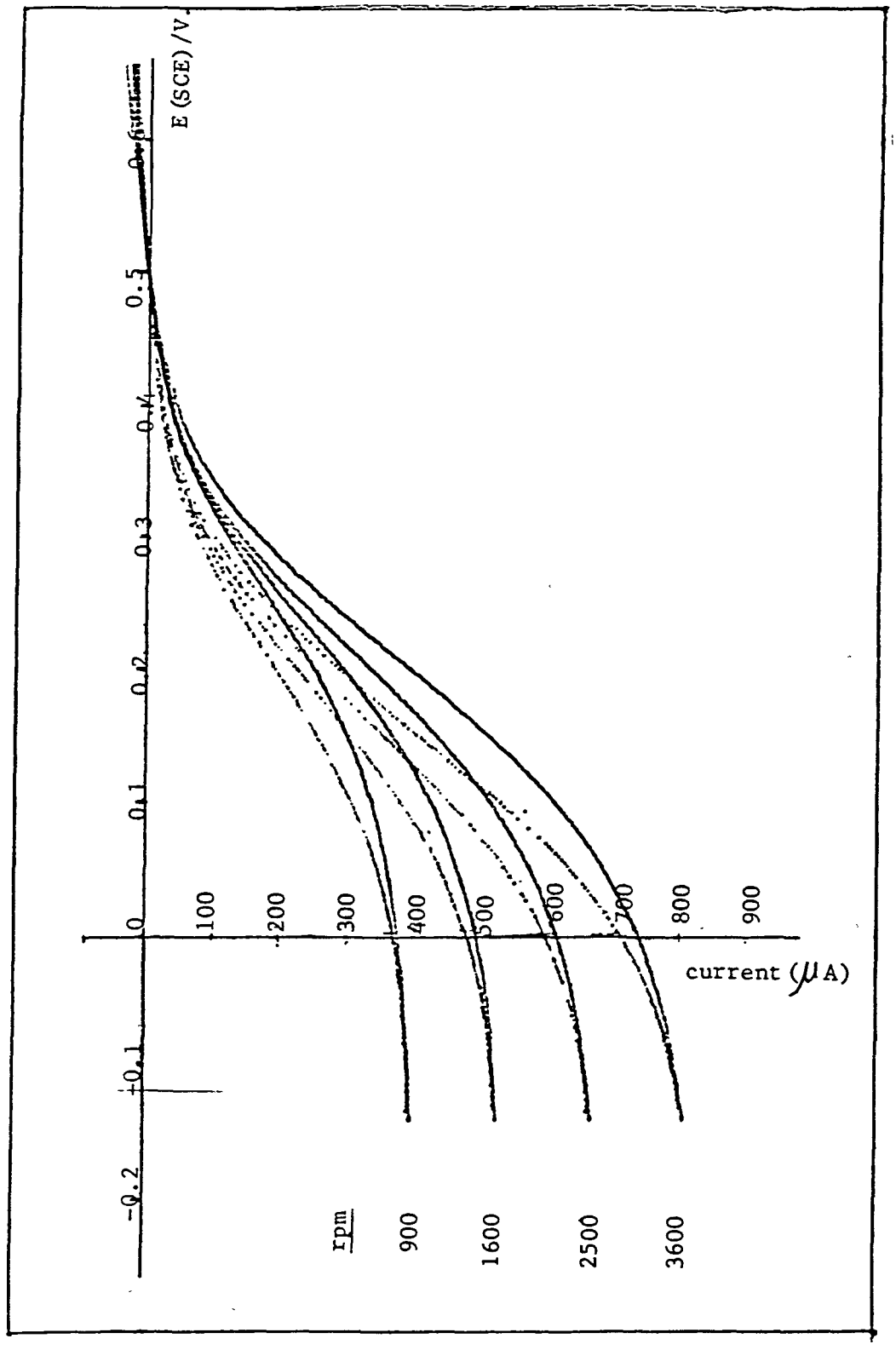

Figure 27: Polarization curves for $Fe(H_2O)_6^{3+}$ reduction on rotating gold disk electrde in acid media. Solution: 6mM $Fe(ClO_4)_3$ in 0.5 M $HClO_4$. Electrode area: 0.458 cm^2. Sweep rate: 10 mv/s. Rotation rates as specified.

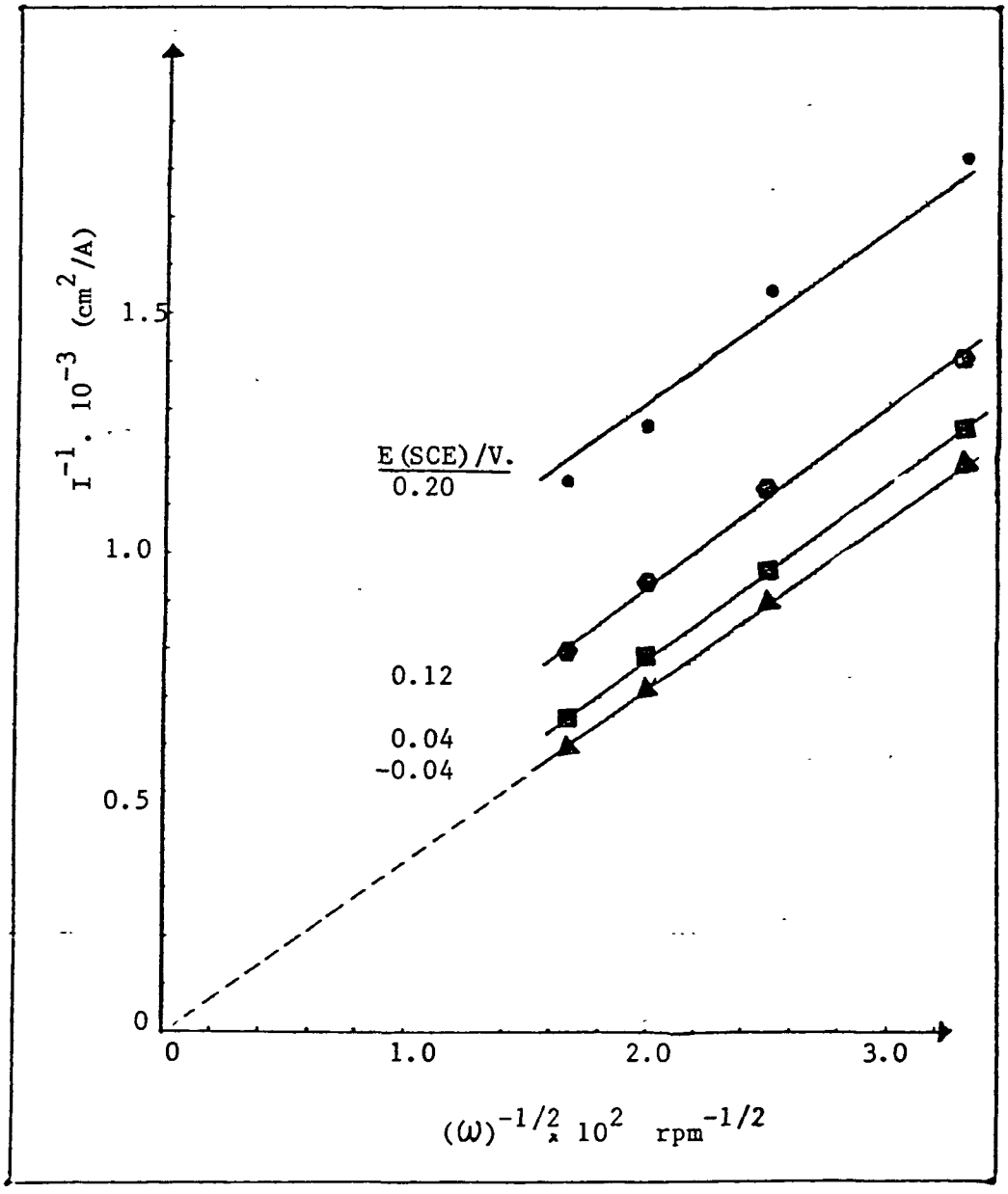

Figure 28: I^{-1} vs. $\omega^{-1/2}$ plot of data in Fig. 27.

A. Effect of Halides

The electrode reaction of the $Fe(H_2O)_6^{3+}/Fe(H_2O)_6^{2+}$ couple is strongly affected by halide anions adsorbed on the electrode surface. In the absence of halides the shape of the voltammogram with separated cathodic and anodic waves indicates a relatively slow electrode reaction. However, it was found that the addition of even a small amount of halides leads to a change in polarization curves to a shape corresponding to a much more rapid electrode reaction. The marked increase in the rate of the electrode reaction of $Fe(H_2O)_6^{3+}/Fe(H_2O)_6^{2+}$ couple has long been believed due to changing the electron-transfer process from outer-sphere mechanism to inner-sphere mechanism with halide as a bridge between electrode and iron complex. Corresponding cyclic voltammogram and polarization curves of iron(II)/(III) couple with halides presence in solution are shown in the following figures.

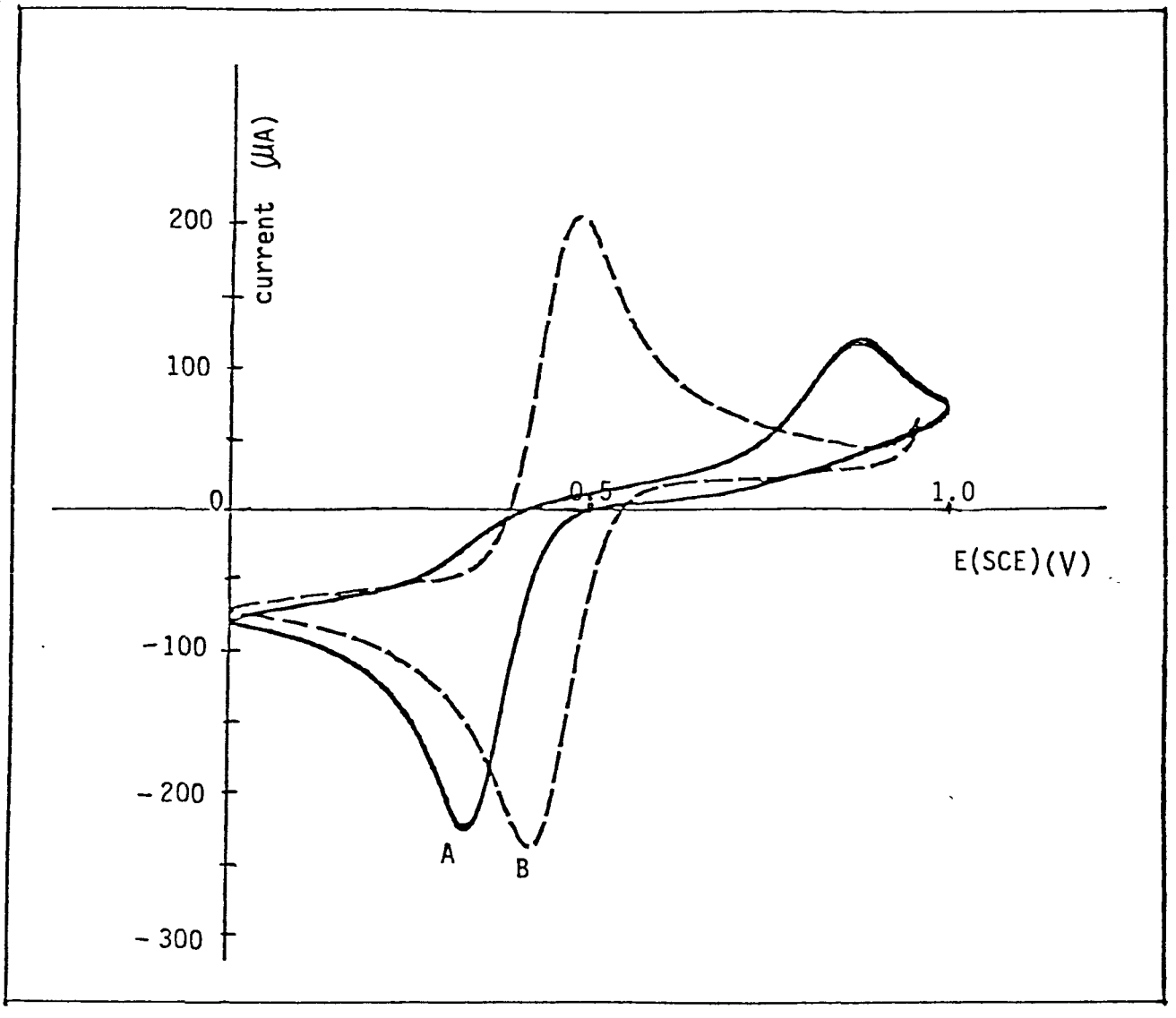

Figure 29: Effect of chloride on the kinetics of iron(II)/(III) couple on gold electrode in acidic media. Solution: 6 mM $Fe(ClO_4)_3$ in 0.5 M $HClO_4$. Electrode: gold disk (Pine) Area: 0.458 cm^2. Sweep rate: 50 mV/s. A). No chloride B). 3 mM NaCl added.

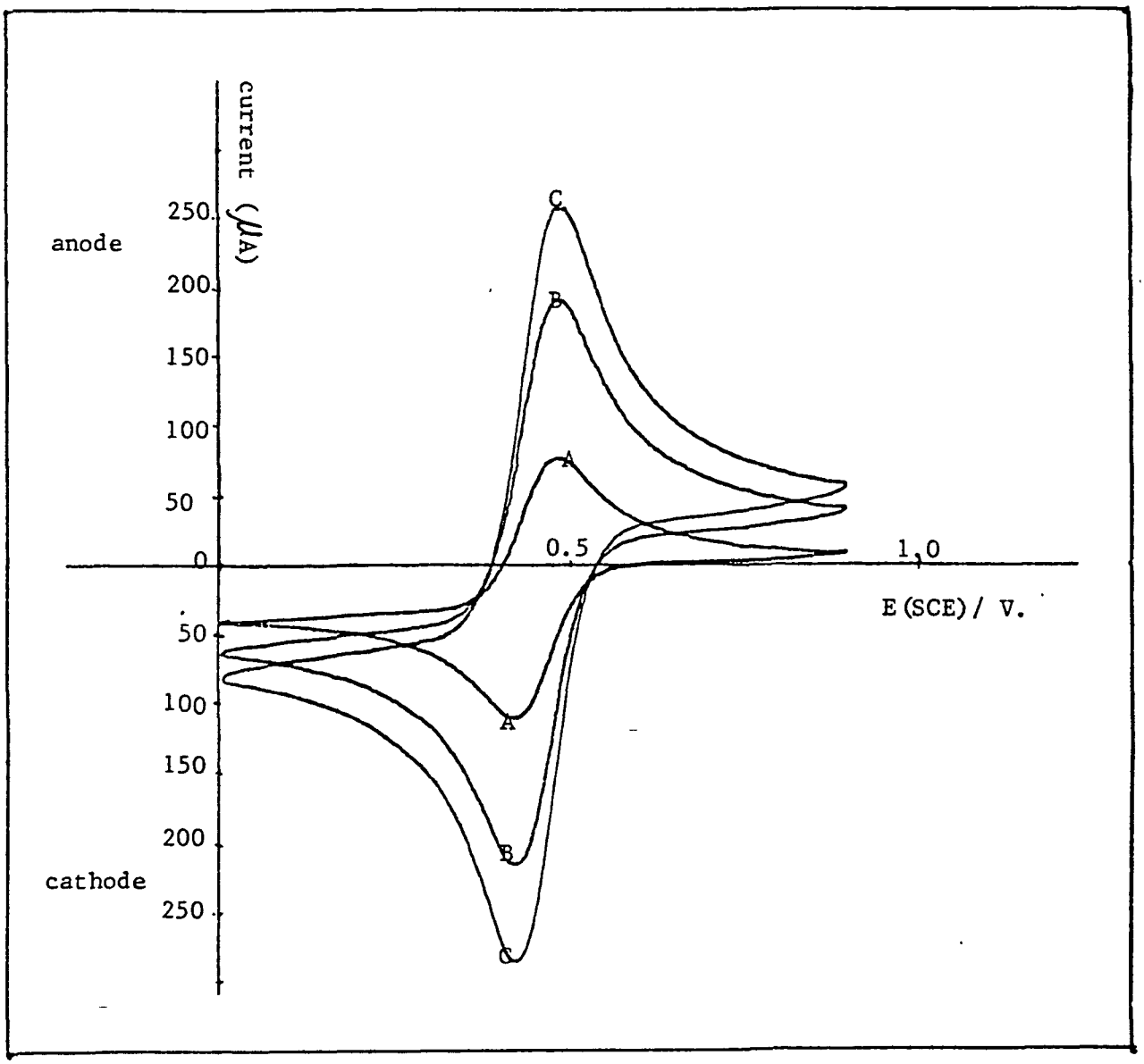

Figure 30: Voltammetry curves for ferric-ferrous couple on gold disk electrode in acid media containing chloride. Solution: 6mM $Fe(ClO_4)_3$ in 0.5 M $HClO_4$ and 3mM NaCl. Electrode area: 0.458 cm^2 (Pine). Sweep rate: A: 10mV/s, B: 50mV/s, C: 100mV/s.

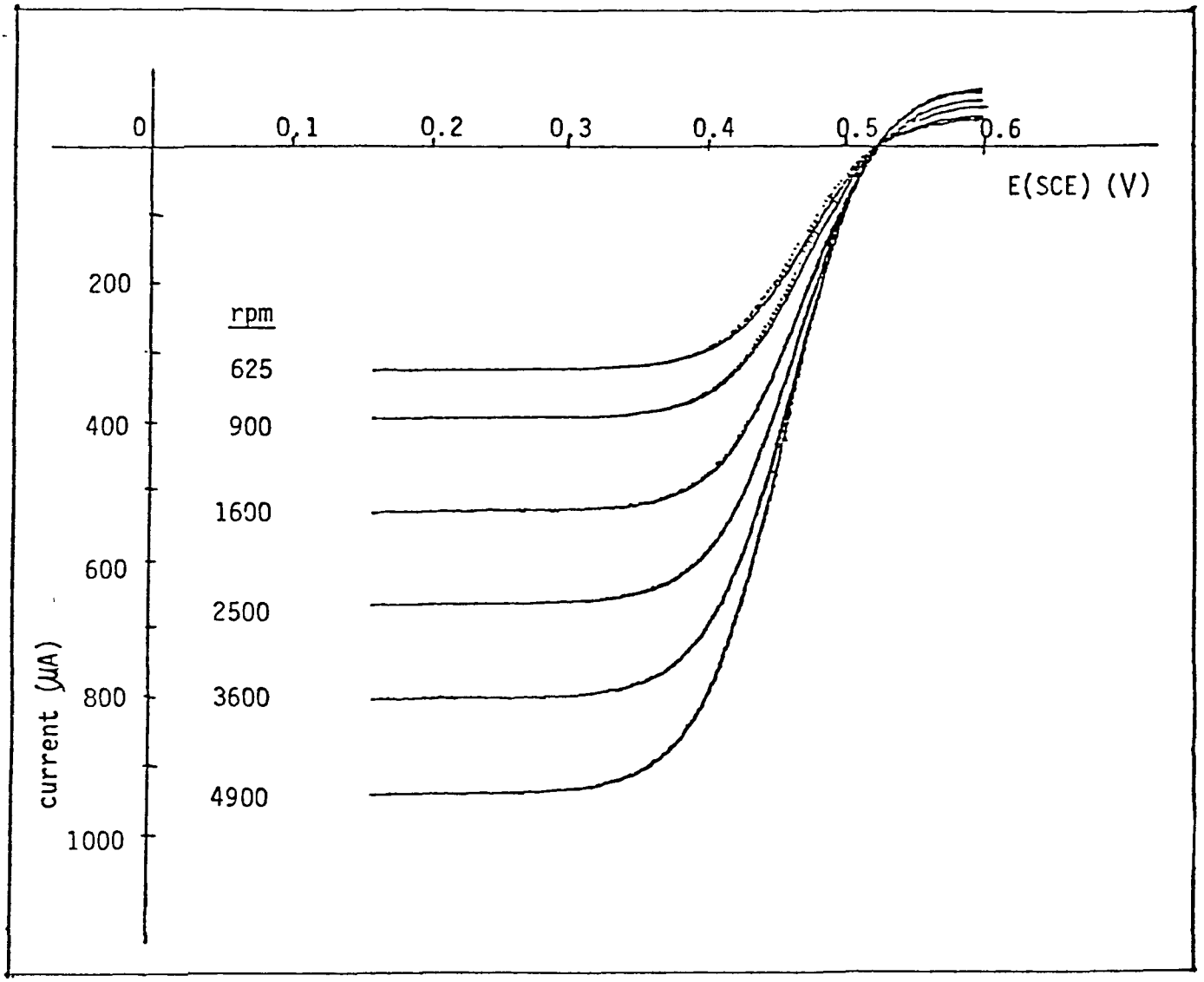

Figure 31: Polarization curves for 6 mM $Fe(ClO_4)_3$ in 0.5 M $HClO_4$, 3 mM NaCl on rotating gold disk electrode. Electrode area: 0.458 cm^2. (Pine). Sweep rate: 10 mV/s. Rotation rate as indicated.

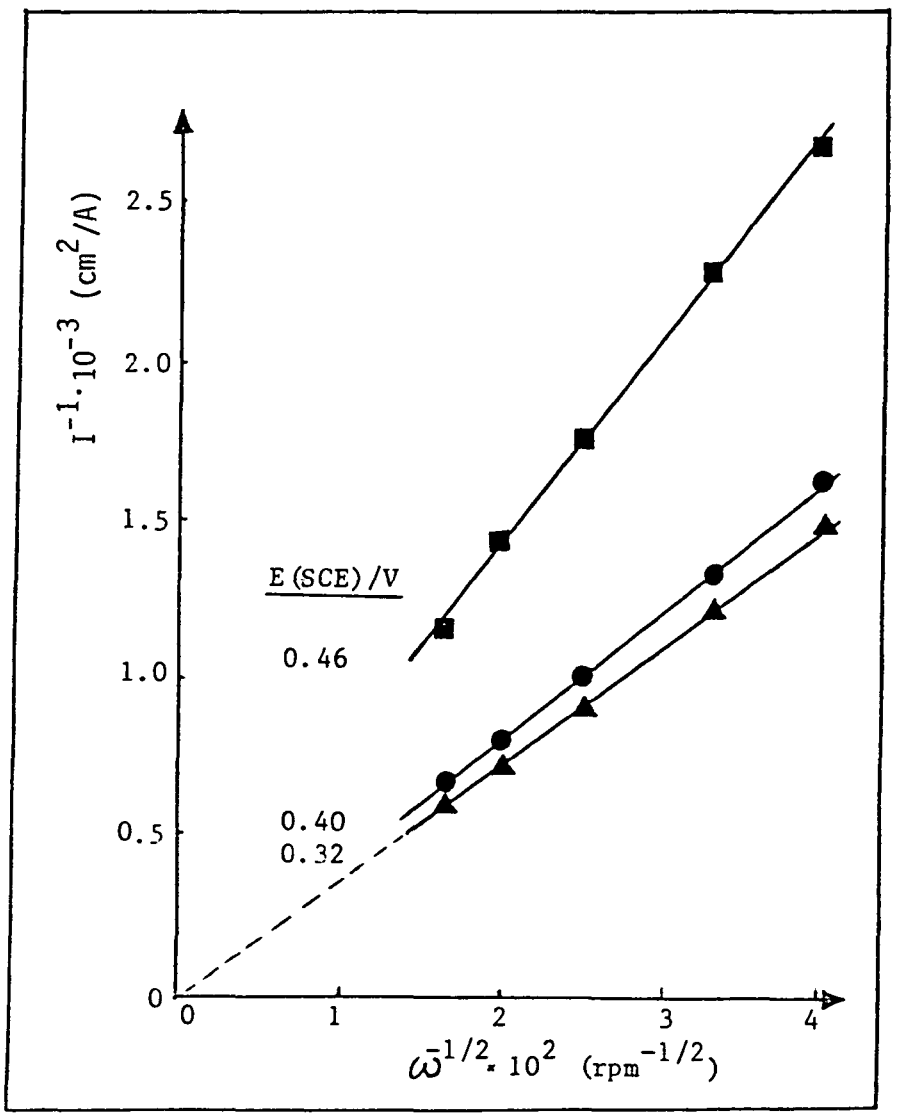

Figure 32: I^{-1} vs. $\omega^{-1/2}$ plot of data in figure 31.

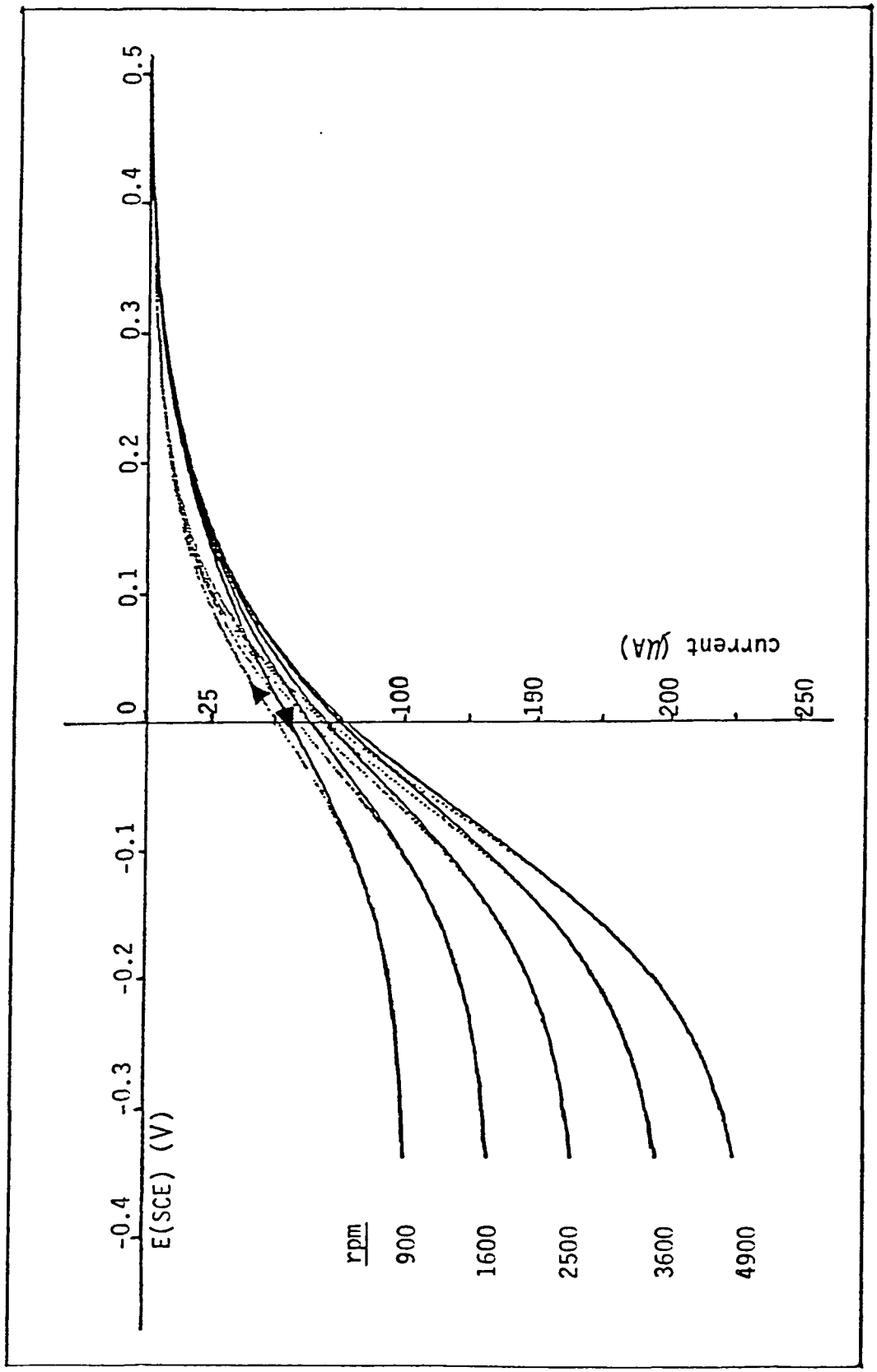

FIGURE 33 : POLARIZATION CURVE FOR $Fe(H_2O)_6^{3+}$ REDUCTION ON ROTATING GOLD DISK ELECTRODE
DISK AREA: ~0.2 cm^2. SCAN RATE: 10 MV/S. SOLUTION: 3MM $Fe(ClO_4)_3$ IN
0.1M $HClO_4$. ROTATION RATE : AS INDICATED. NO CHLORIDE ADDED.

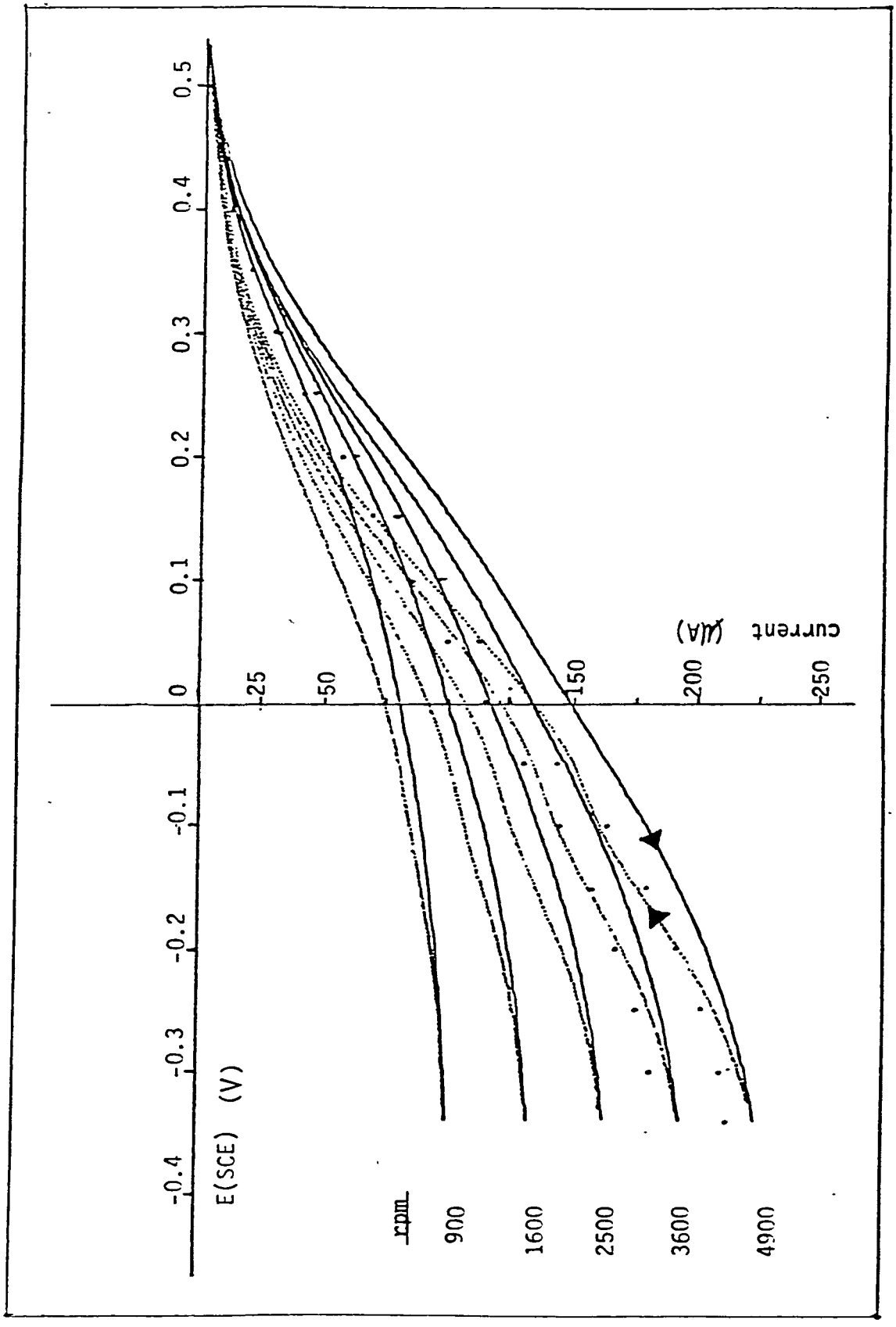

FIGURE 34: SAME AS FIG. 33 IN THE PRESENCE OF $7 \cdot 10^{-5}$M NACL.

'''''' STEADY STATE.

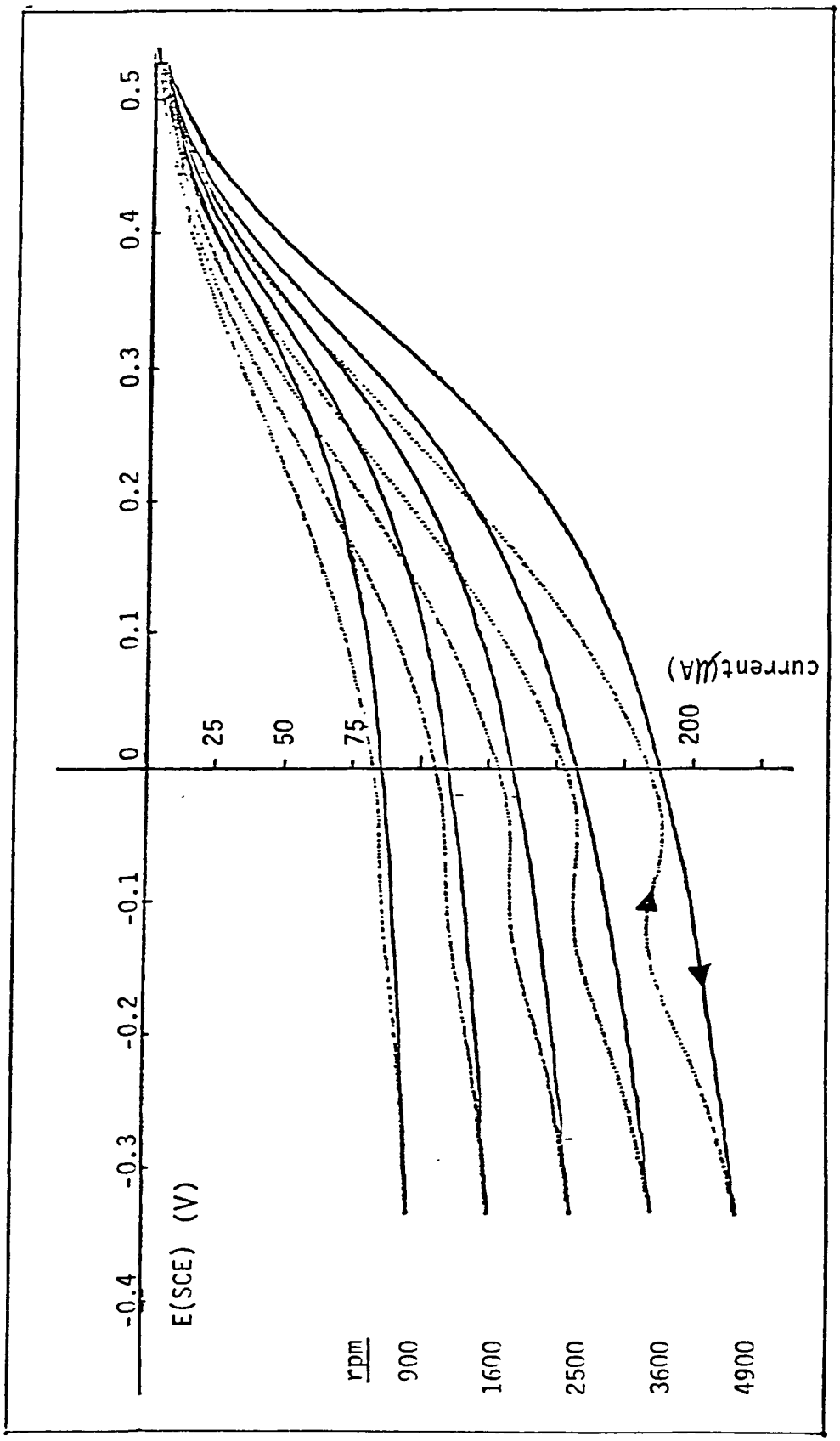

FIGURE 35 : SAME AS FIG. 33 IN THE PRESENCE OF $2'10^{-4}$M NACL

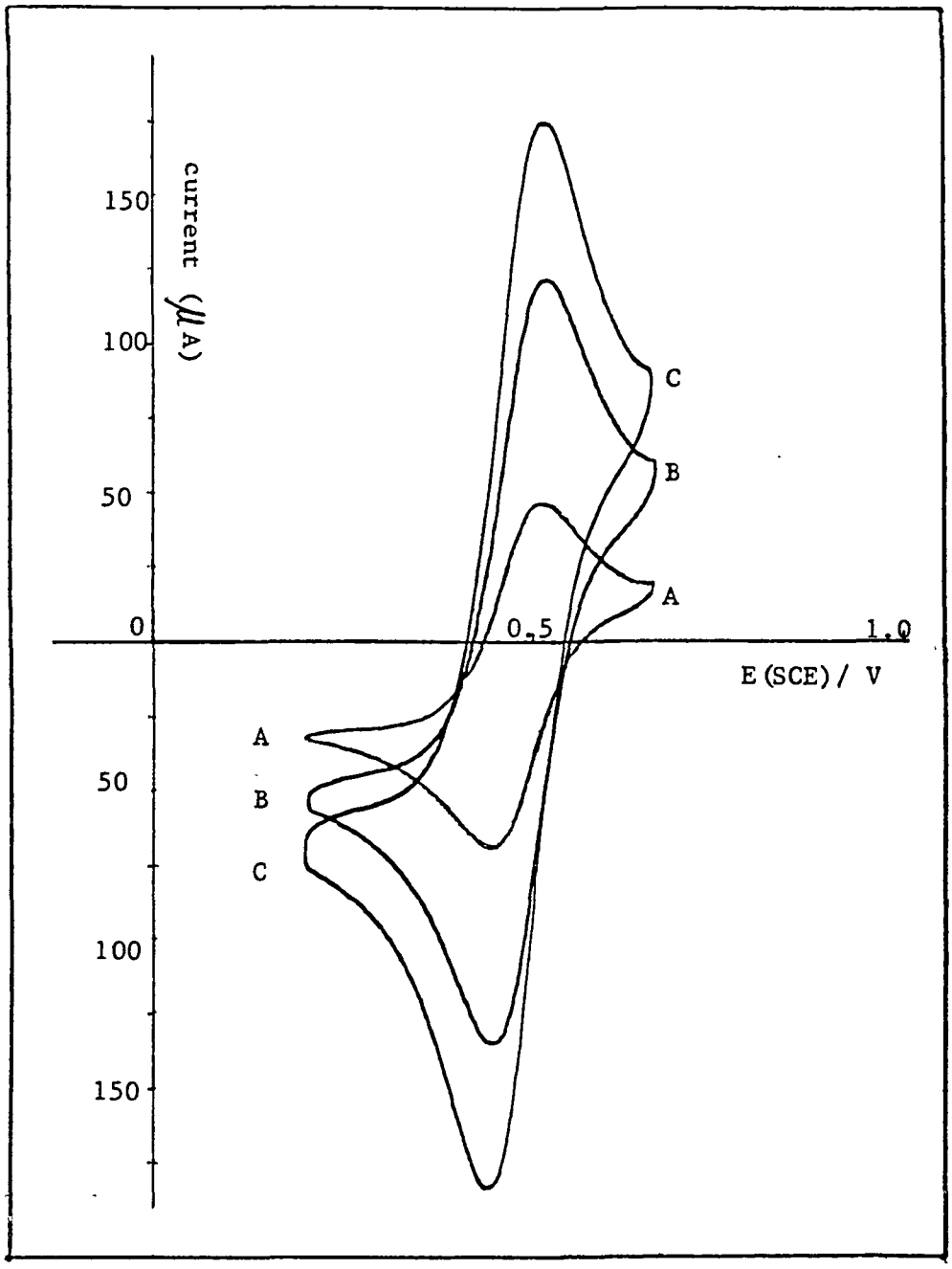

Figure 36 : Voltammetry curves for ferric-ferrous couple on gold disk electrode in acid media containing Br^-. Solution: 6mM $Fe(ClO_4)_3$ in 0.5M $HClO_4$ and 3mM NaBr and 0.32mM $Pb(NO_3)_2$. Electrode area: 0.458cm^2. Sweep rate: A: 10 mv/s, B: 50 mv/s, C: 100 mv/s.

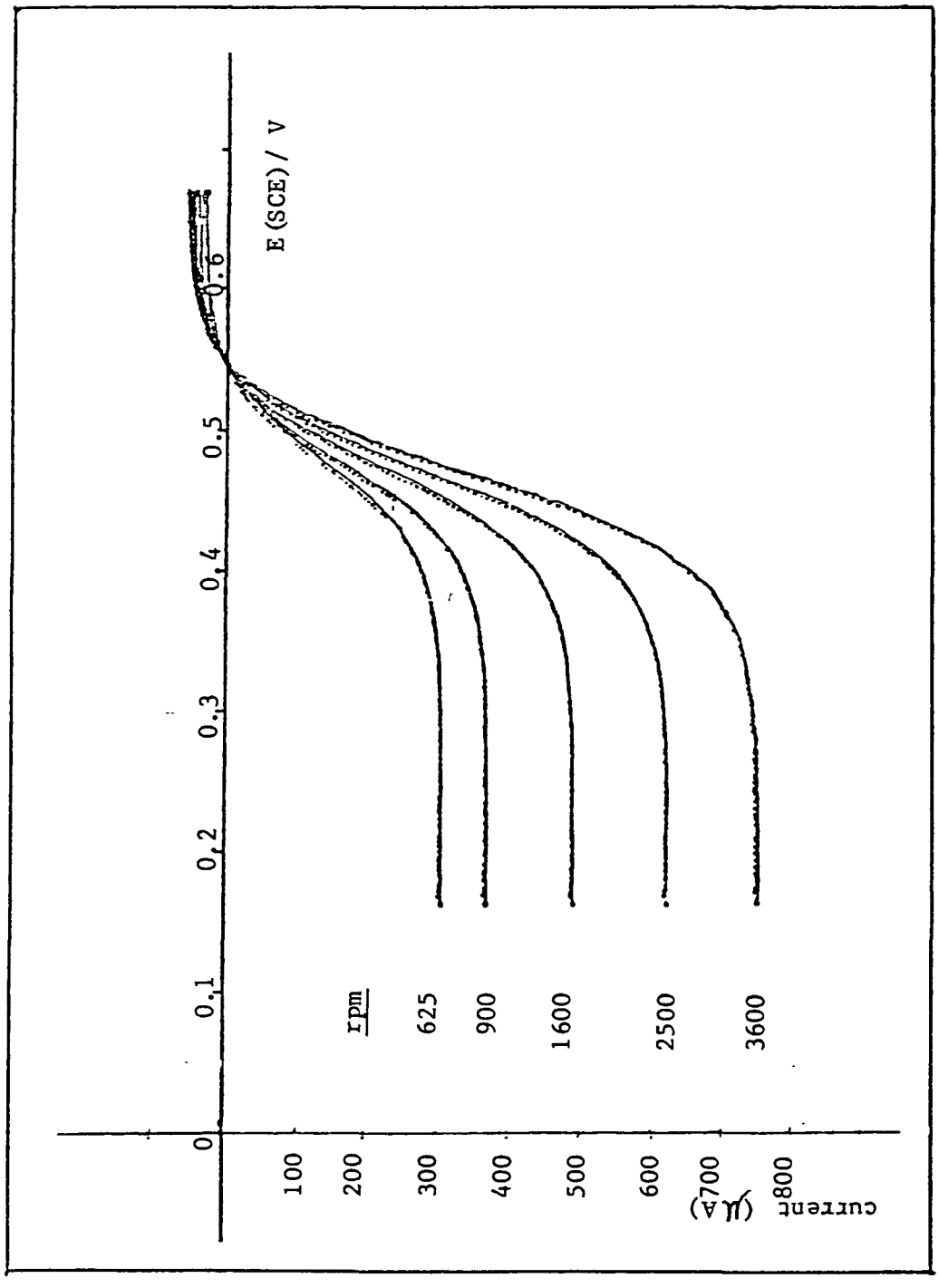

Figure 37 : Polarization curves for $Fe(H_2O)_6^{3+}$ reduction on gold disk electrode with NaBr presence in solution. Electrolyte: 6mM $Fe(ClO_4)_3$, 3mM NaBr, 0.32mM $Pb(NO_3)_2$ in 0.5M $HClO_4$. Electrode area: 0.458 cm^2 (Pine). Sweep rate: 10 mv/s. Rotation rates as specified.

B. Effect of the Underpotential Deposition of Bismuth

The plating and stripping of bismuth on gold was studied in perchloric acid media using a rotating gold disk electrode. The underpotential deposition of bismuth occurs at potential region between -0.05V and +0.40V vs. SCE. where the $Fe(H_2O)_6^{3+}/Fe(H_2O)_6^{2+}$ couple undergoes both diffusion and kinetic controlled reaction. It was found that the underpotential deposition of bismuth on gold results in a net decrease of the reaction kinetics as compared with that on the bare metal for $Fe(H_2O)_6^{3+}$ reduction.

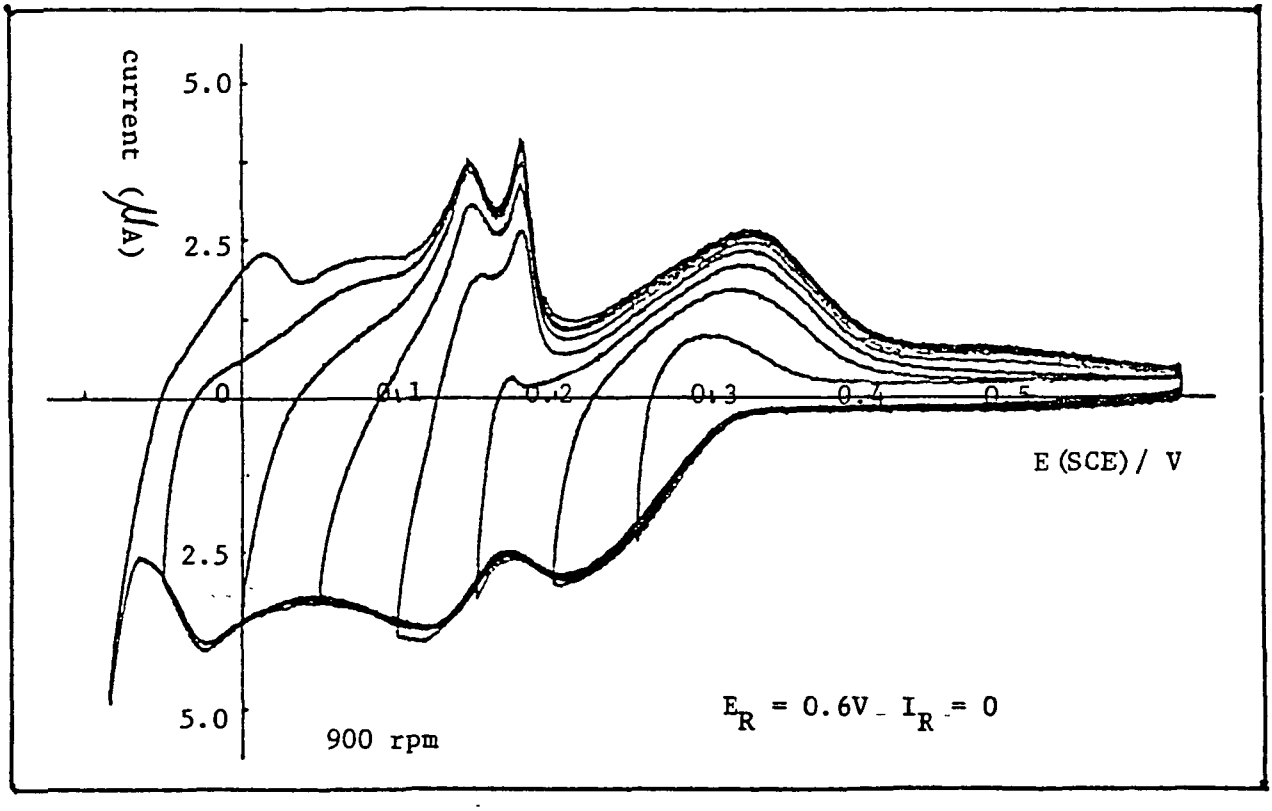

Figure 38: Voltammetry curves for UPD of bismuth on gold disk electrode. Voltage window opening experiments. Electrolyte: 0.1M $HClO_4$, $3.2 * 10^{-5}$M Bi_2O_3. Electrode area: 0.2 cm^2. Sweep rate: 10 mv/s. Rotation rate: 900 rpm

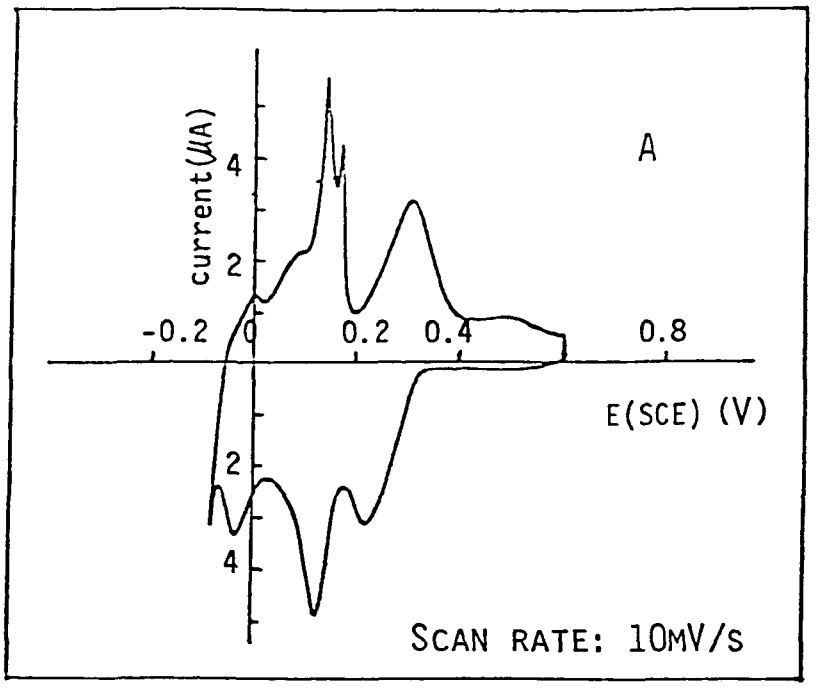

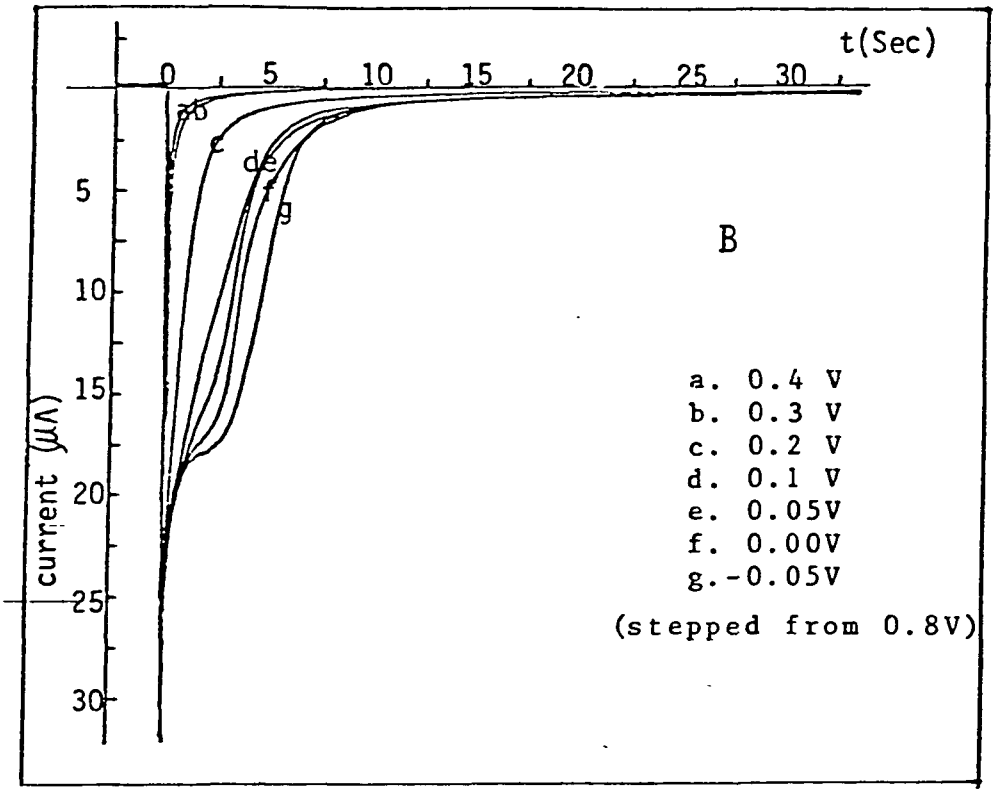

FIGURE 39: UNDERPOTENTIAL DEPOSITION OF Bi ON Au ROTATING DISK ELECTRODE IN A SOLUTION 0.1M $HClO_4$, $3.2 \cdot 10^{-5}$M Bi_2O_3. ELECTRODE AREA: $\sim 0.2 cm^2$. ROTATION RATE: 900 RPM.

A. CYCLIC VOLTAMMOGRAM. B. TRANSIENT EXPERIMENT

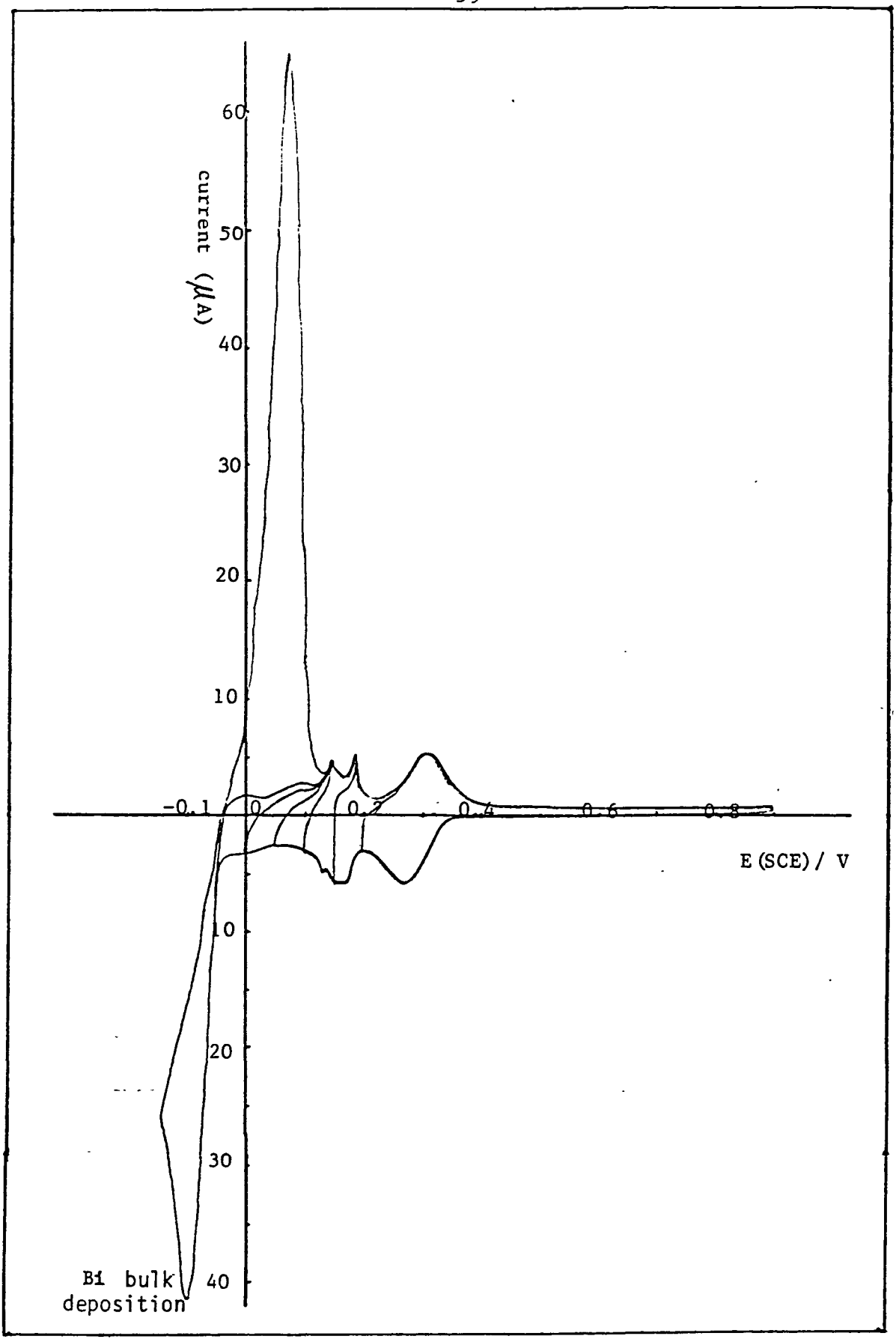

Figure 40 : Deposition and Stripping of bismuth on gold disk electrode. Electrolyte: 3.5×10^{-4}M Bi_2O_3 in 0.1M $HClO_4$. Sweep rate: 10 mv/s. Electrode area: 0.2 cm^2.

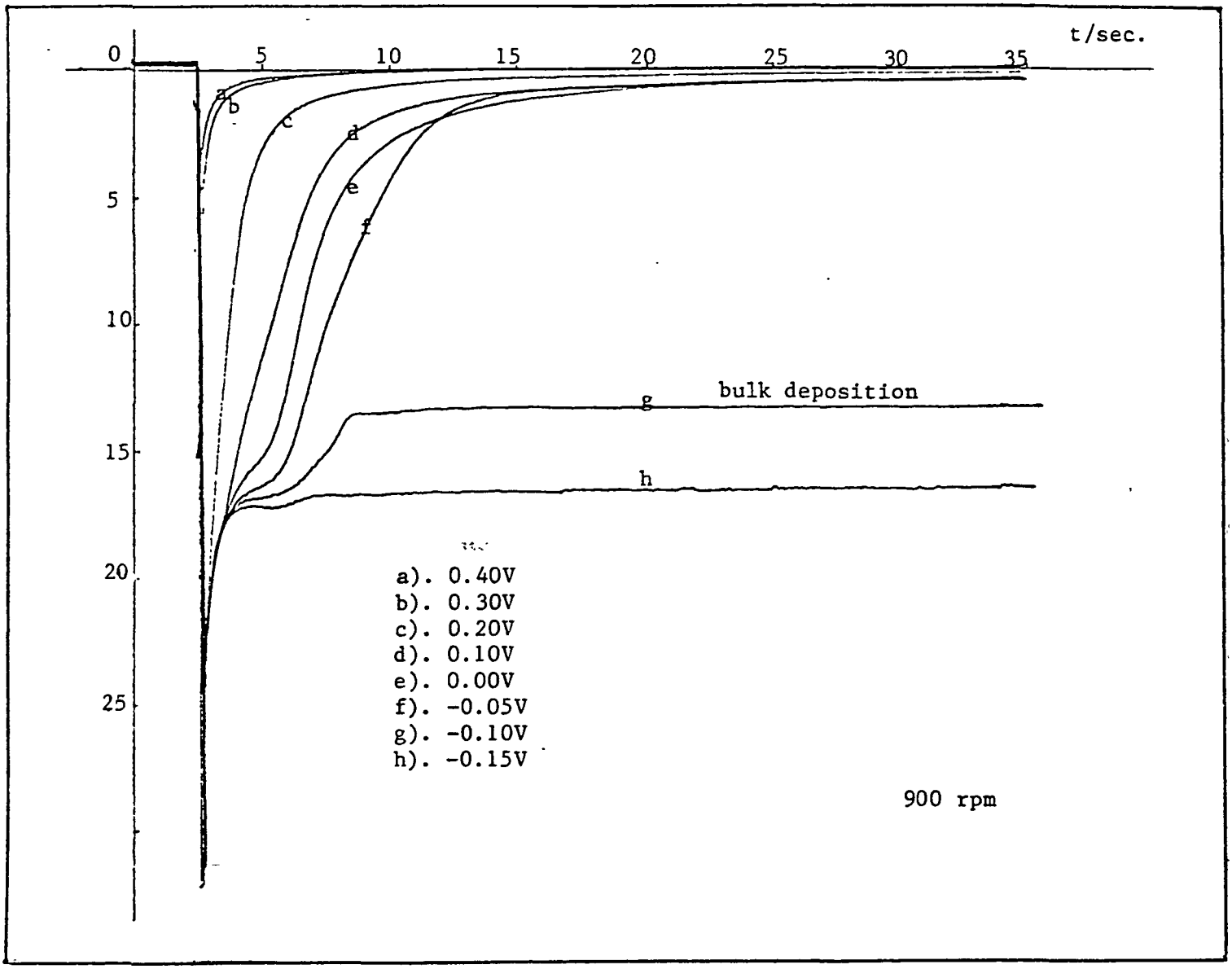

Figure 41: Current vs. Time curves for gold disk electrode in a solution containing 0.1M $HClO_4$ and 3.2 10^{-5}M Bi_2O_3 upon potential step from 0.8V into indicated potential. Rotation rate : 900 rpm. Electrode area: 0.2 cm^2. I_R = 0, E_R=0.8V.

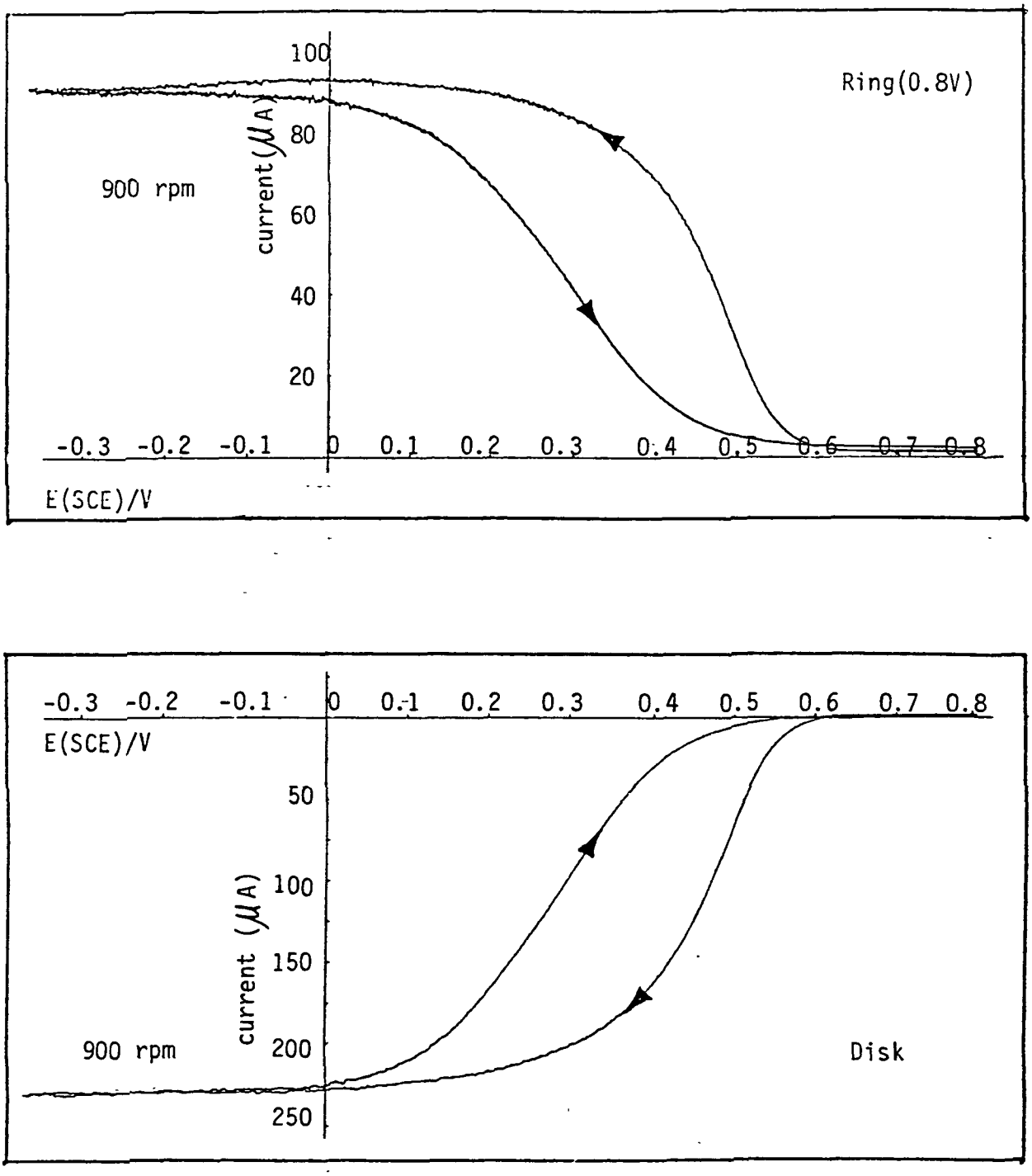

FIGURE 42 : POLARIZATION CURVE FOR $Fe(H_2O)_6^{3+}$ REDUCTION ON ROTATING GOLD RING-DISK ELECTRODE IN ACIDIC MEDIA. SOLUTION: 3MM $Fe(ClO_4)_3$ IN 0.1M $HClO_4$. ROTATION RATE: 900 RPM.

DYNAMIC POLARIZATION . SCAN RATE: 10MV/S.

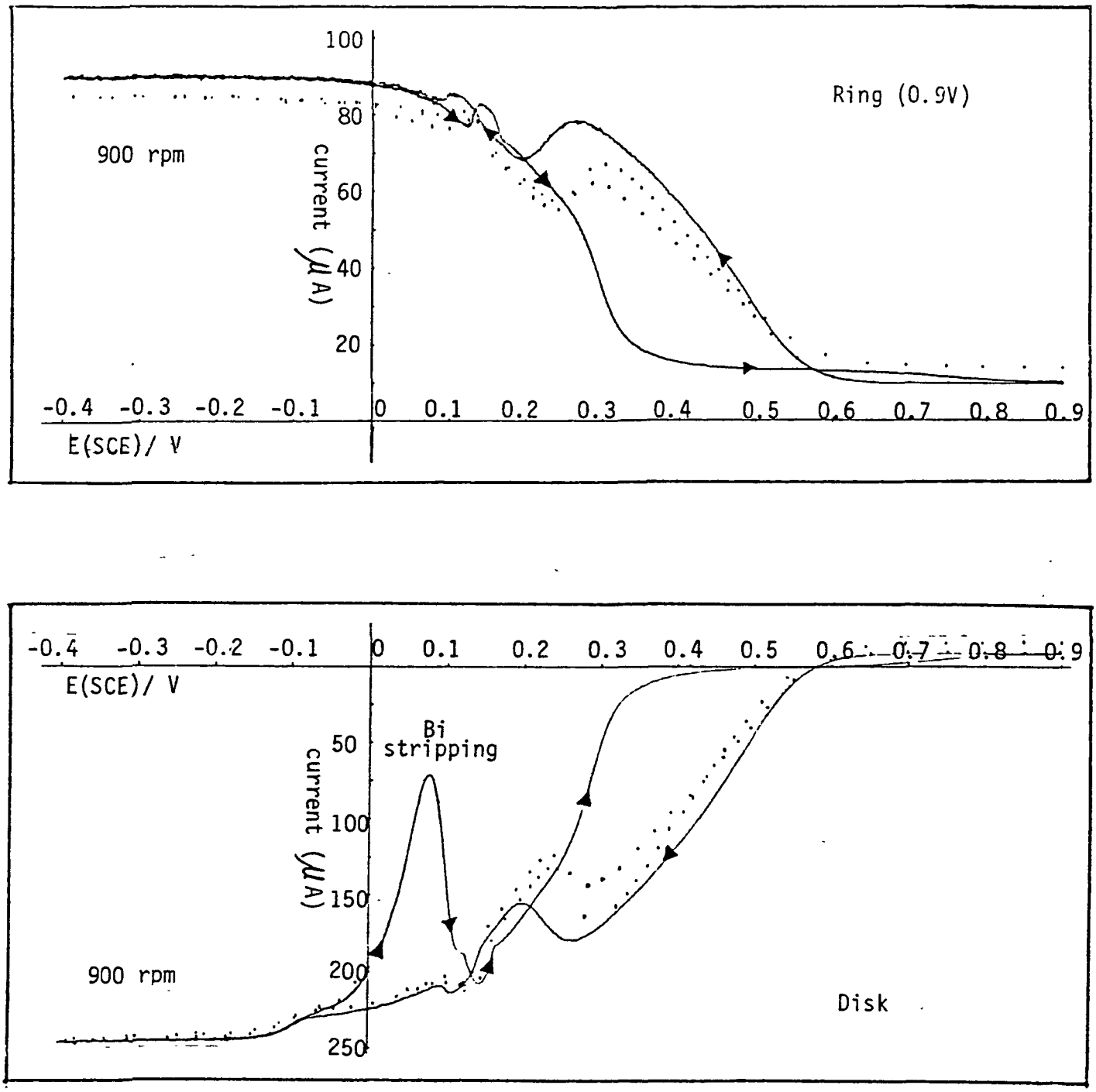

FIGURE 43: EFFECT OF Bi UNDERPOTENTIAL DEPOSITION ON THE REDUCTION OF $Fe(H_2O)_6^{3+}$ ON GOLD RING-DISK ELECTRODE. ELECTRODE AREA: RING=DISK $\sim 0.2 cm^2$. SOLUTION: $3.2 \cdot 10^{-5}$M Bi_2O_3, 3.2mM $Fe(ClO_4)_3$ IN 0.1M $HClO_4$ ROTATION RATE: 900 RPM. RING POTENTIAL: 0. V DYNAMIC POLARIZATION. SCAN RATE: 10mV/s

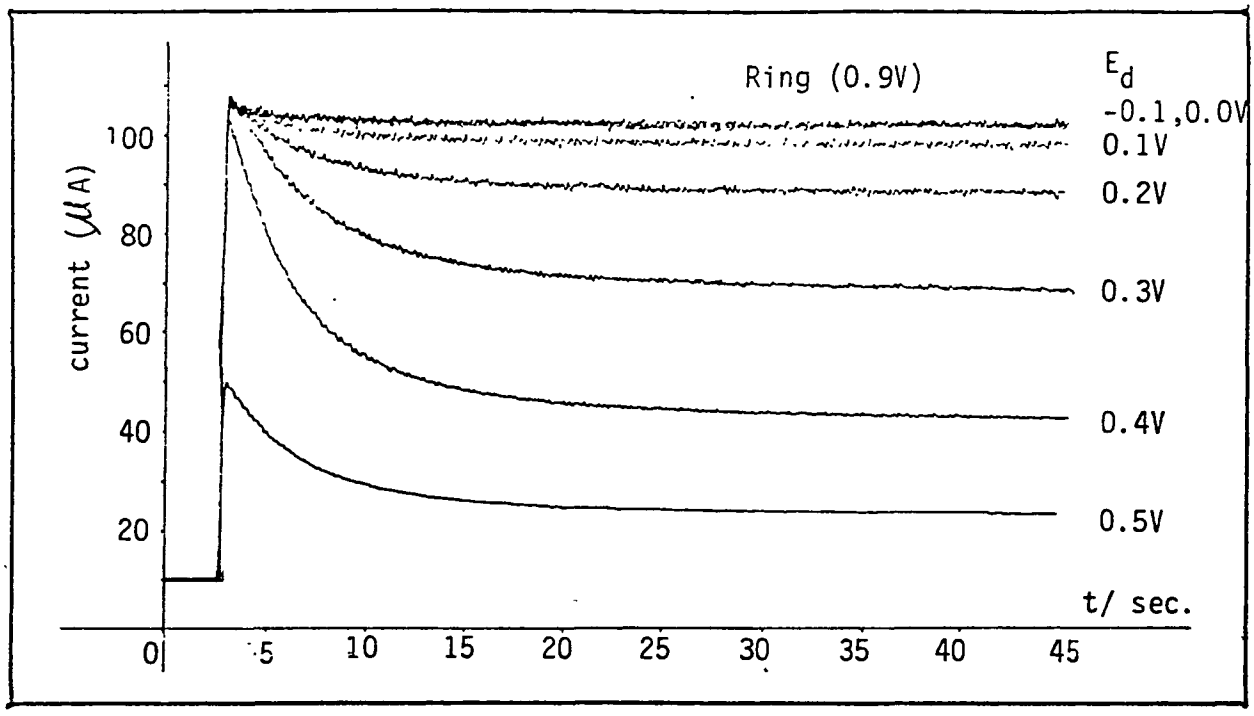

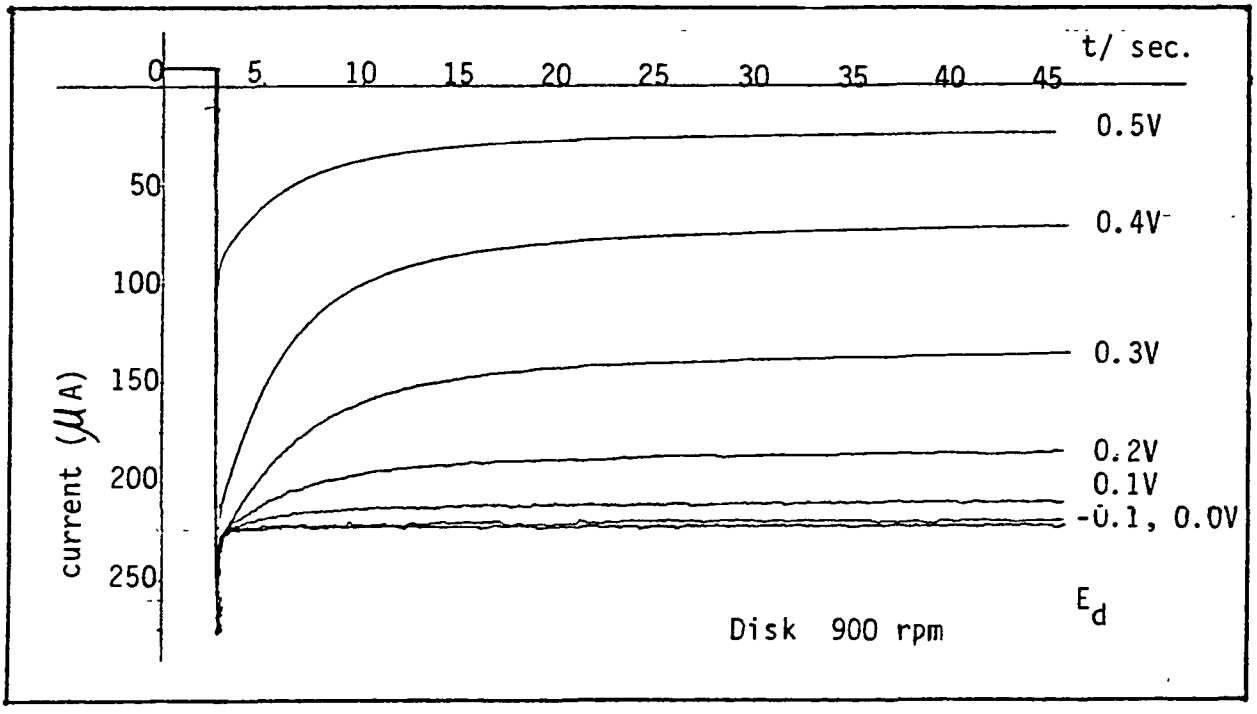

Figure 44: Current vs. Time curves for ferric-ferrous couple on gold ring-disk electrode upon potential step from 0.9V into indicated potential. Solution: 3.2mM $Fe(ClO_4)_3$ in 0.1M $HClO_4$. Rotation rate: 900 rpm. Ring potential: 0.9V. Electrode area: 0.2 cm^2.

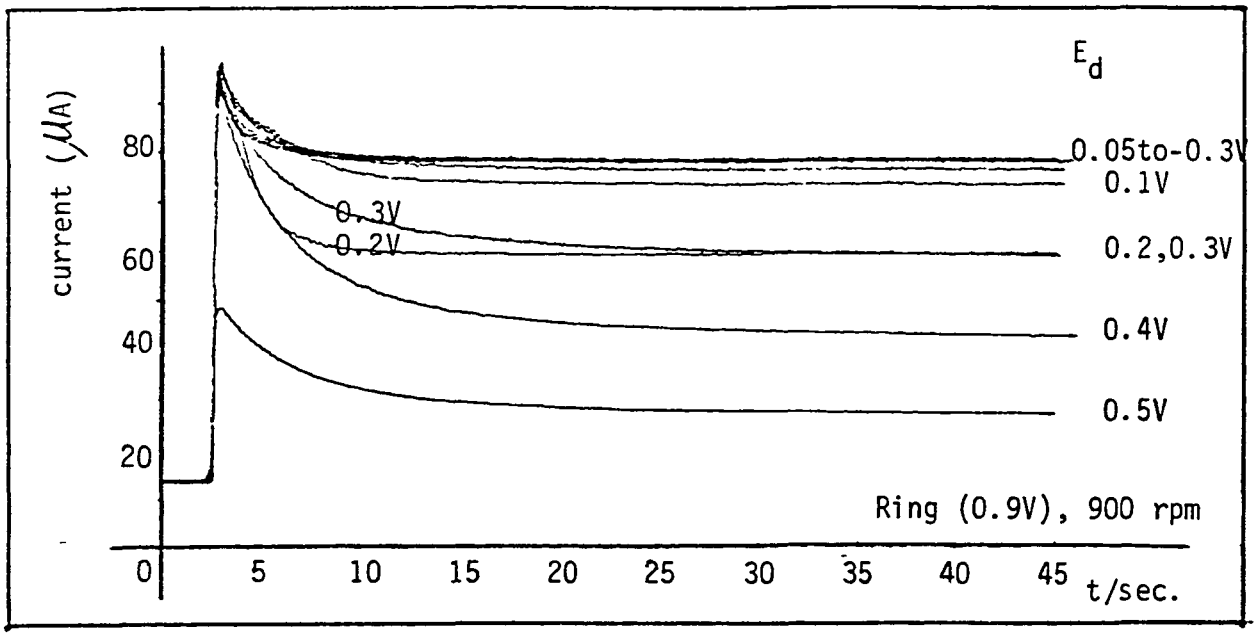

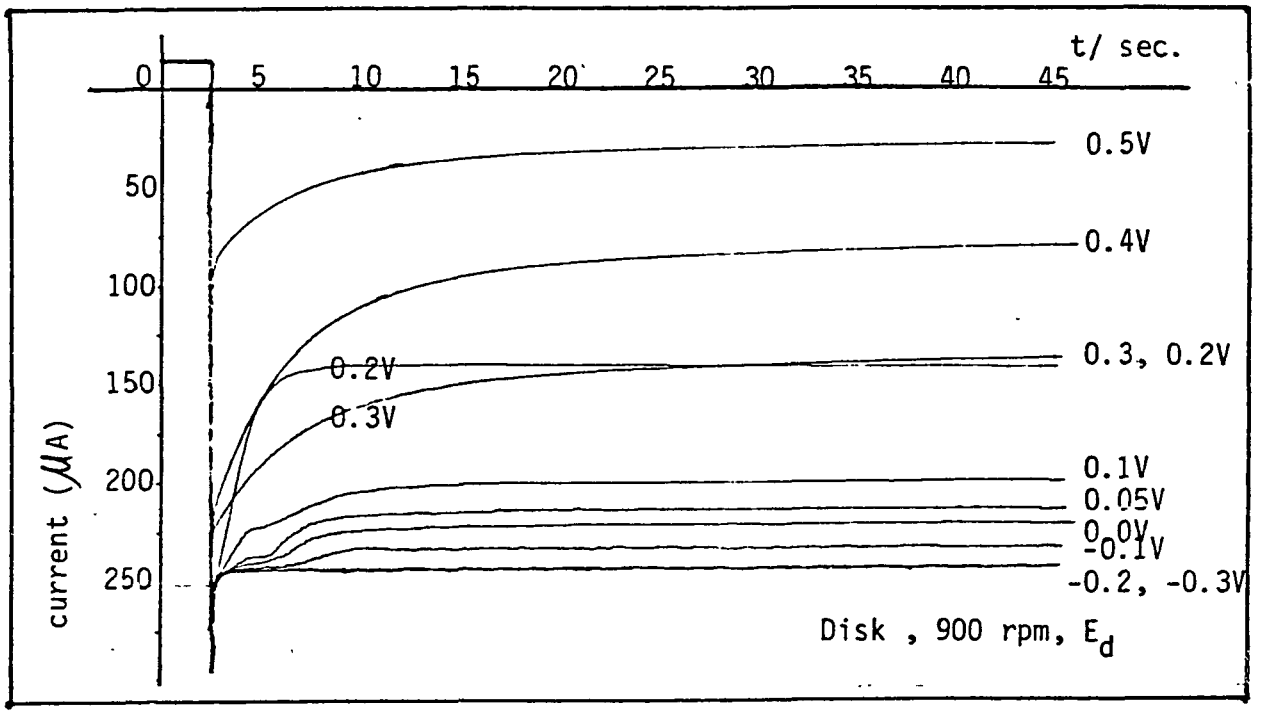

Figure 45: Current vs. Time curves for simultaneous underpotential deposition of bismuth and $Fe(H_2O)_6^{3+}$ reduction on gold ring-disk electrode upon potential step from 0.9V into indicated potential. Solution:3.2mM $Fe(ClO_4)_3$, 5×10^{-5}M Bi_2O_3 in 0.1M $HClO_4$. Rotation rate: 900 rpm. Ring potential: 0.9V. Electrode area: 0.2 cm^2.

4. SPECTROSCOPIC STUDIES

A. Time Effects on Solution Composition. (Visible Spectra).

Ultraviolet and visible spectroscopy have been utilized in connection with the chromium(II)/(III) couple part of NASA's Redox system as a means of analyzing the solution compositions. These studies have been aimed at determining the concertration of individual metal complexes at different states of charge and discharge in an effort to correlate the performance of the overall electrode with the presence of certain species in solution.

The time dependence of absorption spectra of $CrCl_3$ solution is shown in figure 46. It was found that the absorption maximums shift toward shorter wavelength with time. However, the spectrum of $Cr(H_2O)_5Cl^{2+}$ which can be separated using an ion-exchange column eluting with $HClO_4$ does not change even after 12 hours.(Fig. 47).

B. XPS Measurement on pre-electrolysis Gold Cathode

In order to check out the effects of impurity on the reduction kinetics of couple, a pre-electrolyzed gold cathode out from the same supporting electrolyte for the couple is examined by ESCA. No obvious impurity has been detected, except oxygen and carbon which exist else where.(Fig. 48).

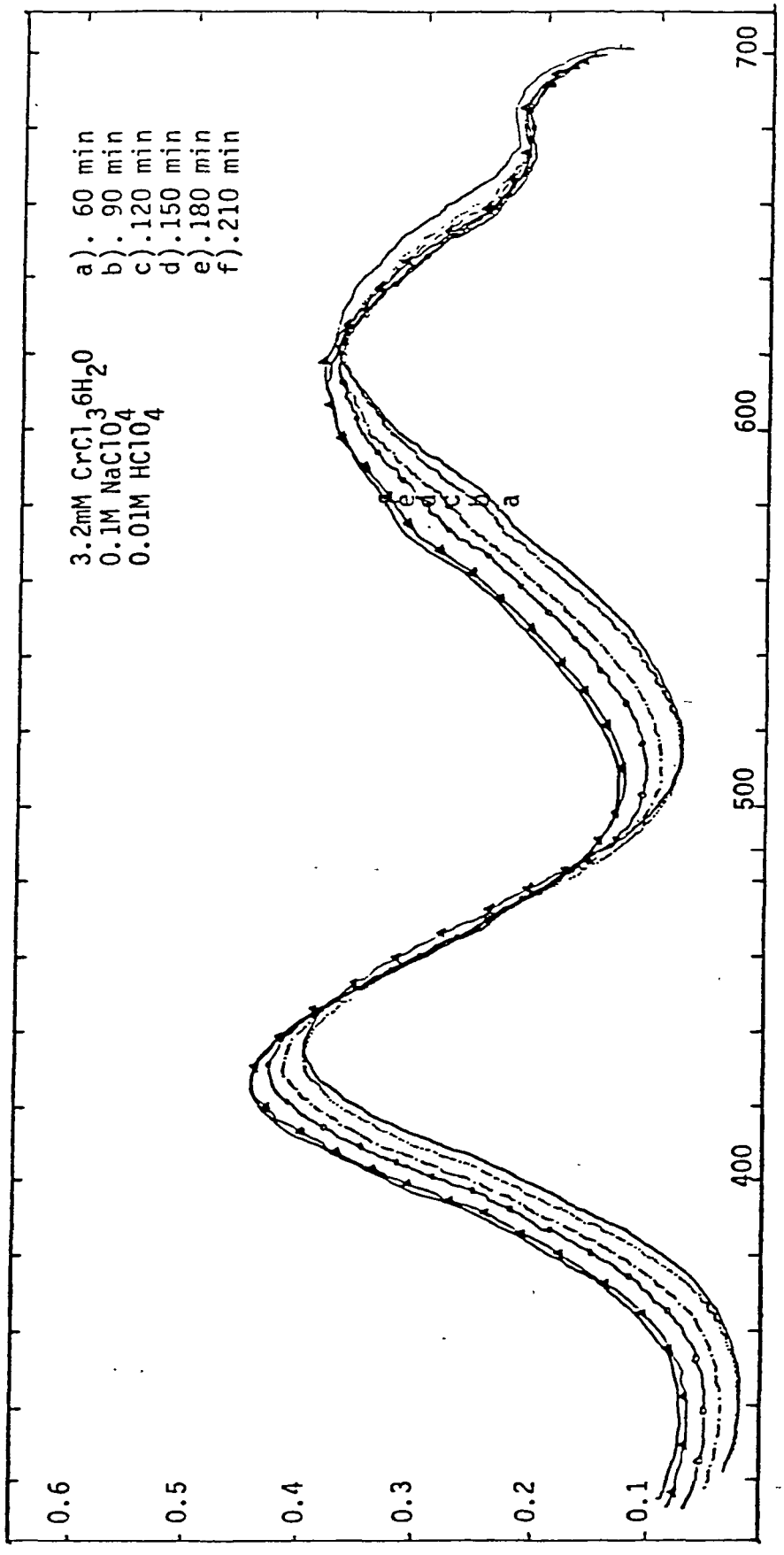

FIGURE 46: VISIBLE SPECTRUM OF 3.2MM $CrCl_3$ IN 0.1M $NaClO_4$, 0.01M $HClO_4$ SOLUTION AS A FUNCTION OF TIME . LENGTH OF TIME REFERS TO TIME OF PREPARATION.

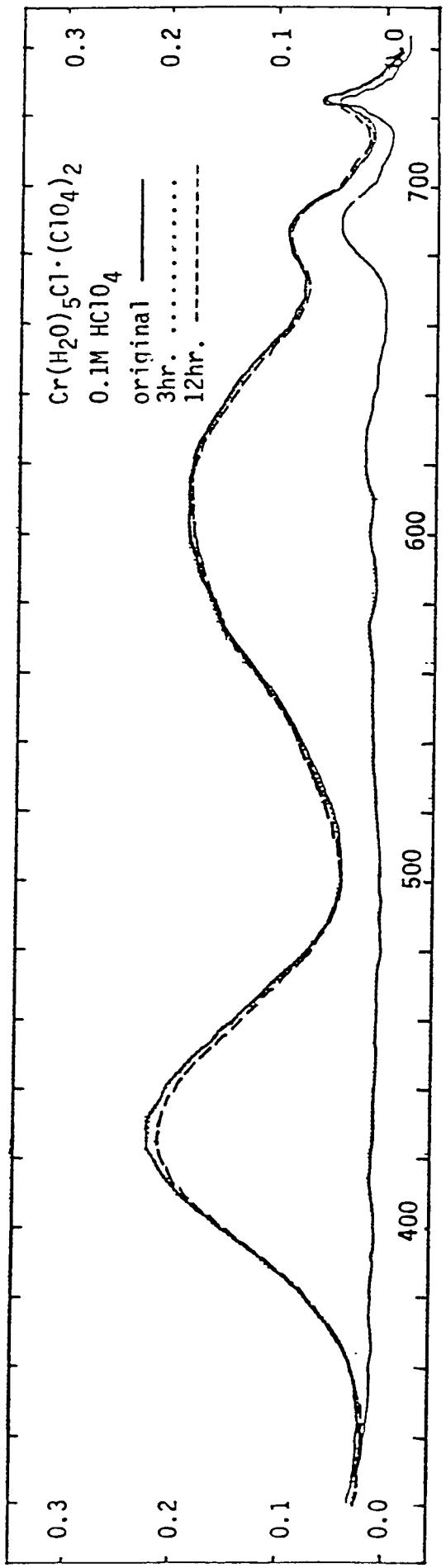

FIGURE 47: VISIBLE SPECTRUM OF $CR(H_2O)_5CL^{2+}$ OBTAINED BY ANION EXCHANGE OF FRESHLY PREPARED $CRCL_3$ IN 0.1M $HCLO_4$ AS A FUNCTION OF TIME.

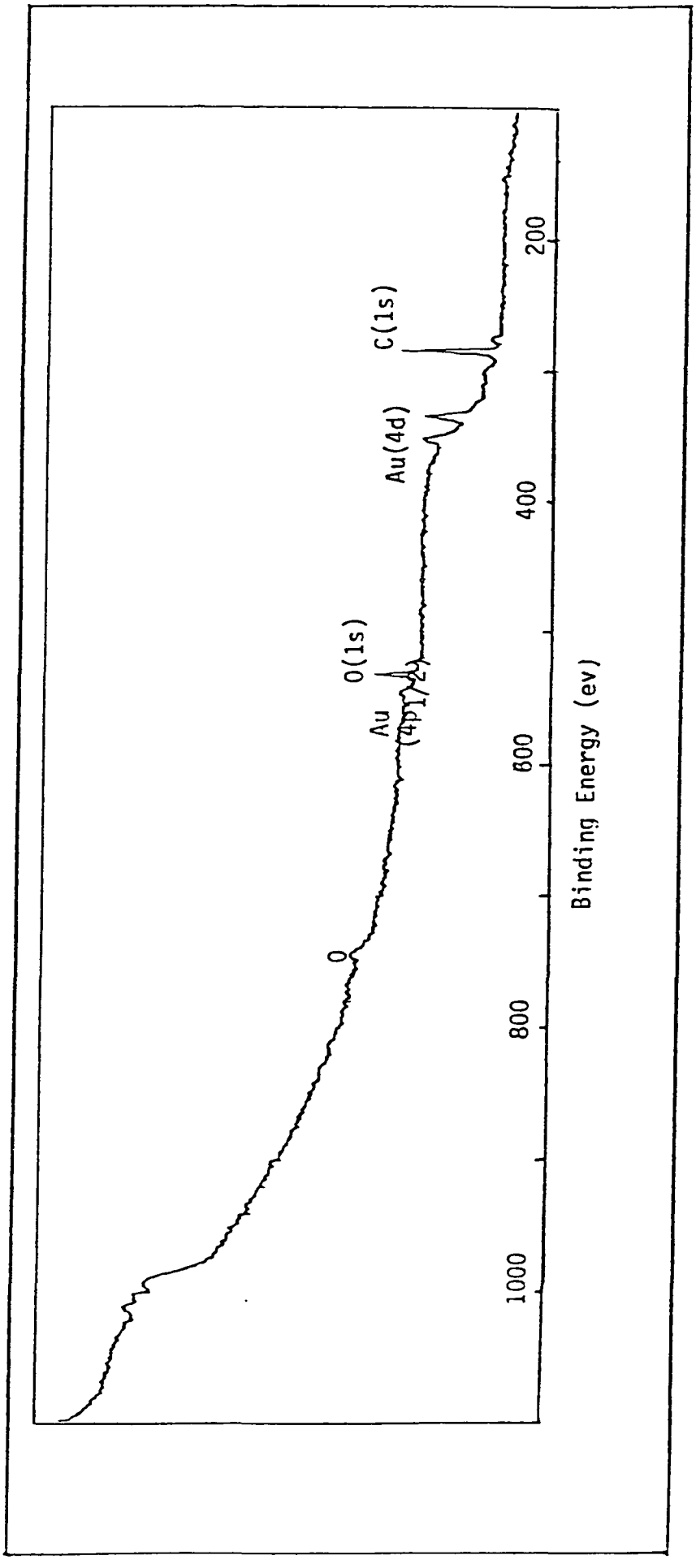

FIGURE 48: X-RAY PHOTOELECTRON SPECTRUM OF A GOLD FOIL CATHODE AFTER PRE-ELECTROLYSIS OF A HYDROGEN SATURATED SOLUTION 0.1M $NaClO_4$ IN 0.01M $HClO_4$ FOR 24 HRS, USING A PLATINUM GAUZE AS ANODE AND REFERENCE ELECTRODE.